LYAPUNOV-BASED NEUROMUSCULAR ELECTRICAL STIMULATION CONTROL

By

QIANG WANG

A DISSERTATION PRESENTED TO THE GRADUATE SCHOOL
OF THE UNIVERSITY OF FLORIDA IN PARTIAL FULFILLMENT
OF THE REQUIREMENTS FOR THE DEGREE OF
DOCTOR OF PHILOSOPHY

UNIVERSITY OF FLORIDA

2012

ACKNOWLEDGMENTS

I would like to sincerely thank my adviser, Warren E. Dixon, for helping me successfully go through the journey of my PhD. Thanks for the guidance he has provided over the years, which led me entering the research field and encouraged me when I got frustrated. Thanks for the patience, time and efforts he has given to help me mature in my research. Thanks for his role models as a adviser, a teacher, a colleague and a friend, which will benefit me in the years coming. I would also like to extend my gratitude to Dr. Gregory, Dr. Sharma, Dr. Johnson, Kamalapurkar, Dinh, Downey, Bellman, and all my colleagues in NCR for the various helps from technical discussions, comments and reviews, and warm words and smiles they provided. I would like to thank my wife for her endless love, support, and patience. Also, I would like to thank my parents and sons, who are my constant source for love and strength.

TABLE OF CONTENTS

LIST OF FIGURES

Abstract of Dissertation Presented to the Graduate School
of the University of Florida in Partial Fulfillment of the
Requirements for the Degree of Doctor of Philosophy

LYAPUNOV-BASED NEUROMUSCULAR ELECTRICAL STIMULATION CONTROL

By

Qiang Wang

December 2012

Chair: Warren E. Dixon
Major: Electrical and Computer Engineering

Neuromuscular electrical stimulation (NMES) or functional electrical stimulation (FES) is a widely used technique for rehabilitation and restoration of motor function. Millions of people suffering from disability and paralysis caused by neural disorders such as a stroke, spinal cord injury, multiple sclerosis, cerebral palsy, or traumatic brain injury can benefit from NMES. Open-loop methods, using grouped electrical pulses with fixed parameters, are widely accepted in clinical settings, primarily for strength training related rehabilitation treatments. The development of closed-loop NMES can provide new rehabilitation treatments where accurate limb movement is essential.

Contributions of this dissertation result from the development of robust closed-loop NMES controllers that account for uncertainties and nonlinearities in the muscle and activation dynamics. Specifically, this dissertation examines an optimal trade-off between performance and muscle fatigue, the effects of modulating the control input, the effects of time delay in the muscle contraction, and switching controllers during the gait cycle.

In Chapter 2 and 3, inverse and direct optimal NMES controller are designed which consider potential overstimulation by NMES controllers. Muscle fatigue is a multiple-factor problem which affects all aspects of NMES. Overstimulation is an avoidable fact that leads to early onset of muscle fatigue. An optimal control framework

provides practitioners a useful tool to balance between stimulation dosage and tracking performance. Experiments are provided to illustrate the performance.

In Chapter 4, a muscle activation model with a pulse modulated control input is developed to capture the discontinuous nature of muscle activation, and a closed-loop NMES controller is designed for the uncertain pulse muscle activation model. The pulse modulated control input in the model results in an explicit condition that relates performance, pulse magnitude, and pulse frequency. Higher frequency results in more rapid muscle fatigue. Given the important role of modulation frequency in managing muscle fatigue, this contribution illustrates how stimulation frequency can be included in the analysis of the closed-loop controller design, which provides a starting point for designing more frequency efficient NMES controllers. Experiments are provided to illustrate the performance.

In Chapter 5, an identifier based control structure is developed. Muscle force output from electrical stimulation exhibits large time delays from the muscle contraction dynamics. Previous results in literature had to use known (or estimated) model parameters to compensate for the muscle contraction dynamics. By using acceleration feedback uncertain muscle contraction model can be used for closed-loop controller design. The use of limb acceleration is problematic for control implementation due to noise. In this chapter, a closed-loop controller is developed which can be implemented only using position and velocity signals.

In Chapter 6, by combining the approaches in Chapter 4 and Chapter 5, an identification-based controller is developed which includes an uncertain muscle contraction dynamics with pulse modulated control input. The controller is implemented only using position and velocity signals and the pulse modulation effect is included in the analysis. Experiments are provided to illustrate the performance.

Ankle motion is important for maintaining normal gait. For individuals who lost their ability to control the ankle, NMES can be used to help restore normal gait. In Chapter

7, a sliding mode based controller is developed to control ankle motion during gait. Ankle motion is modeled as a hybrid system and a switched sliding mode controller is designed to enable the ankle to track desired trajectories during gait.

CHAPTER 1
INTRODUCTION

1.1 Motivation

An upper motor neuron lesion (UMNL) leads to disability and paralysis, affecting millions of people. UMNL is a condition usually caused by neural disorders such as a stroke, spinal cord injury, multiple sclerosis, cerebral palsy, or traumatic brain injury. The overall reported prevalence is 37,000 people/million/year [1]. Since the lower motor neuron system and muscles are intact in those with an UMNL, muscle contractions can be evoked by directly applying electrical stimulus to the muscles. This technique is widely used for rehabilitation and restoration of motor function and is referred to as functional electrical stimulation (FES), or more generally as neuromuscular electrical stimulation (NMES). Challenges for NMES control design include the nonlinear response from muscle to electrical input, load changing during functional movement, unmodeled disturbances, delayed muscle response, and muscle fatigue.

Open-loop methods, which apply grouped electrical pulses with fixed parameters, are widely used in clinical settings. Closed-loop NMES control is promising based on its ability to achieve accurate limb movement which is essential for functional rehabilitation tasks. Several PID-based linear NMES controllers have been developed [2–6], but these methods are typically based on an assumed linear muscle model or lack a stability analysis. Neural network (NN) based NMES controllers [7–21] have also been developed based on the idea that the universal approximation property of NNs can be used to approximate the nonlinear (unstructured) dynamics. Robust NMES methods have also recently been developed in [13] and [22] that achieve guaranteed asymptotic limb tracking.

Muscle fatigue has been described as a "failure to maintain the required or expected force" from a muscle [23]. The onset of muscle fatigue during electrical stimulation is faster than that during volitional contractions, which hinders the application of

functional and therapeutic NMES. Biological factors such as the reversed recruitment order of motor units, synchronous recruitment of motor units and stimulation settings related to stimulation intensity, frequency, and the grouping of electrical pulses help to explain the possible mechanisms for the rapid onset of muscle fatigue during artificial electrical stimulation [24]. Closed-loop control of muscle has been proven to yield accurate limb positioning, but continuous external stimulation of muscle can lead to rapid fatigue (especially if the controller requires high gains to include robustness to disturbances/uncertainty in the dynamics). Rehabilitative procedures seek to maximize the number of repetitive steps, so muscle fatigue is a critical concern. While various stimulation strategies have been investigated (cf. [25–28]) such as choosing different stimulation patterns and parameters, improving fatigue resistance through muscle retraining, sequential stimulation, and size order recruitment, reducing the onset of fatigue remains a largely open research topic.

Closed-loop control can achieve precise limb tracking despite unpredictable perturbations due to muscle spasms and central neural system (CNS) feedback loops [24]. However, closed-loop methods often need high gain to guarantee performance in the presence of uncertainty, and high-gain feedback can amplify high frequency effects, which lead to muscle fatigue. For different rehabilitation tasks, the practitioner may value limb trajectory accuracy over dosage (i.e. number of repetitions) or vice versa. Motivated by the need to arbitrate between these potentially conflicting objectives, an optimal control method is developed that provides a cost function which can be adjusted to place greater emphasis on accuracy versus dosage for uncertain nonlinear muscle dynamics.

The underlying idea of optimal control is to develop a value function that is the steady state solution to the Hamilton-Jacobi-Bellman equation (HJB), stabilizes a nonlinear system, and guarantees optimality by minimizing a cost functional. Nonlinearities in the system dynamics pose challenges in developing controllers that can guarantee both

stability and optimality, thus inverse optimal control [29, 30] is used to avoid the complexity of solving the steady state HJB equations. Rather than minimizing a given cost functional, inverse optimal control aims to parameterize a family of stabilizing controllers that minimize a meaningful *derived* cost functional. The derived cost functional is meaningful in the sense that it contains a positive function of the state and a positive definite function of the feedback control. The general form of the meaningful cost functional is given as

$$J = \lim_{t \to \infty} \int_0^t l(x) + u(x)^T R(x) u(x) dx,$$

where $l(x)$ is a semi-positive definite and radially unbounded function of the state $x(t)$, $u(x)$ denotes the control input and $R(x)$ is a positive real valued function.

Feedback linearization is an another commonly used technique to achieve optimal control. A quadratic cost functional can be expressed as

$$J = \int_0^\infty \frac{1}{2} x^T Q x + \frac{1}{2} u^T R u \ dt,$$

where $x(t)$ denotes the state, and $u(t)$ denotes the control effort, respectively and Q and R are positive semi-definite and positive definite, respectively. The tradeoff between limb position accuracy and dosage can be achieved by tuning Q and R with guaranteed robustness. These parameters are included in the Hamiltonian of optimization, and the optimal controller is derived by solving the respective Hamilton-Jacobi-Bellman (HJB) equation. For nonlinear dynamic systems, solving the HJB equation can be intractable. Feedback linearization is a commonly used technique to cancel nonlinear elements, leaving a residual linear system where the HJB equation reduces to an Algebraic Riccati Equation (ARE). Combined with adaptive and learning-based approaches, methods have been developed to successfully minimize a cost functional despite uncertainty in a dynamic system [31, 32].

Chapter 2 and 3 examine inverse and direct asymptotic optimal NMES controllers.

NMES is delivered in the form of electrical current pulses which create a localized electric field to elicit action potentials in the nearby neurons. The output of muscle force is determined by the pulse amplitude, duration, frequency, and the muscle fatigue state. Pulse duration and amplitude determine the activation region, i.e., how many motor units are recruited, and are equivalent regarding the total applied electric charge. This effect is often referred to as spatial summation. Each electric pulse causes a twitch in the muscle fibers. If a second pulse is applied before the first twitch finishes, the two twitches sum and a higher force output from the muscle is achieved. This effect is often referred to as temporal summation. When the pulse frequency is higher than a threshold called the fusion frequency, continuous muscle force output is observed. Larger force can be achieved with higher frequencies. However, higher stimulation frequencies cause the muscle to fatigue faster. In practice, muscle force is controlled by modulating the pulse amplitude or pulse duration, and the frequency is set to a constant value that is as low as possible to maintain fused force output while avoiding fatiguing the muscle prematurely [33]. Recent results demonstrated that frequency-modulation can yield better performance for both peak forces and force-time integrals than pulse-duration-modulation, while producing similar levels of muscle fatigue [34]. Since the NMES control input is implemented as a series of pulses, hybrid systems theory provides a mathematical framework to investigate the effect of the discontinuous modulation strategy. Since the modulation strategy has significant impact on the muscle performance and fatigue, the ability to examine the impact of the control signal and modulation strategy in analysis may open new insight into the development of NMES controllers. Chapter 4 investigates the use of a hybrid control method that explicitly accounts for the modulation strategy.

There exists a time delay between the application of electrical stimulation and muscle force output. Muscle contraction dynamics account for the majority of the total time delay in muscle force output. The contraction dynamic time delay is 20ms

14

for fast glycolytic (FG) and 120ms for slow oxidative (SO) fibers [35]; however, since this time delay is related to the contraction dynamics, it varies with the input signal frequency. To account for this delay, some authors have developed controllers for the delay without considering the underlying delay mechanism [36]. Other results seek to compensate for the delay by modeling the underlying delay causing muscle contraction dynamics. In [5] and [37], muscle contraction dynamics were modeled as a first order system with known parameters. The exact parameters of the muscle dynamics are not easy to determine, and these parameters are likely to change over time due to muscle fatigue or muscle strength training. In addition, muscle contraction states are not directly measurable. Acceleration measurements can be used as a substitute as in [5] and [37]. In practice, limb position and velocity are measurable with acceptable noise levels, while acceleration is not directly available and often contaminated with noise. Derivative estimation is challenging. For example, numerical differentiation approaches such as backward differencing are very sensitive to sensor noise. Considerable high frequency noise can be introduced to the acceleration signal. A low pass filter (LPF) can be used to suppress the noise, but the use of a LPF introduces extra phase lag. An identifier/observer approach is shown less sensitive to noise in [38]. Chapter 5 explores the potential to improve the tracking performance and robustness of controllers that include the muscle dynamics in the closed-loop control design without the use of acceleration measurements..

Neurological disorders resulting from an UMNL can have lasting impairments. For example, of the 730,000 individuals who survive a stroke each year, 73% have residual disability [39]. Stroke has significant impact on walking ability resulting in characteristic post stroke gait. Inadequate dorsiflexion during swing phase and decreased plantarflexion force generation during the stance phase are both common impairments of post stroke gait causing foot dragging and slapping, larger metabolic cost on walking, slow walking speed, and gait asymmetry. By delivering pulsed electrical current into affected

15

muscles or nerves, desired muscle contractions can be obtained. FES is commonly used as an effective rehabilitation tool to enable muscle training and gait correction to improve post stoke recovery and achieve daily life independence. Traditionally with the help of foot switches or employing tilt sensors, FES can be delivered to activate ankle dorsiflexor muscles during the swing phase of the gait to correct "foot drop", a common symptom caused by stroke, spinal cord injury and other neurological diseases. However, stimulating ankle dorsiflexor muscles only during the swing phase does not prevent foot slap, decreased swing phase knee flexion, or slow walking speed. Resent research [40, 41] has shown that delivering FES to both the plantarflexor and dorsiflexor muscles during gait can help to correct post stroke gait deficits at multiple joints (ankle and knee) during both the swing and stance phases of gait resulting in improved functional ambulation. These FES treatments are typically applied open-loop and have led to some promising results including some commercial products. However, such approaches offer limited precision and predictability without feedback, and typically over stimulate the muscle potentially leading to a more rapid onset of fatigue.

Previous controllers have been developed (with associate stability analysis) without considering the discrete nature of a walking gait. As described in [42], the ankle motion is continuous during normal gait, but the plantarflexor and dorsiflexor muscles alternate and the moving segment is the foot during initial stance phase and swing phase while the moving segment is the shank from toe strike to toe off. The ankle movement is a continuous evolution of the angle between foot and shank, yet an isolated discrete signal is needed to denote the transition between plantarflexion and dorsiflexion. The transition is important to maintain a continuous ankle motion. The switching property of gait control suggests the need to model and analyze the ankle motion control system using hybrid systems control theory. Generally, coexistence and interaction between continuous dynamics and discrete events (such as switching) in a system result in unique properties that are not inherited from individual subsystems. A well known

16

example can be found in [43] that shows switching between globally exponentially stable subsystems does not guarantee the stability of the hybrid dynamic system. The stability of switched systems depends on the interplay of the dynamics of subsystems and the properties of the switching signals. Chapter 7 address the switching dynamics during gait through the development of a hybrid NMES controller.

1.2   Contribution

In Charter 2, a NN-based inverse optimal NMES controller is developed to enable the lower limb to track a desired trajectory through electrical stimulation of the quadriceps despite uncertainties in the considered muscle activation and limb model. Experimental results for tracking a desired trajectory and a functional experiment (standing) illustrated the performance of the controller. Motivation for this result is a framework that can be used to examine the interplay between the performance and the control authority for rehabilitation clinicians. An inverse optimal method was used to ensure optimality for a derived meaningful cost functional. The framework illustrates that NN controllers augmented by a PD feedback mechanism can minimize a cost functional which can be adjusted (e.g., through Q and R) to place more emphasis on tracking error performance versus the feedback control input. While this work makes a contribution as the first analysis to explore an optimal controller for NMES given a nonlinear uncertain muscle model, the development is limited by the restriction to use a derived cost functional.

In Charter 3, an NMES controller is designed which minimizes a quadratic cost functional while also yielding asymptotic limb position tracking. The controller has the potential to reduce the effect of overstimulation by penalizing the tracking performance and the control input, which provides a framework for clinicians to examine the balance/interplay between performance and control authority. Experiments illustrate tracking performance of the controller and the ability to achieve adjustment between tracking errors and the feedback control through error penalty and control penalty. This

17

work explores the application of an optimal controller which is obtained by feedback linearizing the uncertain nonlinear dynamics through a NN and implicit learning method.

In Chapter 4, for the first time, a muscle contraction model with a pulse modulated control input is developed to capture the discontinuous nature of muscle activation, and a closed-loop NMES controller is designed for the uncertain pulse muscle activation model. Semi-globally uniformly ultimately bounded (SUUB) tracking is guaranteed. The closed-loop system is analyzed through Lyapunov-based methods and a pulse frequency related gain condition is obtained. Simulation results are provided to illustrate the performance of the developed controller. For the first time, this chapter brings together an analysis of the controller and modulation scheme.

In Chapter 5, for the first time, the uncertainties in the muscle contraction dynamics were taken into consideration when compensating for the muscle contraction dynamics. A controller is designed together with an identifier/observer, which could potentially improve the tracking performance and achieve more robust control. Since the muscle contraction state is not measurable, the dynamics are manipulated to remove the dependence on muscle contraction state. By designing a identifier/observer to generate the second order derivative of the estimated position, the controller can be implemented without acceleration measurements. The overall stability of the identifier-controller system is analyzed through Lyapunov methods. Semi-global UUB tracking and estimation are achieved. Simulation results illustrate the controller performance.

In Chapter 6, an acceleration free NMES controller is developed based on an identifier/observer frame work incorporating modulated control inputs with muscle contraction dynamics. The overall stability of the identifier-controller system is analyzed through Lyapunov methods. Semi-global UUB tracking and estimation are achieved. Experiment results illustrate the controller performance.

In Chapter 7, a switched sliding mode based controller is developed to address the challenge that at different phase of the gait, the moving limb segments and the

muscle groups are switching back and forth, ensuring that the ankle asymptoticly tracks a designed or recorded trajectory during gait which can be used for gait retraining. Semi-global asymptotic tracking is obtained for the switched controller during gait, which is analyzed based on multiple Lyapunov functions and the performance is illustrated though simulations.

1.3 Outline

Chapter 1 serves as an introduction. The motivation, problem statement and the contributions of the dissertation are discussed in this chapter.

In Chapters 2 and 3, inverse and direct optimal NMES controllers are developed with guaranteed stability, which address the problem of possible over stimulation by balancing the performance and the control effort, potentially reducing muscle fatigue.

Chapter 4 considers a modulated control input. Using hybrid analysis, an explicit frequency condition is developed.

In Chapter 5, an uncertain muscle contraction model is included in the control design to address the problem of muscle contraction time delay. To mitigate the problem that the limb acceleration is not always available, an identification-based frame is designed to implement an acceleration free NMES controller.

Chapter 6 developed an identification-based acceleration free NMES controller considering a muscle contraction dynamics with a pulse modulated input.

Chapter 7 examines the problem of applying NMES controller to the system of ankle during walking. A hybrid controller is designed to address the challenge of controlling the ankle motion during the gait.

Chapter 8 provides a conclusion and future works.

CHAPTER 2
ADAPTIVE INVERSE OPTIMAL NEUROMUSCULAR ELECTRICAL STIMULATION

Efforts in this chapter focus on the development of an adaptive inverse optimal NMES controller. The controller yields desired limb trajectory tracking while simultaneously minimizing a cost functional that is positive in the error states and stimulation input. The development of this framework allows trade-offs to be made between tracking performance and control effort by putting different penalties on error states and control input depending on the clinical goal or functional task. The controller is examined through a Lyapunov-based analysis. Experiments on able-bodied individuals are provided to demonstrate the functionality and performance of the developed controller.

2.1   Muscle Activation and Limb Model

The dynamics of a free swinging shank when the subject is seated can be segregated into body segmental dynamics and muscle activation and contraction dynamics. The complete dynamic model is given by [5]

$$M_I + M_e + M_g + M_v + \tau_d = \tau. \tag{2--1}$$

In (2–1), $M_I(\ddot{q}) \in \mathbb{R}$ denotes the inertial effects of the shank-foot complex about the knee-joint, $M_e(q) \in \mathbb{R}$ denotes the nonlinear elastic effects due to joint stiffness, $M_g(q) \in \mathbb{R}$ denotes the gravitational component, $M_v(\dot{q}) \in \mathbb{R}$ denotes the nonlinear viscous effects due to damping in the musculotendon complex [44], $\tau_d(t) \in \mathbb{R}$ is considered as an unknown bounded disturbance which represents an unmodeled reflex activation of the muscle (e.g., muscle spasticity) and other unknown unmodeled phenomena (e.g., dynamic fatigue), and $\tau(t) \in \mathbb{R}$ denotes the torque produced at the knee joint, where $q(t), \dot{q}(t), \ddot{q}(t) \in \mathbb{R}$ denote the generalized angular position, velocity, and acceleration of the lower limb about the knee-joint, respectively. The inertial component $M_I(q) \in \mathbb{R}$ is defined as

$$M_I(\ddot{q}(t)) = J\ddot{q}(t). \tag{2--2}$$

The elastic effects are modeled on the empirical findings by Ferrarin and Pedotti in [44] as

$$M_e = -k_1(e^{-k_2 q})(q - k_3),$$ (2–3)

where k_1, k_2, $k_3 \in \mathbb{R}$ are unknown positive coefficients. As shown in [5], the viscous moment $M_v(\dot{q})$ can be modeled as

$$M_v = B_1 \tanh(-B_2 \dot{q}) - B_3 \dot{q},$$ (2–4)

where B_1, B_2, and $B_3 \in \mathbb{R}$ are unknown positive constants. The torque produced at the knee joint can be modeled as

$$\tau(t) = \zeta V(t),$$ (2–5)

where $V(t) \in \mathbb{R}$ is the electrical stimulus applied to the quadriceps muscle group, $\zeta(q, \dot{q}) \in \mathbb{R}$ is a mapping function between the generated knee torque and the applied electrical stimulus on quadriceps. For complete details of the dynamics in (2–1), see [22].

Assumption 1: Based on the results in [45], the nonlinear function $\zeta(q, \dot{q})$ is assumed to be continuously differentiable, positive, and a bounded function.

Assumption 2: The disturbance term $\tau_d(t)$ and its first time derivative are assumed to be bounded. This assumption is reasonable for typical disturbances such as muscle spasticity, fatigue, and load changes during functional tasks.

To facilitate the subsequent analysis, the expression in (2–1) is rewritten as

$$J_\zeta \ddot{q}(t) + M_\zeta + \tau_{d\zeta} = V(t),$$ (2–6)

where $J_\zeta(q, \dot{q})$, $M_\zeta(q, \dot{q})$, $\tau_{d\zeta}(q, \dot{q}) \in \mathbb{R}$ are defined as

$$J_\zeta = \zeta^{-1}J, \ M_\zeta = \zeta^{-1}(M_e + M_g + M_v), \ \tau_{d\zeta} = \zeta^{-1}\tau_d.$$ (2–7)

Based on Assumptions 1 and 2, the following inequalities can be developed

$$\xi_0 \leq |J_\zeta| \leq \xi_1, \ |\tau_{d\zeta}| \leq \xi_2,$$ (2–8)

where ξ_0, ξ_1, $\xi_2 \in \mathbb{R}$ are known positive constants.

2.2 Control Development

A rehabilitative goal of NMES is to elicit a desired muscle response that can lead to restored independent function. For rehabilitative outcomes, repetitive training is essential; yet, electrically stimulated muscle can often fatigue quickly due to overstimulation and various other factors such as synchronous excitation and non-physiological motor unit recruitment order. As an inroad to address these concerns, the control objective is to stimulate the quadriceps muscle group to enable the shank to track a desired time-varying trajectory, denoted by $q_d(t) \in \mathbb{R}$, despite uncertainties in the dynamic model, while also minimizing a given performance index that includes a penalty on the tracking error and the control effort.

To quantify the tracking objective, lower limb angular position tracking error and an auxiliary tracking error denoted by $e(t)$, $r(t) \in \mathbb{R}$, respectively, are defined as

$$e = q_d - q, \quad r = \dot{e} + \alpha e, \tag{2–9}$$

where $\alpha \in \mathbb{R}$ is a positive constant gain.

After taking the time derivative of $r(t)$, multiplying it by $J_\zeta(q, \dot{q})$, and utilizing Equations 2–6 and 2–9 the following open-loop error system can be obtained:

$$J_\zeta \dot{r} = \tau_{d\zeta} + f_1 + f_2 - V, \tag{2–10}$$

where $f_1(t)$, $f_2(t) \in \mathbb{R}$ are defined as

$$f_1 = J_\zeta \alpha \dot{e}, \qquad f_2 = J_\zeta \ddot{q}_d + M_\zeta. \tag{2–11}$$

Based on (2–10) and the subsequent stability analysis (given in Theorem 1), the voltage control input $V(t)$ is designed as

$$V = u_2 - u_1 = \hat{f}_2 - u_1, \tag{2–12}$$

where $u_1(t) \in \mathbb{R}$ is subsequently designed control input, and $u_2(t) = \hat{f}_2(t) \in \mathbb{R}$ is a NN estimate of $f_2(t)$. A three-layer NN can be used to represent f_2 as

$$f_2(y) = W^T \sigma \left(U^T y \right) + \epsilon(y) \tag{2–13}$$

where $U \in \mathbb{R}^{(N_1+1) \times N_2}$ and $W \in \mathbb{R}^{(N_2+1) \times 1}$ are bounded constant ideal weight matrices, $\sigma(\cdot) : \mathbb{R}^{N_1+1} \to \mathbb{R}^{N_2+1}$ is an NN activation function, $y(t) \in \mathbb{R}^{N_1+1}$ is an input vector defined as

$$y(t) = [1 \ q(t) \ \dot{q}(t) \ \ddot{q}_d(t)]^T, \tag{2–14}$$

and $\epsilon(y) : \mathbb{R}^{N_1+1} \to \mathbb{R}$ is a functional reconstruction error that can be upper bounded as

$$|\epsilon(y)| \le \delta, \tag{2–15}$$

where $\delta \in \mathbb{R}$ is a known positive constant. The estimate $\hat{f}_2(t)$ is designed as

$$\hat{f}_2 = \hat{W}^T \sigma \left(\hat{U}^T y \right), \tag{2–16}$$

where, $\hat{U}(t) \in \mathbb{R}^{(N_1+1) \times N_2}$, $\hat{W}(t) \in \mathbb{R}^{(N_2+1) \times 1}$ are weight estimate matrices. The ideal weight matrix estimates $\hat{U}(t)$ and $\hat{W}(t)$ are updated on-line using the projection algorithm

$$\dot{\hat{W}} = proj \left(\Gamma_w \hat{\sigma} r^T \right), \ \dot{\hat{U}} = proj \left(\Gamma_u y \left(\hat{\sigma}'^T \hat{W} r \right)^T \right), \tag{2–17}$$

where $\Gamma_w \in \mathbb{R}^{(N_2+1) \times (N_2+1)}$ and $\Gamma_u \in \mathbb{R}^{(N_1+1) \times (N_1+1)}$ are constant, positive definite, symmetric gain matrices, $\hat{\sigma} = \sigma \left(\hat{U}^T y \right)$, and $\hat{\sigma}' = \sigma' \left(\hat{U}^T y \right) = d\sigma \left(U^T y \right) / d \left(U^T y \right)_{|U^T y = \hat{U}^T y}$.

The weight mismatch errors $\tilde{U}(t) \in \mathbb{R}^{(N_1+1) \times N_2}$ and $\tilde{W}(t) \in \mathbb{R}^{(N_2+1) \times 1}$ are denoted as

$$\tilde{W} = W - \hat{W}, \quad \tilde{U} = U - \hat{U}, \tag{2–18}$$

and the hidden-layer output mismatch $\tilde{\sigma}(y) \in \mathbb{R}^{N_2+1}$ for a given $y(t)$ is defined as

$$\tilde{\sigma} = \sigma - \hat{\sigma} = \sigma \left(U^T y \right) - \sigma \left(\hat{U}^T y \right). \tag{2–19}$$

By using a Taylor Series approximation, the hidden-layer output mismatch $\tilde{\sigma}(y)$ can be expressed as

$$\tilde{\sigma} = \hat{\sigma}'\tilde{U}^T y + O\left(\tilde{U}^T y\right)^2, \tag{2–20}$$

where $O\left(\tilde{U}^T y\right)^2$ denotes the higher order terms.

Substituting (2–12) into (2–10) and performing some algebraic manipulation yields

$$J_\zeta \dot{r} = N + \tilde{W}^T \hat{\sigma} + \hat{W}^T \hat{\sigma}' \tilde{U}^T y + u_1, \tag{2–21}$$

where the auxiliary term $N\left(\tilde{W}, \tilde{U}, y\right) \in \mathbb{R}$ is defined as

$$N = f_1 + \tilde{W}^T \hat{\sigma}' \tilde{U}^T y + W^T O\left(\tilde{U}^T y\right)^2 + \epsilon(y) + \tau_{d\zeta}. \tag{2–22}$$

Based on Equations 2–8, 2–15, and 2–17 $N\left(\tilde{W}, \tilde{U}, y\right)$ can be upper bounded as [46]

$$\|N\| \le c_1 + c_2 \|z\|, \tag{2–23}$$

where $c_1, c_2 \in \mathbb{R}$ are known positive constants, and $z(t) \in \mathbb{R}^2$ is defined as

$$z(t) = [e \quad r]^T. \tag{2–24}$$

Based on (2–10) and the subsequent stability analysis, the stabilizing PD controller u_1 in (2–21) is designed as

$$u_1 = -R^{-1}r = -(k_{s_1} + k_{s_2} + k_{s_3})r, \tag{2–25}$$

where $R^{-1}, k_{s_1}, k_{s_2}, k_{s_3} \in \mathbb{R}$ denote positive adjustable gains.

From Assumption 1, Equations 2–10−2–12 and 2–25, it can be shown that

$$\frac{1}{2}\left|\dot{J}_\zeta\right| \le \rho(\|z\|), \tag{2–26}$$

where $\rho(\|z\|) \in \mathbb{R}$ is a positive, global invertible function.

2.3 Stability Analysis

Theorem 2.1. *The controller given in (2–12), (2–16), and (2–25) ensures that all closed-loop signals are bounded, and the position tracking error is semi-global uniformly*

ultimately bounded (SUUB) in the sense that

$$|e(t)| \leq \epsilon_0 \exp(-\epsilon_1 t) + \epsilon_2, \tag{2-27}$$

where ϵ_0, ϵ_1, $\epsilon_2 \in \mathbb{R}$ denote positive constants in $\mathcal{D} \triangleq \{ z \subset \mathbb{R}^2 \mid \|z\| \leq \rho^{-1}\left(\sqrt{k_{s_3}}\right)) \}$, provided the control gains α, and k_{s_2} introduced in (2–9) and (2–25) are selected based on the sufficient conditions

$$\min(k_{s_2} - \frac{1}{2}, \alpha - \frac{1}{2}) > c_2, \quad k_{s_2}, \alpha > \frac{1}{2}. \tag{2-28}$$

Proof. Consider a positive definite, continuously differentiable, and radially unbounded function $V_L\left(e, r, \tilde{W}, \tilde{U}\right) \in \mathbb{R}$ defined as

$$V_L = \frac{1}{2}e^2 + \frac{1}{2}J_\zeta r^2 + \frac{1}{2}tr\left(\tilde{W}^T \Gamma_w^{-1} \tilde{W}\right) + \frac{1}{2}tr\left(\tilde{U}^T \Gamma_u^{-1} \tilde{U}\right). \tag{2-29}$$

By using (2–8) and typical NN properties [47], $V_L(t)$ can be upper and lower bounded as

$$\gamma_1 \|z\|^2 \leq V_L \leq \gamma_2 \|z\|^2 + \gamma_3, \tag{2-30}$$

where γ_1, γ_2, $\gamma_3 \in \mathbb{R}$ are known positive constants. Taking the time derivative of (2–29), utilizing (2–17) and (2–21), and canceling common terms yields

$$\dot{V}_L = e\dot{e} + \frac{1}{2}\dot{J}_\zeta r^2 + rN + ru_1. \tag{2-31}$$

Using (2–9) and Young's inequality, the expression in (2–31) can be bounded as

$$\dot{V}_L \leq -\left(\alpha - \frac{1}{2}\right)e^2 + r^2\left(\frac{1}{2}\dot{J}_\zeta + \frac{1}{2}\right) + rN + ru_1. \tag{2-32}$$

By utilizing (2–23), (2–25), and (2–26), the expression in (2–32) can be upper bounded as

$$\dot{V}_L \leq -\left(\alpha - \frac{1}{2}\right)e^2 - \left(k_{s_2} - \frac{1}{2}\right)r^2 \tag{2-33}$$

$$- \left(k_{s_1}r^2 - c_1|r|\right) + c_2\|z\|^2 - \left(k_{s_3} - \rho(\|z\|)\right)r^2.$$

Applying nonlinear damping and neglecting negative terms, the expression in (2–33) can be upper bounded as

$$\dot{V}_L \le -\gamma_4 \|z\|^2 + \frac{c_1^2}{4k_{s_1}}, \forall \|z\| \in \mathcal{D}, \tag{2–34}$$

and $\gamma_4 = \min(k_{s_2} - \frac{1}{2}, \alpha - \frac{1}{2}) - c_2 > 0$ provided the sufficient gain conditions in (2–28) are satisfied. The inequality in (2–30) can be used to rewrite (2–34) as

$$\dot{V}_L \le -\frac{\gamma_4}{\gamma_2} V_L + \varepsilon, \forall \|z\| \in \mathcal{D}, \tag{2–35}$$

where $\varepsilon \in \mathbb{R}$ is a positive constant. The linear differential inequality in (2–35) can be solved as

$$V_L(t) \le V_L(0) e^{-\frac{\gamma_4}{\gamma_2}t} + \varepsilon \frac{\gamma_2}{\gamma_4} \left[1 - e^{-\frac{\gamma_4}{\gamma_2}t} \right], \forall \|z\| \in \mathcal{D}. \tag{2–36}$$

Provided the sufficient conditions given in (2–28) are satisfied, the expressions in (2–29) and (2–36) can be used to prove the control input and all the closed-loop signals are bounded in $\mathcal{D}$. Larger value of k_{s_3} and k_{s_1} will expand the size of the domain $\mathcal{D}$ to include any initial conditions (i.e., a semi-global type of stability result) and reduce the residual error. From (2–29) and (2–36), the result in (2–27) can be obtained. □

2.4 Cost Functional Minimization

An inverse optimal controller [29, 48, 49] is optimal with respect to an *a posteriori* cost functional that is derived from a Lyapunov-based analysis (in comparison to minimizing an *a priori* given cost functional in direct optimal control). Due to the use of a NN to compensate for the unstructured uncertainty in the muscle model, a residual disturbance is present in the system (i.e., the UUB stability result). Given this residual disturbance, the following analysis is formulated in the spirit of a two player zero-sum differential game where the objective is to minimize the cost functional with respect the control input in the presence of the maximum "worst-case" disturbance. The feedforward NN element estimates the non-LP dynamics, while the feedback element is penalized by the cost functional.

Theorem 2.2. *The feedback law given by*

$$u_o^* = -\beta R^{-1} r, \tag{2–37}$$

with the scalar gain constant selected as $\beta > 2$ and the update law given in (2–17),
minimizes the cost functional

$$J = \lim_{t \to \infty} \left\{ 2\beta V_L(t) + \int_0^t \left[l + u_1^2 R \right] - 2\beta \frac{c_1^2}{4k_{s_1}} d\sigma \right\}, \tag{2–38}$$

where $l(z, t) \in \mathbb{R}$ is a positive function of the tracking error

$$l = -2\beta \left(e\dot{e} + \frac{1}{2} \dot{J}_\zeta r^2 + rf_1 + rN - \frac{c_1^2}{4k_{s_1}} \right) + \beta^2 r^2 R^{-1}, \tag{2–39}$$

provided the sufficient conditions in (2–28) are satisfied.

The cost functional in (2–38) is said to be meaningful if the bracketed terms in (2–39) are positive (i.e., positive state and control functions). To examine the sign of $l(z, t)$, the expressions in (2–25), (2–31), (2–34) and the condition in (2–28) can be used to determine that

$$e\dot{e} + \frac{1}{2} \dot{J}_\zeta r^2 + rf_1 + rN - \frac{c_1^2}{4k_{s_1}} - r^2 R^{-1} \leq 0. \tag{2–40}$$

After multiplying both sides by -2β and adding $\beta(\beta - 2)r^2 R^{-1}$, the expression in (2–40) can be rewritten as

$$l \geq \beta(\beta - 2)r^2 R^{-1} = Qr^2, \tag{2–41}$$

where $Q \in \mathbb{R}$ is a positive constant. The inequality in (2–41) indicates that $l(z, t)$ is positive since R is positive and $\beta > 2$. Therefore $J(t)$ is a meaningful cost functional that penalizes the error function in $z(t)$ and the feedback control $u_1(t)$. The cost functional in (2–38) and the result in (2–41) indicates that larger values of Q place a greater penalty on the tracking error, whereas larger values of R place a greater penalty on the feedback control. The effects of selecting different values for Q and R are illustrated in Section 2.5.

To show that u_o^* minimizes $J(t)$, the auxiliary signal $v(t) \in \mathbb{R}$ is defined as

$$v = u_1 + \beta R^{-1} r. \tag{2–42}$$

Substituting (2–39) and (2–42) into (2–38) and performing some algebraic manipulation yields

$$J = \lim_{t \to \infty} \left\{ 2\beta V_L(t) + \int_0^t v^2 R \, d\sigma - 2\beta \int_0^t \dot{V}_L d\sigma \right\}. \tag{2–43}$$

After integrating (2–43), the cost functional $J(t)$ can be expressed as

$$J = 2\beta V_L(0) + \lim_{t \to \infty} \left\{ \int_0^t v^2 R \, d\sigma \right\}. \tag{2–44}$$

By substituting (2–37) into (2–31), it can be shown that u_o^* stabilizes the system. Since $J(t)$ is minimized if $v(t) = 0$, then control law $u_1 = u_o^*$ is optimal with respect to the meaningful cost functional in (2–38).

2.5 Experiment Results

The proposed inverse optimal controller was implemented on healthy normal volunteers to evaluate the performance of the controller. The focus of this paper is to develop and analyze an inverse optimal controller as a means to provide a method for understanding the tradeoff of the control parameters Q and R that are included in a cost functional composed of terms such as the limb tracking error and stimulation input. This section describes the performance of the developed strategy when implemented on a group of healthy normal volunteers. The performance of the developed method may vary when implemented in populations of individuals affected with different neurological disorders: clinical trials on specific affected populations of interest are motivated as future work to further the clinical implications of the following outcomes. The results obtained from healthy normal subjects in this section may provide some insight into further clinical trials. For example, in [50] (and in results such as [10, 17, 51] which directly or indirectly cite the work in [50]) a relaxed limb is shown to behave like a recently paralyzed limb. However, there are differences in the muscle response that

are associated with different conditions. For example, a limb that has been paralyzed for some time will exhibit muscle atrophy with disuse, will fatigue more rapidly, and may exhibit clonus and muscle spasticity [51]. The inverse optimal controller has been developed and analyzed while including added unmodeled disturbances (i.e., $\tau_d(t)$), the aforementioned effects for paralyzed muscle are not present in the healthy normal volunteer subjects. Able-bodied volunteers can potentially execute unintentional muscle contractions (which may also be captured by $\tau_d(t)$) that can aid or hinder the desired limb motion. To mitigate this potential, volunteers were instructed to relax and to allow the stimulation to control the limb motion (i.e., the subjects were not supposed to influence the leg motion voluntarily and were not allowed to observe the desired limb trajectory).

The study volunteers were seated in a non-motorized leg extension machine (LEM). The free swinging legs of the volunteer were attached to the movable arm of the LEM where the position of the LEM arm is measured by an optical encoder and used as a feedback signal. Adjustments were made before each trial to ensure the centers of the knee and the encoder were aligned. A 4.5 kg (10lb.) weight was attached on the weight bar of the LEM arm, and a mechanical stop was used to prevent hyperextension. Self-adhesive reusable neuromuscular stimulation electrodes were used in the experiments. One electrode was placed over the distal-medial portion of the quadriceps femoris muscle groups and the other was placed over the proximal-lateral portion. Electrical pulses were delivered through a custom built stimulator. Data acquisition was performed at 1000 Hz and two digital-to-analog signals were used as inputs to the stimulation circuitry that produces a positive square pulse between 3-100 Hz with a voltage output between 1-50 volts peak.

The modulated pulse width was set to a constant $400\,\mu\sec$ and the frequency of the pulse sequence was 28 Hz. The motivation for choosing a $400\,\mu\sec$ pulse is due to the fact that it generates reliable output based on its force-frequency and force-amplitude

relationship relative to other pulse widths. The stimulation frequency was selected based on force-frequency curves [52], which show that as stimulation frequency is increased muscle force increases to a saturation limit. Higher frequencies can be chosen to generate more force up to a saturation limit but muscles tend to fatigue faster at higher frequencies. The 28 Hz pulse wave yields reduced fatigue in comparison to higher frequencies but lower frequencies tend to produce rippled knee motion [52, 53].

2.5.1 Tracking Experiments

Tracking experiments were conducted on five volunteers (two females and three males, ages $22-40$ yrs.). The desired angular trajectory for the knee joint was

$$q_d = \begin{cases} \frac{35}{2}(1 + \sin(\frac{2\pi}{T}t + \frac{3}{2}\pi)), & t < \frac{T}{2}, \\ 15(1 + \sin(\frac{2\pi}{T}t + \frac{3}{2}\pi)) + 5, & t \geq \frac{T}{2}, \end{cases} \tag{2-45}$$

with a frequency of 1.5Hz and range of motion (ROM) between 5° and 35°. The reason to select this trajectory is the sinusoidal functions are sufficient smooth and easy to implemented. The values were selected to approximate the frequency and ROM of the lower limb during walking. Any sufficiently smooth desired trajectory could have been selected. For the tracking experiments, Q and R are adjusted by trial and error for each individual to yield the best performance. Each individual was stimulated for 5 to 10 trials with a minimum rest of 5 minutes between trials. Each trial was 30s. The steady state Root Mean Square (RMS) and Peak (i.e., $max|e(t)|$) tracking error is calculated from 3s to 30s. Table 1 summarizes the RMS and Peak errors for given Q and R gains. Figure 2-1 illustrates a typical knee/limb tracking error. The Q and R gains were adjusted to obtain the results in Table 1. The mean steady state RMS is $1.92°$ with a standard deviation (STD) of $0.18°$, and the mean Peak error is $6.57°$ with a STD of $1.29°$.

Unit step tests were conducted on three volunteers (one females and two males, ages 25-40 yrs.). The results are summarized in Table 2. A representative trial is shown in Fig. 2-2.

Table 2-1. Steady-state root mean square (RMS) and peak error for five healthy normal individuals

Subject	Peak	RMS	Peak(3-30s)	RMS(3-30s)	Q	R
A	9.67°	2.34°	8.91°	2.10°	44.9	2000
B	6.14°	1.89°	5.06°	1.81°	79.8	2000
B	9.69°	2.20°	6.07°	1.59°	19.9	2000
C	15.47°	3.37°	7.18°	2.13°	9.73	2000
D	13.72°	3.07°	6.88°	1.98°	19.9	2000
E	8.47°	2.31°	5.34°	1.91°	499.5	2000
Mean	10.53°	2.54°	6.57°	1.92°		
STD	3.45°	0.59°	1.41°	0.20°		
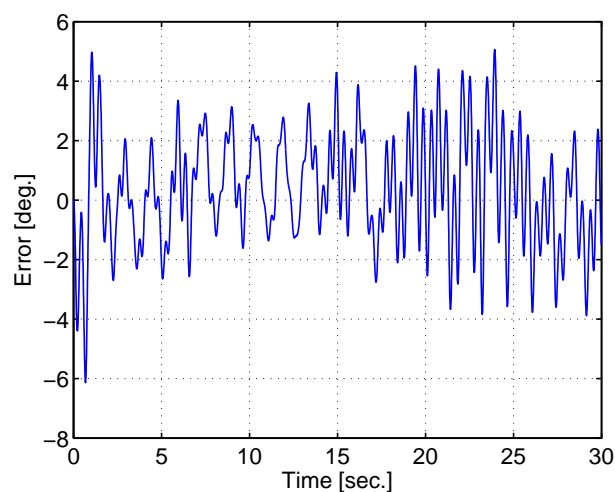
Figure 2-1. Tracking error for a representative trial

2.5.2 Performance Trade-offs

To demonstrate the ability for a clinician to choose different combinations of Q and R to place a greater emphasis on tracking performance or feedback control input, tracking experiments were conducted on three healthy normal volunteers (ages $25-40$ yrs). Two groups of experiments were conducted with fixed NN update gains. The first experiments fixed $Q = 1$ and varied R from 8 to 10000 to illustrate the effect of penalizing the control input. Additional experiments varied Q between 8 to 600 for a fixed $R = 2000$ to show the effect of penalizing the performance. Each session was 20s, and RMS values were calculated for the error, total control input, and optimal control input (i.e. $u_1(t)$), respectively. Figure 2-3 illustrates that the feedback control input decreases
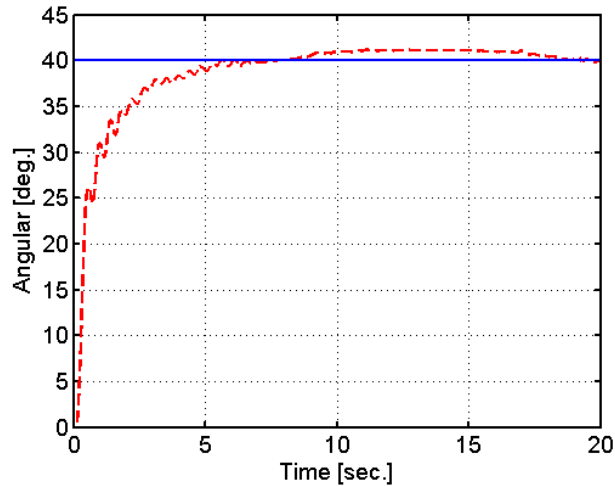
Figure 2-2. Step test for a representative trial. The solid line depicts the desired angle and the dotted line depicts the actual trajectory

and the tracking error increases by increasing R. Figure 2-4 illustrates that the error decreases and the feedback control input increases with increasing Q. The results in Figure 2-3 and Figure 2-4 represent the outcome for one volunteer, but the results showed the same trends for the other two subjects with different adjustable ranges.

2.5.3 Changing Gravity Load

To illustrate that the proposed inverse optimal controller can be used for a task which involves a changing load (i.e. the moment arm of gravity force changes), a sit-to-stand transition-like experiment was conducted on a 38 year old healthy normal male. Note that a physiological sit-to-stand transaction involves a mixed eccentric-concentric contraction of the muscles due to the biarticular nature of the quadriceps group. For this experiment, the electrodes were placed on one leg, and the volunteer was seated on the edge of a chair. The knee joint angle was measured by a goniometer (Biometrics Ltd.,VA), where the goniometer measured $90°$ in the seated position and approximately 180° in the standing position. Given the large initial condition of error (i.e., $90°$) an experimentally determined desired "rise to standing" trajectory was designed as $q_d = 135 + 45\sin(\frac{2\pi}{5}t + \frac{3}{2}\pi)$, if $t < \frac{5}{2}$ and $180°$ if $t \geq \frac{5}{2}$. Fig. 2-5, depicts the actual versus desired trajectory for the standing experiment. The maximum positive and negative

Table 2-2. The step test for a representative trial

Subject	Leg	Final Value	Rising Time	Setting Time	RMS
A	left	20°	3.25	3.46	0.40°
B	left	20°	0.31	0.46	0.54°
C	left	20°	3.66	3.91	0.49°
Mean			2.41	2.61	0.48°
A	left	40°	2.55	2.80	1.31°
B	left	40°	2.31	2.54	1.10°
C	left	40°	1.43	1.62	1.72°
Mean			2.32		1.38°
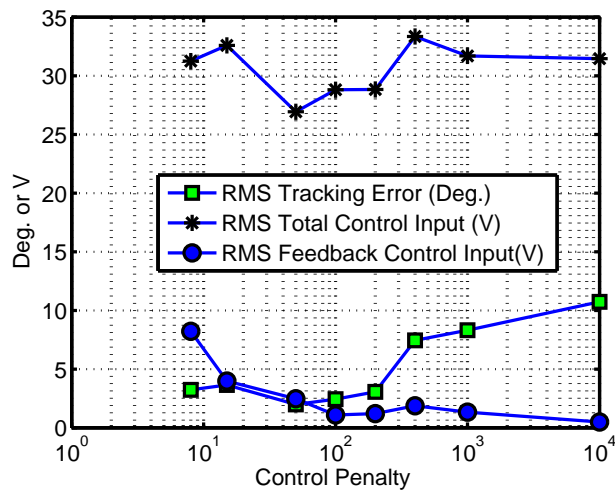
Figure 2-3. Experiments with $Q = 1$ where R varied from 8 to 10000
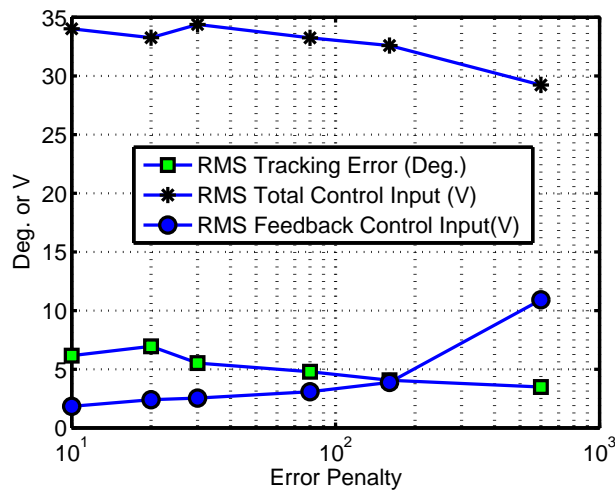
Figure 2-4. Experiments where Q varied from 10 to 600 and $R = 2000$

transient errors are $+6.0°$ and $-5.3°$, respectively. The steady state error is $-0.63 \pm 0.17°$ with a maximum stimulation voltage of 30 volts.
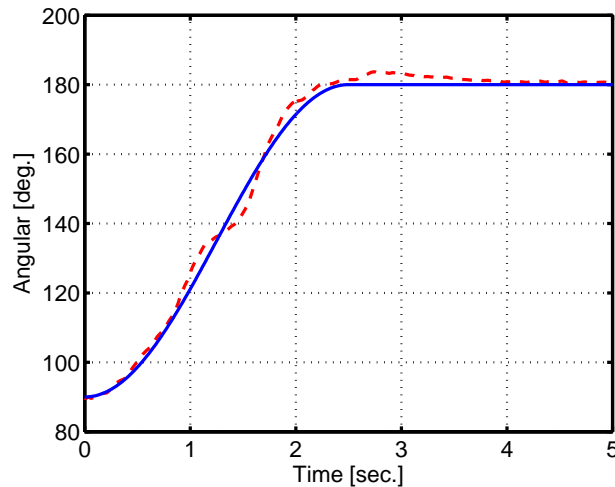
Figure 2-5. Trajectories of the standing experiment. The solid line depicts the desired trajectory and the dashed line depicts the actual trajectory

2.6   Discussion

A NN-based inverse optimal controller is proposed and evaluated. The controller is proven to achieve uniformly ultimately bounded tracking in the presence of bounded unmodeled disturbances. The structure of the controller is organized as a combination of a NN feedforward and a PD feedback element. The NN element compensates for the nonlinear uncertainties present in the dynamics such as passive constraints on joint movement and muscle stimulation which include nonlinear recruitment, torque-angle, torque-velocity scaling, etc. A cost functional is constructed to allow gains to be adjusted to scale the relative penalty of the tracking error or the feedback control portion of the control. As indicated in Table 1, a mean RMS error of 1.92°±0.2° (for 3-30 seconds) was achieved for the given desired trajectory. The sit-to-stand transition-like experiment shows that the controller also yields promising results where the maximum positive and negative transient errors are +6.0° and -5.3°, respectively, with a steady state error within -0.63°±0.17°. The control accuracy from these experiments is sufficient for typical functional tasks. In addition to developing a controller (and associated stability

34

proof) that can yield desired tracking error performance, a contribution of this effort is to develop a framework to adjust the performance versus control effort. The trade-off between tracking performance and feedback control effort can be achieved by choosing different values of Q and R. Larger values of Q yield better tracking performance at the expense of a larger feedback control effort while larger values of R yield reduced feedback control effort with larger tracking errors. As illustrated in Figure 2-3, with Q=1, increasing R from 8 to 10000 results in a reduction of the RMS feedback control input from 8.2 volts to 0.5 volts. Figure 2-4 illustrates that with R=2000, increasing Q from 20 to 600 reduces the RMS tracking error from 7° to 3.5°. Additional development remains to examine the effects on fatigue of increased control input. Moreover, the current development is not able to include the entire control input in the cost functional (i.e., only the feedback portion of the controller is included). The results validate the ability to directly alter the feedback control through R, but the results do not show a correlation between changes in the feedback portion versus changes in the overall control (i.e., the overall control output was relatively invariant to changes in R). This can be explained by the NN feedforward component compensating for the differences. However, heuristically, it is well accepted that larger feedback gains result in noise amplification and higher frequency control. It is also well accepted that higher frequency stimulation can lead to more rapid fatigue. These results point to the need for further studies in future work to investigate the relationship between fatigue as a function of feedback control versus feedforward control. From a theoretical perspective, the approach in [54] provides an inroad to developing an inverse optimal controller that includes a portion of the feedforward component in the cost functional for the parametric strict-feedback systems.

Able-bodies individuals are a heterogeneous group due to muscle size, strength and fatigability varying greatly which is seen in the experiment group. The results reflect the robustness of the controller that the controller is bale to account for individual differences in response to electrical stimulation. The response of muscles to electrical

35

stimulation could be different between able-bodied individuals and individuals with various disorders. For example, a person with SCI that occurred prior to a few weeks has muscles that are atrophied, experience more rapid fatigue, and are potentially subject to disturbances such as spasticity and clonus. The muscle atrophy and rapid fatigue can be improved through muscle re-conditioning using electrical stimulation. The experimental population used in this study produces a proof-of-concept that the controller works to regulate electrically stimulated limb tracking, but the results should not be extrapolated to the potential performance of the system in individuals who have disorders without clinical trials in such application.

CHAPTER 3
ASYMPTOTIC OPTIMAL NEUROMUSCULAR ELECTRICAL STIMULATION

Muscle fatigue during electrical stimulation onsets early and is comparatively more substantial than during volitional contractions, hindering successful application of FES/NMES. One of the avoidable causes of muscle fatigue can be attributed to the overstimulation during NMES. In this chapter, a NMES controller is developed to minimize a quadratic cost functional to balance asymptotic trajectory tracking performance and control effort, potentially reducing overstimulation of the muscle. A Lyapunov-based analysis is used to prove the asymptotic convergence of closed-loop tracking error and asymptotic minimization of the given cost functional. Experiments on health normal individuals are provided to further validate the performance of the developed controller.

3.1 Control Objective

Trajectory tracking is an essential task in many rehabilitative exercises and function restoration tasks. Therefore, the control objective is to ensure the knee angle $q(t)$ tracks a desired trajectory, denoted by $q_d(t) \in \mathbb{R}$. The following development is based on the assumption that $q(t)$ and $\dot{q}(t)$ are measurable. The desired trajectory can be any continuous signal (or a simple constant setpoint).

To quantify the tracking objective, a lower limb angular position tracking error, denoted by $e_1(t) \in \mathbb{R}$, is defined as

$$e_1 \triangleq q_d - q, \tag{3--1}$$

where $q_d(t)$ is an a priori trajectory, designed such that $q_d(t)$, $q_d^i(t) \in \mathcal{L}_\infty$, where $q_d^i(t)$ denotes the ith derivative for $i = 1, 2, 3, 4$. To facilitate the subsequent control design and stability analysis, filtered tracking errors denoted by $e_2(t)$, $r(t) \in \mathbb{R}$ are also defined as

$$e_2 = \dot{e}_1 + \alpha_1 e_1, \tag{3--2}$$

$$r = \dot{e}_2 + \alpha_2 e_2, \tag{3--3}$$

where α_1, $\alpha_2 \in \mathbb{R}$ are positive constant gains. The filtered tracking error $r(t)$ is not measurable since the expression in (3–3) depends on $\ddot{q}(t)$.

3.2 Feedback Linearizing Optimal Control Design

To motivate the control development for the uncertain muscle dynamics, the development in this section assumes that all the system parameters and disturbance are known (this assumption is relaxed in the next section). A controller is developed that minimizes a quadratic cost functional which penalizes the states and control input.

Multiplying the time derivative of (3–2) by $J_\zeta(q)$ and using (2–6) and (3–1), yields

$$J_\zeta \dot{e}_2 = -\frac{1}{2} \dot{J}_\zeta e_2 + h + \tau_{d\zeta} - V, \tag{3–4}$$

where the function $h(q, \dot{q}, \dot{q}_d, \ddot{q}_d) \in \mathbb{R}$ is defined as

$$h = \frac{1}{2} \dot{J}_\zeta e_2 + J_\zeta \alpha_1 \dot{e}_1 + J_\zeta \ddot{q}_d + M_\zeta. \tag{3–5}$$

The (unmodulated) voltage applied to the muscle is designed as

$$V = h + \tau_{d\zeta} - u, \tag{3–6}$$

to yield the feedback linearized dynamics

$$J_\zeta \dot{e}_2 = -\frac{1}{2} \dot{J}_\zeta e_2 + u, \tag{3–7}$$

where $u(t) \in \mathbb{R}$ is an auxiliary control input that will be designed to minimize the given cost functional $J(z, u) \in \mathbb{R}$ defined as

$$J = \int_0^\infty \frac{1}{2} z^T Q z + \frac{1}{2} R u^2 \, dt, \tag{3–8}$$

where $z(t) \in \mathbb{R}^2$ is

$$z = \begin{bmatrix} e_1 & e_2 \end{bmatrix}^T, \tag{3–9}$$

$Q \in \mathbb{R}^{2 \times 2}$ is a positive semi-definite symmetric constant matrix and $R \in \mathbb{R}$ is a positive gain to weight the influence of the states and (partial) control effort, respectively. The resulting optimal control voltage input, denoted by $V^*(t)$, for the feedback linearized system is

$$V^* = h + \tau_{d\zeta} - u^*, \tag{3–10}$$

where the optimal value of $u(t) = u^*(t)$ is designed as

$$u^*(t) = -R^{-1} e_2 \tag{3–11}$$

to minimize (3–8) with respect to the differential constraints in (3–2) and (3–7).

The expression in Equations 3–2 and 3–7 can be rewritten in state space form as

$$\dot{z} = A(q, \dot{q}) z + B(q, \dot{q}) u, \tag{3–12}$$

where $A(q, \dot{q}) \in \mathbb{R}^{2 \times 2}$ and $B(q, \dot{q}) \in \mathbb{R}^{2 \times 1}$ are

$$A = \begin{bmatrix} -\alpha_1 & 1 \\ 0 & -\frac{1}{2} J_\zeta^{-1} \dot{J}_\zeta \end{bmatrix}, \quad B = \begin{bmatrix} 0 \\ J_\zeta^{-1} \end{bmatrix}. \tag{3–13}$$

The optimal control law $u^*(t)$ minimizes (3–8) subject to (3–12) if and only if there exists a value function $V_o(z, t)$ where

$$-\frac{\partial V_o}{\partial t} = \frac{1}{2} z^T Q z + \frac{1}{2} u^{*T} R u^* + \frac{\partial V_o}{\partial z} \dot{z}, \tag{3–14}$$

satisfies the HJB equation

$$\frac{\partial V_o}{\partial t} + \min_u \left[H \left(z, u, \frac{\partial V_o}{\partial t}, t \right) \right] = 0, \tag{3–15}$$

where the Hamiltonian of optimization $H \left(z, u, \frac{\partial V_o}{\partial t}, t \right) \in \mathbb{R}$ is defined as

$$H = \frac{1}{2} z^T Q z + \frac{1}{2} u^T R u + \frac{\partial V_o}{\partial z} \dot{z}. \tag{3–16}$$

The minimum of (3–8) is obtained for the optimal controller $u(t) = u^*(t)$, where the respective Hamiltonian is

$$H^* = \min_u \left[H\left(z, u, \frac{\partial V_o}{\partial t}, t \right) \right] = -\frac{\partial V_o}{\partial t}. \qquad (3\text{–}17)$$

To facilitate the subsequent development, let $P(q, \dot{q}) \in \mathbb{R}^{2\times 2}$ be defined as

$$P = \begin{bmatrix} K & 0 \\ 0 & J_\varsigma \end{bmatrix}, \qquad (3\text{–}18)$$

where $K \in \mathbb{R}$ is a positive constant gain, and let Q in (3–8) be partitioned as

$$Q = \begin{bmatrix} Q_{11} & Q_{12} \\ Q_{12} & Q_{22} \end{bmatrix}. \qquad (3\text{–}19)$$

If α_1, R, and K introduced in (3–1), (3–8), and (3–18), satisfy the following algebraic relationships

$$K = -Q_{12} > 0, \qquad (3\text{–}20)$$

$$Q_{11} = 2\alpha_1 K,$$

$$R^{-1} = Q_{22},$$

and then $P(q)$ satisfies the differential Riccati equation

$$PA + A^T P^T - PBR^{-1}B^T P + \dot{P} + Q = 0,$$

and the value function $V_o(z, t) \in \mathbb{R}$

$$V_o = \frac{1}{2} z^T P z, \qquad (3\text{–}21)$$

satisfies the HJB equation in (3–17). Lemma 1 of [55] can be used to conclude that the optimal control $u^*(t)$ that minimizes (3–8) subject to (3–12) is

$$u^* = -R^{-1} B^T \left(\frac{\partial V_o(z, t)}{\partial z} \right)^T = -R^{-1} e_2. \qquad (3\text{–}22)$$

So the feedback linearizing optimal control voltage input is given by (3–10).

To associate the error penalty with controller gains, using (3–2), (3–9), (3–19) and (3–20), $z^T(t) Qz(t) \in \mathbb{R}$ can be developed as

$$z^T Qz = 2\alpha_1 K e_1^2 - 2K e_1 e_2 + R^{-1} e_2^2. \tag{3–23}$$

3.3 Adaptive Control Design

In the previous section, $h(q, \dot{q}, \dot{q}_d, \ddot{q}_d)$ and $\tau_{d\zeta}(q, t)$ are assumed to be known to develop the optimal controller u^* for the residual dynamics in (3–7). The assumption of known dynamics is relaxed by using an adaptive controller that combines the universal approximation property of NNs with the implicit learning characteristics of RISE feedback to asymptotically converge to V^*.

Multiplying (3–3) by $J_\zeta(q)$ and using (3–4) yields

$$J_\zeta r = \bar{h} + f_d + \tau_{d\zeta} - V, \tag{3–24}$$

where $f_d(q_d, \dot{q}_d, \ddot{q}_d)$, $\bar{h}(q, \dot{q}, q_d, \dot{q}_d, \ddot{q}_d) \in \mathbb{R}$ are defined as

$$f_d = J_\zeta(q_d)\ddot{q}_d + M_\zeta(q_d, \dot{q}_d), \tag{3–25}$$

$$\bar{h} = \alpha_2 J_\zeta e_2 + J_\zeta \alpha_1 \dot{e}_1 + J_\zeta \ddot{q}_d + M_\zeta - f_d. \tag{3–26}$$

The NN estimate $\hat{f}_d(t) \in \mathbb{R}$ is denoted as

$$\hat{f}_d = \hat{W}^T \sigma\left(\hat{U}^T x_d\right), \tag{3–27}$$

where $\hat{U}(t) \in \mathbb{R}^{(N_1+1) \times N_2}$, $\hat{W}(t) \in \mathbb{R}^{(N_2+1) \times 1}$ are weight estimate matrices for the ideal weights between the first-to-second and the second-to-third layers of a NN, respectively. The input vector $x_d(t) \in \mathbb{R}^4$ is defined as

$$x_d(t) = [1 \; q_d, \dot{q}_d, \ddot{q}_d]^T. \tag{3–28}$$

Based on (3–24) and the subsequent stability analysis, the controller in (3–10) is redesigned as

$$V = \hat{f}_d + \mu - u^*, \tag{3–29}$$

which consists of optimal control $u^*(t)$ given in (3–11), where $\hat{f}_d(t)$ is designed in (3–27), and the RISE feedback $\mu(t)$ is defined as

$$\mu = k_s e_2(t) - k_s e_2(0) + \nu, \tag{3–30}$$

where $\nu(e_2(t)) \in \mathbb{R}$ is the solution to the generalized equation

$$\dot{\nu} = k_s \alpha_2 e_2 + \beta sgn(e_2), \tag{3–31}$$

where $k_s, \beta \in \mathbb{R}$ are positive control gains. Using Filippov's theory of differential inclusions [56–59], the existence of solutions can be established for $\dot{\nu} \in K[h_1](e_2, t)$, where $h_1(e_2, t) \in \mathbb{R}$ is defined as the right-hand side of $\dot{\nu}$ in (3–31) and $K[h_1] \triangleq \bigcap_{\delta > 0} \bigcap_{\mu S_m = 0} \overline{co} h_1(B(\nu, \delta) - S_m)$, where $\bigcap_{\mu S_m = 0}$ denotes the intersection over all sets S_m of Lebesgue measure zero, $\overline{co}$ denotes convex closure, and $B(\nu, \delta) = \{\varsigma \in \mathbb{R} | \|\nu - \varsigma\| < \delta\}$ [60, 61]. The differential equation given in (3–31) is continuous except for the Lebesgue measure zero set when $e_2(e_1, \dot{e}_1, t) = 0$.

A multi-layer NN is used to express $f_d(q_d, \dot{q}_d, \ddot{q}_d)$ as

$$f_d = W^T \sigma(U^T x_d) + \epsilon(x_d), \tag{3–32}$$

where $U \in \mathbb{R}^{(N_1+1) \times N_2}$ and $W \in \mathbb{R}^{(N_2+1) \times 1}$ are bounded constant ideal weight matrices for the first-to-second layer and second to third layer, respectively; N_1, N_2, 1 are the numbers of neurons in the first, second, and third layer of the NN, respectively; $\sigma(\cdot) : \mathbb{R}^{N_1+1} \to \mathbb{R}^{N_2+1}$ is an activation function for the NN, and $\epsilon(\cdot) : \mathbb{R}^4 \to \mathbb{R}$ is a functional reconstruction error. The input vector $x_d(t) \in \mathbb{R}$ is introduced in (3–28).

Based on the assumption that the desired trajectory is bounded, the following inequalities hold

$$|\epsilon\left(x_d\right)| \le \delta_0, \quad |\dot{\epsilon}\left(x_d, \dot{x}_d\right)| \le \delta_1, \quad |\ddot{\epsilon}\left(x_d, \dot{x}_d, \ddot{x}_d\right)| \le \delta_2, \tag{3–33}$$

where δ_0, δ_1, and $\delta_2 \in \mathbb{R}$ are known constants. The NN estimate $\hat{f}_d\left(t\right)$ is defined in (3–27). The update law is designed as

$$\dot{\hat{W}} = proj\left(\Gamma_w \hat{\sigma}' \hat{U}^T \dot{x}_d e_2^T\right),$$
$$\dot{\hat{U}} = proj\left(\Gamma_u \dot{x}_d \left(\hat{\sigma}'^T \hat{W} e_2\right)^T\right), \tag{3–34}$$

where $\Gamma_w \in \mathbb{R}^{(N_2+1)\times(N_2+1)}$ and $\Gamma_u \in \mathbb{R}^{(N_1+1)\times(N_1+1)}$ are constant, positive definite and symmetric gain matrices, $\hat{\sigma} = \sigma\left(\hat{U}^T x_d\right)$, and $\hat{\sigma}' = \sigma'\left(\hat{U}^T x_d\right) \equiv d\sigma\left(U^T x_d\right)|_{U^T x_d = \hat{U}^T x_d}$. The projection algorithm ensures that the $\hat{U}(t)$ and $\hat{W}(t)$ remain bounded inside known bounded convex regions [62].

The weight mismatch errors $\tilde{U}(t) \in \mathbb{R}^{(N_1+1)\times N_2}$ and $\tilde{W}(t) \in \mathbb{R}^{(N_2+1)\times 1}$ are denoted as

$$\tilde{W} = W - \hat{W}, \quad \tilde{U} = U - \hat{U}.$$

By using (3–24)−(3–31), the closed loop error system can be expressed as

$$J_\zeta r = \alpha_2 J_\zeta e_2 + J_\zeta \alpha_1 \dot{e}_1 + J_\zeta \ddot{q}_d \tag{3–35}$$
$$+ M_\zeta + \tau_{d\zeta} - \hat{W}^T \sigma\left(\hat{U}^T x\right) + \mu + R^{-1} e_2. \tag{3–36}$$

Taking the time derivative of (3–35)yields

$$J_\zeta \dot{r} = -\frac{1}{2}\dot{J}_\zeta r - k_s r - \beta_1 sgn\left(e_2\right) - e_2 - R^{-1} r + N + \tilde{N}, \tag{3–37}$$

where the unmeasurable auxiliary functions $\tilde{N}(e_1, e_2, r, t)$ and $N\left(\hat{W}, \hat{V}, x_d, \dot{x}_d\right) \in \mathbb{R}$ are defined as

$$\tilde{N} = M_\zeta - M_\zeta(q_d, \dot{q}_d) + \dot{M}_\zeta - \dot{M}_\zeta(q_d, \dot{q}_d, \ddot{q}_d) + \dot{\tau}_{d\zeta} - \dot{\tau}_{d\zeta}(q_d, \dot{q}_d, t) \tag{3-38}$$
$$+ \dot{J}_\zeta \left(-\frac{1}{2}r + \alpha_1 e_1 + \alpha_2 e_2 + \ddot{q}_d\right) - \dot{J}_\zeta(q_d, \dot{q}_d)\ddot{q}_d + \alpha_2 J_\zeta \dot{e}_2 + J_\zeta \alpha_1 \ddot{e}_1$$
$$- \dot{\hat{W}}^T \sigma\left(\hat{U}^T x_d\right) - \hat{W}^T \sigma'\left(\hat{U}^T x_d\right) \dot{\hat{U}}^T x_d,$$

$$N = N_D + N_B. \tag{3-39}$$

In (3–390, $N_D(x_d, \dot{x}_d, t) \in \mathbb{R}$ is defined as

$$N_D = \tau_{d\zeta} + \dot{\tau}_{d\zeta}(q_d, \dot{q}_d, t) + J_\zeta \dddot{q}_d + \dot{J}_\zeta(q_d, \dot{q}_d)\ddot{q}_d + M_\zeta(q_d, \dot{q}_d) + \dot{M}_\zeta(q_d, \dot{q}_d, \ddot{q}_d), \tag{3-40}$$

while $N_B(\hat{W}, \hat{U}, x_d, \dot{x}_d, t) \in \mathbb{R}$ is defined as

$$N_B = N_{B_1} + N_{B_2}, \tag{3-41}$$

where $N_{B_1}(\hat{W}, \hat{U}, x_d, \dot{x}_d, t) \in \mathbb{R}$ and $N_{B_2}(\hat{W}, \hat{U}, x_d, \dot{x}_d, t) \in \mathbb{R}$ are defined as

$$N_{B_1} = -W^T \hat{\sigma}'\left(\hat{U}^T x_d\right) \hat{U}^T \dot{x}_d - \hat{W}^T \hat{\sigma}'\left(\hat{U}^T x_d\right) \tilde{U}^T \dot{x}_d, \tag{3-42}$$

and

$$N_{B_2} = \hat{W}^T \hat{\sigma}'\left(\hat{U}^T x_d\right) \tilde{U}^T \dot{x}_d + \tilde{W}^T \hat{\sigma}'\left(\hat{U}^T x_d\right) \hat{U}^T \dot{x}_d. \tag{3-43}$$

In a similar manner as in [63], the Mean Value Theorem can be used to develop the following upper bound

$$\left\|\tilde{N}\right\| \leq \rho\left(\|y\|\right) \|y\|, \tag{3-44}$$

where $y(t) \in \mathbb{R}^3$ is defined as

$$y = \begin{bmatrix} e_1^T & e_2^T & r^T \end{bmatrix}^T, \tag{3-45}$$

and the bounding function $\rho\left(\|y\|\right)$ is a positive globally invertible non-decreasing function. The following inequalities can be developed based on Assumption 2, (3–33)

and (3–34),

$$\|N_D\| \le \xi_2, \quad \|N_B\| \le \xi_3, \quad \left\|\dot{N}_D\right\| \le \xi_4, \quad \left\|\dot{N}_B\right\| \le \xi_5 + \xi_6 e_2, \qquad (3\text{–}46)$$

where $\xi_i \in \mathbb{R}, i = 2 - 6$ are known positive constants.

3.4 Stability Analysis

Theorem 3.1. *The control law given in (3–11) and (3–27)–(3–31) ensures all closed-loop signals are bounded and the knee joint tracking error is regulated in the sense that $|e_1(t)| \to 0$ as $t \to \infty$, provided the sufficient conditions*

$$\alpha_1 > \frac{1}{2}, \ \alpha_2 > \xi_6 + 1, \qquad (3\text{–}47)$$

$$\beta > \xi_2 + \xi_3 + \frac{1}{\alpha_2}\xi_4 + \frac{1}{\alpha_2}\xi_5, \qquad (3\text{–}48)$$

are satisfied, where k, α_1, α_2, and β are controller gains, respectively, and ξ_i, $i = 2 - 6$ are known bounds of the terms in the dynamic system. Furthermore, the controller asymptotically minimizes the cost function in (3–8) provided conditions in (3–47) and (3–48) are satisfied.

Proof. Let $\mathcal{D} \subset \mathbb{R}^5$ be a domain containing $\Phi(t) = 0$, where $\Phi(t) \in \mathbb{R}^5$ is defined as

$$\Phi \triangleq \left[y(t)^T \quad \sqrt{P_v(t)} \quad \sqrt{G(t)}\right]^T, \qquad (3\text{–}49)$$

where $P_v(t) \in \mathbb{R}$ is defined as the generalized Filippov solution to the following differential equation

$$\dot{P}_v = r\left(N_{B_1} + N_D - \beta sgn(e_2)\right) + \dot{e}_2 N_{B_2} - \xi_6 e_2^2, \qquad (3\text{–}50)$$

$$P_v\left(e_2(t_0), t_0\right) \triangleq \beta\left|e_2(0)\right| - e_2(0)N(0), \qquad (3\text{–}51)$$

where $\beta \in \mathbb{R}$ is known positive control gain. Similar to the development in (3–31), existence of solutions for $P_v(e_2, t)$ can be established using Filippov's theory of differential inclusions for $\dot{P}_v \in K[h_2](r, \dot{e}_2, e_2, t)$, where $h_2(r, \dot{e}_2, e_2, t) \in \mathbb{R}$ is defined as the right-hand side of $\dot{P}v$. When β is chosen according to the sufficient condition in (3–48), then

45

$P_v(e_2, t) \geq 0$ (See [64] for proof). The auxiliary function $G(t) \in \mathbb{R}$ in (3–49) is defined as

$$G \triangleq \frac{\alpha_2}{2} tr\left(\tilde{W}^T \Gamma_w \tilde{W}\right) + \frac{\alpha_2}{2} tr\left(\tilde{U}^T \Gamma_u \tilde{U}\right), \tag{3–52}$$

where Γ_w, $\Gamma_u \in \mathbb{R}$ are positive definite matrices, and $\alpha_2 \in \mathbb{R}$ is a positive control gain.

Let $V(\Phi, t) : \mathscr{D} \times [0, \infty) \to \mathbb{R}$ be a positive-definite, Lipschitz continuous, regular function defined as

$$V_L \triangleq e_1^2 + \frac{1}{2}e_2^2 + \frac{1}{2}r^2 J_\zeta + P_v + G. \tag{3–53}$$

$V_L(\Phi, t)$ can be upper and lower bounded

$$\gamma_1 \|\Phi\|^2 \leq V_L(\Phi, t) \leq \gamma_2 \|\Phi\|^2, \tag{3–54}$$

where γ_1, $\gamma_2 \in \mathbb{R}$ are some known constants defined as

$$\gamma_1 = \frac{1}{2} \min\{1, \xi_0\}, \quad \gamma_2 = \frac{1}{2} \max\{2, \xi_1\}. \tag{3–55}$$

In (3–55), ξ_0 and $\xi_1 \in \mathbb{R}$ are defined in (2–8).

Under Filippov's framework, a generalized Lyapunov stability theory can be used to establish strong stability of the closed-loop system $\dot{y} = h_3(\Phi, t)$, where $h_3(\Phi, t) \in \mathbb{R}$ denotes the right-hand side of the closed-loop error signals. The time derivative of (3–53) exists almost everywhere (a.e.) and $\dot{V}(\Phi, t) \overset{a.e.}{\in} \dot{\tilde{V}}(\Phi, t)$ where

$$\dot{\tilde{V}} = \bigcap_{\xi \in \partial V(\Phi, t)} \xi^T K \left[\dot{e}_1 \ \dot{e}_2 \ \dot{r} \ \frac{1}{2} P_v^{-\frac{1}{2}} \dot{P}_v \ \frac{1}{2} G^{-\frac{1}{2}} \dot{G} \ 1 \right]^T$$

where ∂V is the generalized gradient of $V(\Phi, t)$ [65]. Since $V(\Phi, t)$ is a Lipschitz continuous regular function,

$$\dot{\tilde{V}} \subset \left[2e_1 \ e_2 \ rJ_\zeta \ 2P_v^{\frac{1}{2}} \ 2G^{\frac{1}{2}} \ \frac{1}{2}\dot{J}_\zeta r^2 \right] K[\cdot]^T. \tag{3–56}$$

Using the calculus for $K[\cdot]$ from [61], $V_L(\Phi, t)$ can be determined as

$$\dot{\tilde{V}} \subset 2e_1\dot{e}_1 + e_2\dot{e}_2 + \frac{1}{2}r^2\dot{J}_\zeta + rJ_\zeta\dot{r} + \dot{P}_v + \dot{G}. \tag{3–57}$$

46

By utilizing (3–2), (3–3), and (3–37), substituting for the time derivative of P_v and G, using Young's Inequality, and (3–34), (3–44), (3–57) can be developed as

$$\dot{V} \overset{a.e.}{\leq} -\lambda \|y\|^2 + \frac{\rho^2 (\|y\|) \|y\|^2}{4k_s}, \tag{3–58}$$

where $\lambda = \min\{2\alpha_1 - 1, \alpha_2 - 1 - \xi_6, R^{-1}\}$. The expression in (3–58) can be further upper bounded by a continuous, positive semi-definite function

$$\dot{V} \overset{a.e.}{\leq} -\gamma_3 \|y\|^2 \qquad \forall y \in \mathscr{D} \tag{3–59}$$

for some positive constant $\gamma_3 \in \mathbb{R}$ and domain $\mathscr{D} = \left\{ \Phi(t) \in \mathbb{R}^5 \mid \|\Phi\| < \rho^{-1}\left(2\sqrt{\lambda k_s}\right) \right\}$. Larger values of k_s will expand the size of the domain $\mathscr{D}$. The inequalities in (3–54) and (3–59) can be used to show that $V_L(\Phi, t) \in \mathcal{L}_\infty$ in $\mathscr{D}$. Thus, $e_1(t), e_2(t), r(t) \in \mathcal{L}_\infty$ in $\mathscr{D}$. The closed-loop error system can be used to conclude that the remaining signals are bounded in $\mathscr{D}$, and the definitions for $\Phi(t)$ can be used to show that $\Phi(t)$ is uniformly continuous in $\mathscr{D}$. Let $S_{\mathscr{D}} \subset \mathscr{D}$ denote a set defined as

$$\mathcal{S}_{\mathscr{D}} \triangleq \left\{ \Phi(t) \subset \mathscr{D} \mid \gamma_2 \|\Phi\|^2 < \gamma_1 \left(\rho^{-1}\left(2\sqrt{\lambda k_s}\right)\right)^2 \right\}. \tag{3–60}$$

The region of attraction in (3–60) can be made arbitrarily large to include any initial conditions by increasing the control gain k_s. The inequation in (3–59) can be used to indicate that

$$\gamma_3 \|y(t)\|^2 \to 0 \quad \text{as} \quad t \to \infty \quad \forall y(0) \in \mathcal{S}_{\mathscr{D}}. \tag{3–61}$$

Based on the definition of $y(t)$, (3–61) can be used to show that

$$|e_1(t)| \to 0 \quad \text{as} \quad t \to \infty \quad \forall y(0) \in \mathcal{S}_{\mathscr{D}}. \tag{3–62}$$

The results in (3–61) indicates that as $t \to \infty$, (3–35) reduces to

$$\hat{f}_d + \mu = h + \tau_{d\zeta}. \tag{3–63}$$

47

Therefore, the dynamics in (3–4) converges to the state space system in (3–12). Hence, $u(t)$ converges to an optimal control law that minimizes (3–8) subject to (3–12), provided the conditions in (3–47), (3–48), and (3–20) are satisfied. □

3.5   Experiment Results

The developed controller was implemented on able-bodied volunteers to evaluate the performance. The same testbed and procedure were used as in Chapter 2.

3.5.1   Tracking Experiments

Tracking experiments for the adaptive controller in Section V were conducted on four volunteers (one female and three males, ages $22-40$ yrs.) using the desired trajectory with a frequency of $1.5 Hz$ and range of motion (ROM) between $5°$ and $35°$. These values were selected to approximate the frequency and ROM of the lower limb during walking, but any sufficiently smooth desired trajectory could have been selected. The Root Mean Square (RMS) tracking error is calculated from 5s to 20s. The Q and R gains were adjusted to obtain the best performance without regard to the control input. The mean RMS error is $4.2°$ with a standard deviation (STD) of $1.3°$. The mean peak-to-peak absolute error is $6.6°$ with a STD of $1.7°$. These results demonstrate the performance of the tracking ability of the proposed controller. Figure 3-2 illustrates a typical knee/limb tracking error.

3.5.2   Performance Trade-offs

To demonstrate the ability for a clinician to choose different combinations of Q and R to place a greater emphasis on tracking performance or feedback control input, tracking experiments were conducted. Two groups of experiments were conducted. The first experiments fixed $\alpha_1 = 1$ and varied R from 5 to 120 to illustrate the effect of penalizing the control input. Additional experiments varied α_1 between 0.5 to 4 for a fixed $R = 20$ to show the effect of penalizing the performance. Each session was 20s, and RMS values were calculated for the error, total control input, and feedback control input, respectively. Figure 3-3 illustrates that the feedback control input decreases and the
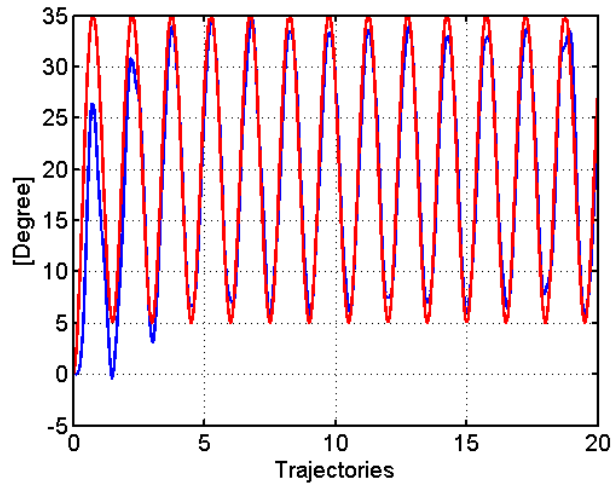
Figure 3-1. Tracking trajectories (dashed line-desired, solid line-actual) for a representative trial on an able-bodied individual

tracking error increases by increasing R. Figure 3-4 illustrates that the error decreases and the feedback control input increases with increasing α_1. The results in Figures 3-3and 3-4 represent the outcome for one volunteer, but the same trends were obtained for the other two subjects with different adjustable ranges.

3.6 Discussion

An adaptive controller which includes a NN term and a RISE term is used to asymptotically minimize a given cost function. The overall controller is proven to achieve asymptotic tracking in the presence of bounded unmodeled disturbances. The asymptotic adaptive controller implicitly compensates for the nonlinear uncertainties present in the dynamics such as passive constraints on joint movement and muscle stimulation which include nonlinear recruitment, torque-angle, and torque-velocity scaling, etc. A quadratic cost functional is adjusted to scale the relative penalty of the tracking error or the feedback control portion of the overall control input.

As indicated in the tracking experiments, a mean RMS error of $4.2°\pm1.3°$ (for 5-20 seconds) was achieved for the given desired trajectory. The limb position accuracy from these experiments is sufficient for typical functional tasks. In addition to developing a

49
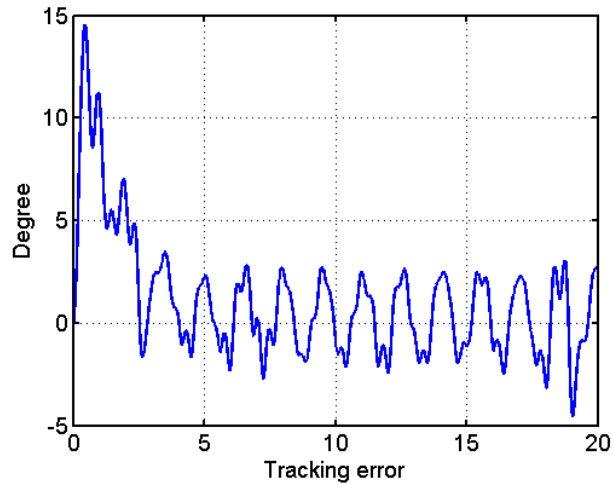
Figure 3-2. Tracking error for a representative trial on an able-bodied individual

controller (and associated stability proof) that can yield desired tracking error performance, a contribution of this effort is to develop a framework to adjust the performance versus dosage.

The trade-off between tracking performance and feedback control effort can be achieved by choosing different values of Q and R. Larger gains in Q yield better tracking performance at the expense of a larger feedback control effort while larger values of R yield reduced feedback control effort with larger tracking errors. Since the error terms $z^T(t) Qz(t) \in \mathbb{R}$ in (3–8) can be related to controller gains as (3–23), where $K \in \mathbb{R}$ is not included in the controller, the error penalty Q can be increased by increasing either α_1 or R^{-1}. Since increasing R^{-1} is equivalent to decreasing the control penalty, when the control penalty is kept constant, increasing the error penalty only can be implemented by increasing α_1. As illustrated in Figure 3-3, with $\alpha_1 = 1$, increasing R from 5 to 120 results in a reduction of the RMS of the feedback control input from 5.18 volts to 2.35 volts. Figure 3-4 illustrates that with $R = 20$, increasing α_1 from 0.5 to 4 reduces the RMS tracking error from $13.94°$ to $5.48°$. Further research is needed to examine the effects of fatigue due to increased control input. Furthermore, the current development does not include the entire control input in the cost functional (i.e., only the feedback

50
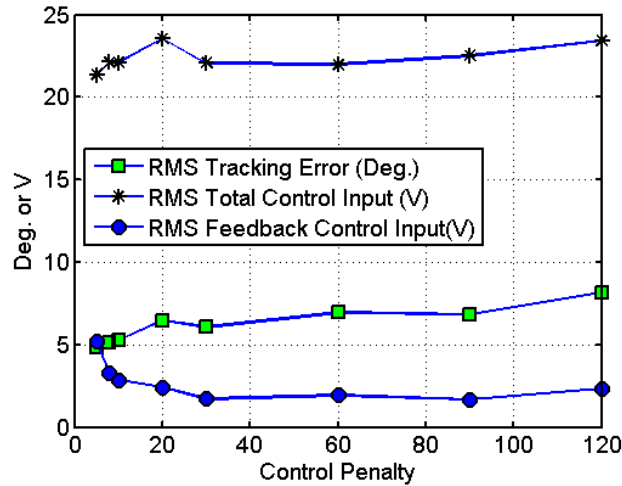
Figure 3-3. Typical experiments on an able-bodied subject with varied R from 5 to 120 for a fixed $\alpha_1 = 1$

portion of the controller is included). These results validate the theoretical ability to directly alter the feedback control through R, but the results do not show a correlation between changes in the feedback portion versus changes in the overall control (i.e., the overall control output was relatively invariant to changes in R).

However, heuristically, it is well accepted that larger feedback gains result in noise amplification and higher frequency control. The RMS total control input $R = 5$ has less value than that when $R = 90$ in Figure 3-3. However, the total control input $R = 5$ has much higher high frequency (>6Hz) components than that when $R = 90$ in Figure 3-5. It is also well accepted that higher frequency stimulation lead to more rapid muscle fatigue. These results point to the need for further studies which investigate the relationship between fatigue as a function of feedback control versus feedforward control.
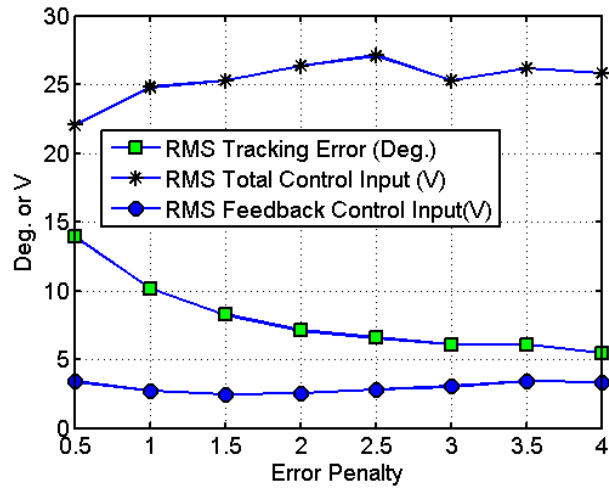
Figure 3-4. Typical experiments on an able-bodied subject with varied α_1 between 0.5 to 4 for a fixed $R = 20$
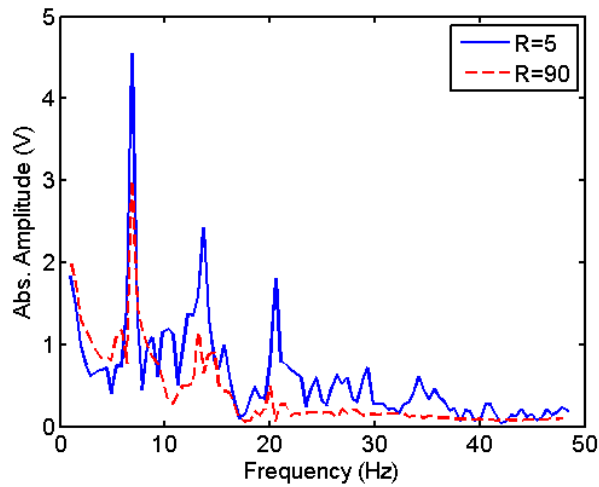
Figure 3-5. Single-sided amplitude spectrums of the total control input from $R = 5$ (solid line) and $R = 90$ (dotted line) for the same experiments in Fig. 3 on an able-bodied person

CHAPTER 4
NEUROMUSCULAR ELECTRICAL STIMULATION LIMB TRACKING WITH A PULSED MODULATED CONTROL INPUT

Typically, stability analysis for closed-loop NMES ignore the modulated implementation of NMES. However, electrical stimulation is applied to muscle as modulated series of pulses and the modulation strategy has significant impact on the muscle performance and fatigue, the ability to examine the impact of the control signal and modulation strategy in analysis may open new insight into the development of NMES controllers.. In this chapter, for the first time, a muscle activation model with a pulse modulated control input is developed to capture the discontinuous nature of muscle activation, and a closed-loop NMES controller is designed and analyzed for the uncertain pulse modulated muscle activation model. Semi-global uniformly ultimately bounded (SUUB) tracking is guaranteed. The stability of the closed-loop system is analyzed with Lyapunov-based methods, and a pulse frequency related gain condition is obtained. Simulation results are provided to validate the controller. For the first time, this paper brings together an analysis of the controller and modulation scheme.

4.1   Muscle Activation and Limb Model

The body segmental dynamics considered in this chapter are the same as those considered in Chapter 2 and 3. In this chapter, the total muscle torque $\tau\left(t\right)$ generated at the knee-joint is considered as product of an unknown nonlinear function $\zeta(q) \in \mathbb{R}$ (moment arm) and the muscle contraction force $x_f(q)$ generated by electric stimulation as

$$\tau \triangleq \zeta x_f. \tag{4--1}$$

After substituting (2–2) and (4–1), and dividing both sides by ζ, the expression in (2–1) can be expressed as

$$x_f = J_\zeta \ddot{q} + f_1 + \tau_1, \tag{4--2}$$

where $J_\zeta(q), f_1(q, \dot{q}), \tau_1(q, t) \in \mathbb{R}$ are defined as

$$J_\zeta \triangleq J_I \zeta^{-1}, \quad f_1 \triangleq (M_e + M_g + M_v)\,\zeta^{-1}, \quad \tau_1 \triangleq \tau_{ds}\zeta^{-1}.$$

Muscle contraction dynamics can be modeled as a first order dynamic system (cf. [5, 37, 66, 67]), which can be expressed as

$$\dot{x}_f + A_f x_f + f_f + \tau_f = bu, \tag{4–3}$$

where $A_f(q), f_f(q), b(q), \tau_f(t) \in \mathbb{R}$ are uncertain functions. The introduction of the unknown nonlinear functions $A_f(q)$ and $f_f(q)$ enable the muscle contraction to be considered under general conditions in the subsequent control development, and $u(t) \in \mathbb{R}$ is the applied electric stimulation voltage. By substituting $x_f(t)$ and $\dot{x}_f(t)$, the dynamics in (4–3) can be expressed as

$$J\dddot{q} = -f_2 - \tau_2 + u, \tag{4–4}$$

where $J(q), f_2(q, \dot{q}, \ddot{q}), \tau_2(t) \in \mathbb{R}$ are defined as

$$
\begin{aligned}
J &= b^{-1} J_\zeta, \\
f_2 &\triangleq b^{-1}\left(\dot{J}_\zeta + A_f J_\zeta\right)\ddot{q} + b^{-1}\left(A_f f_1 + \dot{f}_1 + f_f\right) + b^{-1}\dot{\tau}_1, \\
\tau_2 &\triangleq b^{-1}\left(\tau_f + A_f \tau_1\right).
\end{aligned}
\tag{4–5}
$$

The following assumptions are used to facilitate the subsequent control development and stability analysis.

Assumption 3: The function $\zeta(q)$ is a continuously differentiable, non zero, positive, monotonic, and bounded function [45].

Assumption 4: The function $b(q)$ is the muscle gain (muscle recruitment) which can be assumed to be a continuously differentiable, non zero, positive, monotonic, and bounded function.

Assumption 5: The functions $A_f(q)$, $f_{2m}(q)$, $\tau_{2m}(t)$ are continuously differentiable and bounded functions.

Based on Assumptions $2-5$, the following inequality can be developed

$$\xi_0 \leq J \leq \xi_1, \quad |\tau_2| \leq \xi_2 \tag{4--6}$$

where ξ_0, ξ_1, ξ_2 are known positive constants.

The electrical pulse input $u(t) \in \mathbb{R}$ can be modeled as

$$u = \begin{cases} v, & nT \leq t < nT + d \\ 0, & otherwise \end{cases}, \tag{4--7}$$

$$n = 0, 1, 2, 3...,$$

where v, d, $T \in \mathbb{R}$ denote pulse amplitude, width, and period, respectively. The pulse frequency is defined as $f \triangleq \frac{1}{T}$. Based on (4–7) the system in (4–4) can be expressed as

$$J\dddot{q} = \begin{cases} -f_2 - \tau_2 + v, & nT \leq t < nT + d \\ -f_2 - \tau_2, & otherwise \end{cases} \tag{4--8}$$

$$n = 0, 1, 2, 3...$$

4.2 Control Development

The control objective is to ensure the knee angle $q(t)$ tracks a desired trajectory, denoted by $q_d(t) \in \mathbb{R}$, which is an essential task in many rehabilitative exercises and function restoration tasks.

For the subsequent development, the desired trajectory $q_d(t)$ and its first to third order derivatives, denoted as $\dot{q}_d(t)$, $\ddot{q}_d(t)$, $\dddot{q}_d(t) \in \mathbb{R}$, are assumed to be bounded.

To quantify the tracking objective, a lower limb angular tracking error, denoted by $e_1(t) \in \mathbb{R}$, is defined in (3–1). To facilitate the subsequent control design and stability analysis, filtered tracking errors denoted by $e_2(t)$, $r(t) \in \mathbb{R}$, are also defined in (3–2)

and (3–3). A compositive error signal $z\left(e_1\left(t\right), e_2\left(t\right), r\left(t\right)\right) \in \mathbb{R}^3$ is defined as

$$z \triangleq \begin{bmatrix} e_1 & e_2 & r \end{bmatrix}^T.$$

(4–9)

Using (4–4) and (3–1)–(3–3), the open-loop error system for $e_3\left(t\right)$ can be developed as

$$J\dot{r} = f_3 + \tau_2 - u,$$

(4–10)

where $f_3\left(q, \dot{q}, \ddot{q}, q_d, \dot{q}_d, \ddot{q}_d, \dddot{q}_d\right) \in \mathbb{R}$ is defined as

$$f_3 \triangleq J\dddot{q}_d + (\alpha_1 + \alpha_2)\, Je_3 - \left(\alpha_1^2 + \alpha_1\alpha_2 + \alpha_2^2\right) Je_2 + \alpha_1^3 e_1 + f_2.$$

(4–11)

By Assumptions 2 - 5, $f_3(\cdot)$ can be bounded as

$$\|f_3\| \le c + \rho(\|z\|)\,\|z\|,$$

(4–12)

where $c \in \mathbb{R}$ is a known positive constant and $\rho(\|z\|) \in \mathbb{R}$ is a positive, global invertible function.

Based on (4–10) and the subsequent stability analysis, the NMES controller is designed as

$$v = kr,$$

(4–13)

where $k \in \mathbb{R}$ is a positive gain. The closed-loop error system for $r\left(t\right)$ is

$$J\dot{r} = \begin{cases} f_3 + \tau_2 - kr, & nT \le t < nT + d \\ -f_3 + \tau_2, & otherwise \end{cases},$$

(4–14)

$$n = 0, 1, 2, 3..., .$$

4.3 Stability Analysis

Theorem 4.1. *The closed-loop system in (4–14) with the control law in (4–13) ensures that all closed-loop signals are bounded, and the tracking error is SUUB, provided the control gains k, α_1, α_2 are selected according to initial conditions and the following*

conditions:

$$\alpha_1 > \frac{1}{2}, \ \alpha_2 > 1, \ k > \xi_1, \tag{4--15}$$

$$\gamma_1 > \gamma_2 \left(\frac{T-d}{d} \right), \tag{4--16}$$

where ξ_1 is given in (4–6), T and d are introduced in (4–7), γ_2 is a known bounding constant that depends on ξ_0, ξ_2, and c defined in (4–6) and (4–12), and γ_1 is a gain constant that can be made arbitrarily large by selecting α_1, α_2, and k in (3–2), (3–3), and (4–13) arbitrarily large.

Proof. Let $V(z(t)) \in \mathbb{R}$ be a continuously differentiable positive definite function defined as

$$V \triangleq \frac{1}{2} z^T z. \tag{4--17}$$

From (3–1)$-$(3–3), (4–9), and (4–14), the time derivative of (4–17) is

$$\dot{V} = -\alpha_1 e_1^2 - \alpha_2 e_2^2 + e_1 e_2 + e_2 r + r J^{-1} f_3 + r J^{-1} \tau_3 - r J^{-1} u.$$

Using Young's inequality, $\dot{V}(z(t))$ can be bounded as

$$\dot{V} \leq -\left(\alpha_1 - \frac{1}{2} \right) e_1^2 - (\alpha_2 - 1) e_2^2 + \frac{1}{2} r^2 + r J^{-1} f_3 + r J^{-1} \tau_2 - r J^{-1} u. \tag{4--18}$$

The function $V(z(t))$ can be expressed in segments $V_n(z, \tau)$, where $V_n(z, \tau) \in \mathbb{R}$ is defined as

$$V_n(z, \tau) \triangleq V(z, t - nT), \tag{4--19}$$

where $\tau \triangleq t - nT, \ n \triangleq \lfloor t/T \rfloor$.

On the interval $0 \leq \tau < d$, $\dot{V}_n(z, \tau)$ can be expressed as

$$\dot{V}_n \leq -\left(\alpha_1 - \frac{1}{2} \right) e_1^2 - (\alpha_2 - 1) e_2^2 + \frac{1}{2} r^2 + \xi_0^{-1} \rho(\|z\|) \|z\| \|r\| - k \xi_1^{-1} r^2 + \|r\| \xi_0^{-1} (\xi_2 + c),$$

$$\tag{4--20}$$

where ξ_0, ξ_1, ξ_2 is given in (4–6), and c and $\rho\left(\|z\|\right)$ is given in (4–12). When the conditions in (4–15) and (4–16) hold, after completing the squares

$$\dot{V}_n \leq -\frac{1}{2}\gamma_1 \|z\|^2 + \lambda_1, \quad \forall \|z\| \in \mathscr{D}$$

$$\mathscr{D} = \left\{ z(t) \in \mathbb{R}^3 \mid \|z\| < \rho^{-1}\left(\xi_0\sqrt{\gamma_0 k\xi_1^{-1}}\right)\right\} \tag{4–21}$$

where $\gamma_0 \in \mathbb{R}$ is defined as

$$\gamma_0 \triangleq \min\left(\alpha_1 - \frac{1}{2}, \alpha_2 - 1, \frac{1}{2}k\xi_1^{-1} - \frac{1}{2}\right),$$

$\gamma_1 \in \mathbb{R}$ is a positive constant, which can be made arbitrary large by increasing the control gains α_1, α_2, and k, and $\lambda_1 \in \mathbb{R}$ is a positive constant that can be made arbitrarily small by selecting k arbitrarily large. Larger values of α_1, α_2, and k will expand the size of the domain $\mathscr{D}$ to include any initial conditions (i.e., a semi-global type of stability result). On the interval $d \leq \tau < T$,

$$\dot{V}_n \leq \frac{1}{2}\gamma_2 \|z\|^2 + \lambda_2,$$

where γ_2, $\lambda_2 \in \mathbb{R}$ are known positive bounding constants that depend on ξ_0, ξ_2, and c defined in (4–6) and (4–12). Using (4–17) and (4–19), $\dot{V}_n\left(z,\tau\right)$ is

$$\dot{V}_n \leq \begin{cases} -\gamma_1 V_n + \lambda_1, & 0 \leq \tau < d \\ \gamma_2 V_n + \lambda_2, & d \leq \tau < T \end{cases},$$

which can be solved to obtain $V_n\left(z,T\right)$ as

$$V_n\left(z,T\right) \leq \left(V_n\left(z,d\right) + \frac{\lambda_2}{\gamma_2}\right)e^{\gamma_2(T-d)} - \frac{\lambda_2}{\gamma_2}, \tag{4–22}$$

$$V_n\left(z,d\right) \leq \left(V_n\left(z,0\right) - \frac{\lambda_1}{\gamma_1}\right)e^{-\gamma_1 d} + \frac{\lambda_1}{\gamma_1}. \tag{4–23}$$

By using (4–22) and (4–23), and the fact that $V_{n+1}(z,0) = V_n(z,T)$, the difference between $V_{n+1}(z,0)$ and $V_n(z,0)$ defined as $\tilde{V}_n(z)$ is

$$
\begin{aligned}
\tilde{V}_n &= V_{n+1}(z,0) - V_n(z,0) \\
&\leq V_n(z,d)\,e^{\gamma_2(T-d)} - V_n(z,0) + \frac{\lambda_2}{\gamma_2}\left(e^{\gamma_2(T-d)} - 1\right), \\
&\leq V_n(z,0)\left(e^{-\gamma_1 d}e^{\gamma_2(T-d)} - 1\right) + \frac{\lambda_1}{\gamma_1}\left(1 - e^{-\gamma_1 d}\right)e^{\gamma_2(T-d)} + \frac{\lambda_2}{\gamma_2}\left(e^{\gamma_2(T-d)} - 1\right).
\end{aligned}
\tag{4–24}
$$

Based on (4–24), $\tilde{V}_n(z) < 0$ (i.e., $V(z(0)) > V(z(T)) > V(z(2T)) > \cdots$) when $V_n(z,0) > \bar{d}^2$ where $\bar{d} \in \mathbb{R}$ is defined as

$$
\bar{d} > \sqrt{\frac{\frac{\lambda_2}{\gamma_2}\left(1 - e^{-\gamma_2(T-d)}\right) + \frac{\lambda_1}{\gamma_1}\left(1 - e^{-\gamma_1 d}\right)}{e^{-\gamma_2(T-d)} - e^{-\gamma_1 d}}}.
\tag{4–25}
$$

where the gain condition in (4–16) determines the size of $\bar{d}$ based on the period, pulse width, and control gains. Based on (4–17), $z(t) \in \mathscr{D}$ uniformly converges to the ultimate bound

$$
\|z(t)\| < \sqrt{2}\bar{d}
\tag{4–26}
$$

provided the sufficient conditions in (4–15)−(4–16) are satisfied. $\|e(t)\|$ is semi-global uniformly ultimately bounded [68, Theorem 4.18] in the sense that

$$
\|e(t)\| \leq \|z(t)\| < \sqrt{2}\bar{d},\ \forall t \geq \overline{T}\left(\bar{d}, \|z(0)\|\right),\forall\|z(0)\| \in \mathcal{D},
$$

where $\overline{T}\left(\bar{d},\|z(0)\|\right) \in \mathbb{R}$ is a positive constant that denotes the ultimate time to reach the ball. □

Remark 4.1. Based on (4–16) and (6–26), the interplay between the modulation strategy and the controller can be determined. To minimize muscle fatigue, one is motivated to decrease the stimulation frequency (i.e., increase T). From (4–16) and (6–26), decreasing the stimulation frequency indicates that the control gains should be selected larger (making γ_1 larger) and that the ultimate error will be larger. if the

frequency is increased (leading to faster muscle fatigue) then the control gains can be selected lower and a lower ultimate bound can be obtained.

The ultimate error bound in (4–26) has terms $e^{-\gamma_2(T-d)}$ and $e^{-\gamma_1 d}$ related to the stimulation frequency and control gains, respectively. The control gains only reduce the contribution of the term $e^{-\gamma_1 d}$ in the ultimate error bound, while the term $e^{-\gamma_2(T-d)}$ in the ultimate error bound can only be reduced via increasing the stimulation frequency.

4.4   Experiments

The proposed controller was implemented on able-bodied volunteers (3 males, ages 26-42 yrs.) to evaluate the performance. The same test bed and procedure were used as in Chapter 2. The electrical stimulation is delivered with a constant pulse width of $400\mu s$ and a pulse frequency of $30Hz$ or $100Hz$. The amplitude of the electrical pulses is modulated by the output of the controller. A Butterworth low pass filter with cutoff frequency of 1000Hz was used to reduce the noise in $e_2(t)$. No weight was attached to the weighting bar. Any sufficiently smooth desired trajectory could have been selected. The desired angular trajectory was selected as

$$q_d = \begin{cases} \frac{65}{2}(1 + \sin(\frac{\pi}{1.25}t + \frac{3}{2}\pi)), & t < 1.25 \\ 30(1 + \sin(\frac{\pi}{1.25}t + \frac{3}{2}\pi)) + 5, & t \geq 1.25, \end{cases} \tag{4–27}$$

The trajectory was a sinusoidal trajectory with a period of 2.5s and range of motion (ROM) between 5° and 60° (see Figure 4-1). The largest angle motion can be achieved is 80° on the LEM. The selection of this ROM was to get a large ROM and leave some room for over shooting.

The experiment results are summarized in Table 4-1, where the peak tracking error was calculated as $max(|e(t)|)$. In Table4-1, the total RMS (root mean square) error is recorded, as well as the RMS error in 10 second intervals. A representative trial (i.e. C-left in Table 4-1) is shown in Figures $4\text{-}1 - 4\text{-}3$.

Table 4-1. Tracking errors for a sinusoidal trajectory with a period of 2.5s and ROM between 5° and 60°. The stimulation frequency is 30Hz.

Subject	RMS			Peak		
	Total	0-10s	10-20s	Total	0-10s	10-20s
A-left	4.01	4.64	3.26	10.87	10.87	6.42
A-right	4.07	4.63	3.43	13.64	13.64	7.10
B-left	4.41	5.20	3.44	11.18	11.18	7.23
B-right	3.91	4.52	3.19	14.96	14.96	9.78
C-left	3.83	4.17	3.83	9.59	9.59	9.27
C-right	4.03	4.17	3.89	8.69	8.69	8.69
Mean	4.04	4.55	3.51	11.49	5.60	8.08
STD	0.18	0.35	0.27	2.18	1.49	1.24
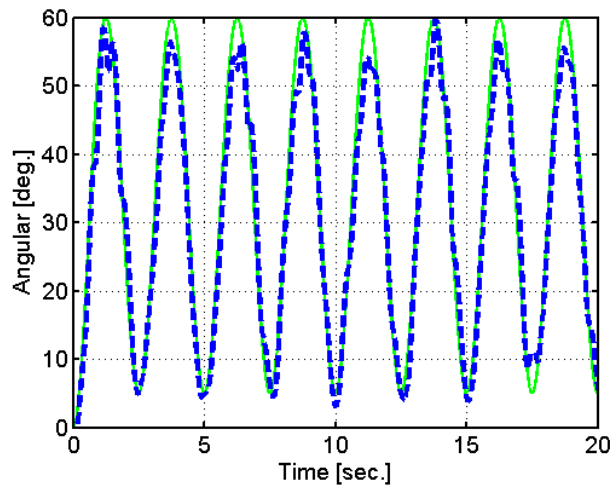
Figure 4-1. Desired (solid line) and measured (dashed line) trajectories. The stimulation pulse frequency is 30Hz

For comparison, the controller was implemented at 100Hz stimulation pulse frequency on the same group of subjects. The tracking errors are listed in Table 4-2. A representative trial (i.e. A-right in Table 4-2) is shown in Figures 4-4 and 4-5. The RMS and peak errors from 0 to 10s and 0 to 20s marked by *s in Table 4-2 are both statistically lower (student T-test, one tail, paired, $p < 0.05$) than the results obtained using 30Hz stimulation pulse frequency. No statistical difference was determined in the RMS and peak error in the range 10 to 20s. The lower error during the initial 10 seconds and from 0-20 seconds is predicted by the theoretical analysis. That is, high frequency stimulation yields a stronger contraction that can be used to decrease the tracking error.
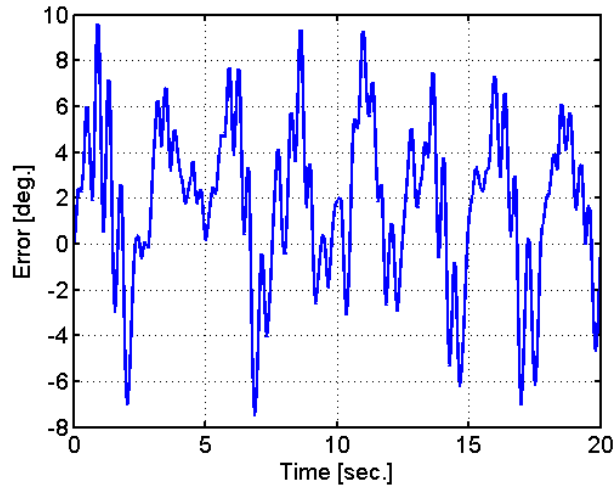
Figure 4-2. Tracking error of a representative sinusoidal trajectory tracking experiment. The stimulation pulse frequency is 30Hz.

The lack of statistic difference from 10-20s is due to the fact that the higher frequency stimulation results in a more rapid muscle fatigue. The errors in Figure 4-4 show a continuous increasing trend. To illustrate the fact that high frequency fatigues the muscle more rapidly than low frequency [23], A 30v pulse train is applied to Subject B-left at 100Hz for 20s, and after 5 minutes rest, a 35v pulse train at 30Hz was applied for 20s. The applied voltage at 30Hz were selected to initially have similar outputs as the result at 100Hz (i.e., the response of 30v at 100Hz was 21.7-25.4° and the response of 35v at 30Hz was 22.3-24v in the time interval of 1-2s). The position of the lower leg is given in Figure 4-6, which illustrate the rapid onset of fatigue with high frequency pulse trains.
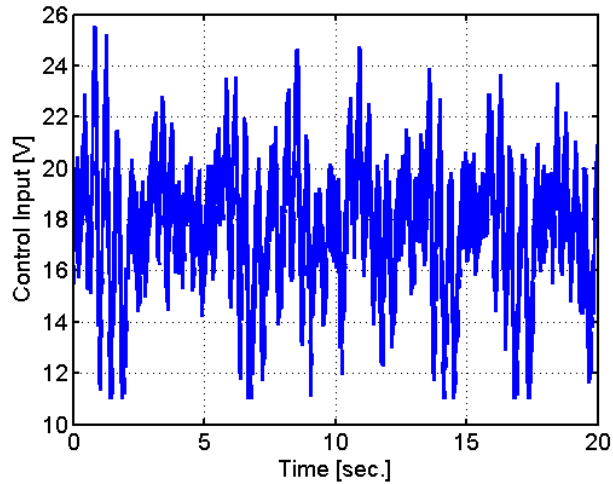
Figure 4-3. Control input (Voltage) for a representative sinusoidal trajectory tracking experiment. The stimulation pulse frequency is 30Hz.

Table 4-2. The tracking errors for a sinusoidal trajectory with a period of 2.5s and ROM between 5° and 60°. The stimulation frequency is 100Hz. The * indicates a statistically significant difference (p<0.05) when compared to the 30Hz experiments.

| Subject	RMS			Peak		
	Total	0-10s	10-20s	Total	0-10s	10-20s
A-left	3.08	2.76	3.36	7.56	5.72	7.56
A-right	2.60	2.23	2.91	6.27	4.97	6.27
B-left	3.66	3.21	3.99	8.02	6.71	8.02
B-right	3.98	2.79	4.87	11.69	6.18	11.69
C-left	3.28	3.39	3.16	7.06	6.53	7.06
C-right	2.81	2.90	2.72	6.75	5.81	6.75
Mean	3.23*	2.88*	3.50	7.89*	5.99*	7.89
STD	0.47	0.37	0.73	1.79	0.58	1.79
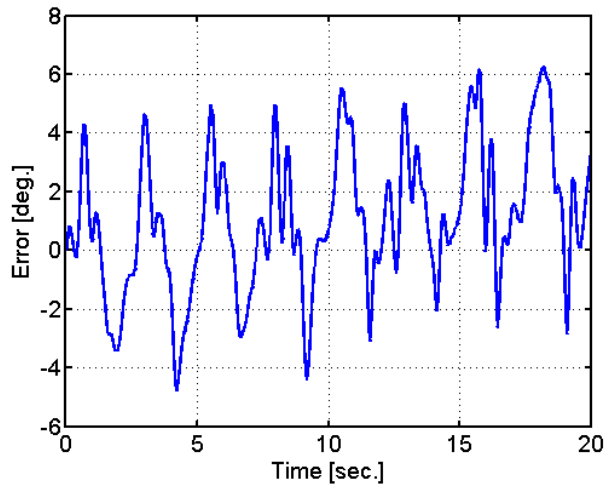
Figure 4-4. Tracking error of a representative sinusoidal trajectory tracking experiment. The stimulation pulse frequency is 100Hz.
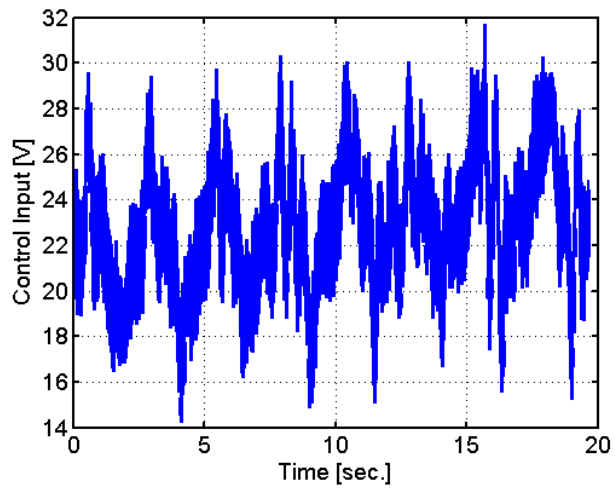

Figure 4-5. Control input (Voltage) for a representative sinusoidal trajectory tracking experiment. The stimulation pulse frequency is 100Hz.
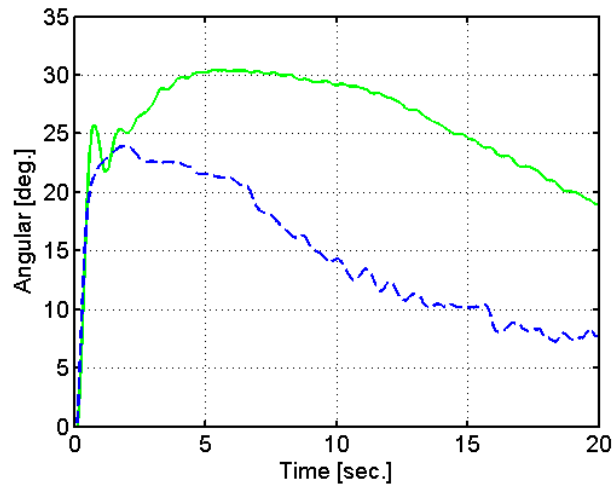
Figure 4-6. Constant voltage response at 30 Hz (solid line) and 100Hz (dashed line)

CHAPTER 5
NEUROMUSCULAR ELECTRICAL STIMULATION WITH A UNCERTAIN MUSCLE CONTRACTION MODEL

In this chapter, uncertainties in the muscle contraction dynamics are taken into consideration when compensating for the muscle contraction dynamics. Accounting for the muscle contraction dynamics is a challenge because of uncertainty, nonlinearity and the fact that the contraction states are not measurable. A neural-network (NN)-based controller together with a dynamic NN-based identifier is designed to enable semi-global uniformly ultimately bounded tracking of a desired limb trajectory and on-line estimation of the limb acceleration. The overall stability of the identifier-controller system is analyzed through Lyapunov methods. Simulation results are provided to illustrate the controller performance.

5.1 Muscle Activation and Limb Model

The same body segmental and muscle contraction dynamics are used as those in Chapter 4 except that input $u(t) \in \mathbb{R}$ is not modulated. The dynamics can be expressed as

$$J\dddot{q} = -f_2 - \tau_2 + u.$$

5.2 Control Development

The control objective is to ensure the knee angle $q(t)$ tracks a desired trajectory, denoted by $q_d(t) \in \mathbb{R}$, which is an essential task in many rehabilitative exercises and function restoration tasks. To quantify the tracking objective, a lower limb angular position tracking error, denoted by $e(t) \in \mathbb{R}$, is defined as in (2–9). To facilitate the subsequent control design and stability analysis, filtered tracking errors denoted by $e_1(t), e_2(t) \in \mathbb{R}$, are also defined as

$$e_1 \triangleq \dot{e} + \alpha_1 e, \tag{5–1}$$

$$e_2 \triangleq \dot{e}_1 + \alpha_2 e_1, \tag{5–2}$$

where α_1 and $\alpha_2 \in \mathbb{R}$ are positive constant control gains. Using (2–9), (5–1) $-$(5–2) , $e_2(t)$ can be expressed as

$$e_2 = \ddot{q}_d - \ddot{q} + (\alpha_1 + \alpha_2)(\dot{q}_d - \dot{q}) + \alpha_1\alpha_2 e. \tag{5–3}$$

The subsequent development is based on the assumption that $q(t)$ and $\dot{q}(t)$ are measurable. The error dynamics in (5–3) depend on the unmeasurable limb acceleration. To compensate for the acceleration dependency, an error estimation is designed based on (5–3) as

$$\hat{e}_2 \triangleq \ddot{q}_d - \ddot{\hat{q}} + (\alpha_1 + \alpha_2)(\dot{q}_d - \dot{\hat{q}}) + \alpha_1\alpha_2 e., \tag{5–4}$$

where $\ddot{\hat{q}}(t), \dot{\hat{q}}(t) \in \mathbb{R}$ denotes the subsequently designed observer output.

To facilitate the subsequent analysis, let $f_{2d}(q_d, \dot{q}_d, \ddot{q}_d) \in \mathbb{R}$ be defined as

$$
\begin{aligned}
f_{2d} \triangleq{} & b^{-1}(q_d, \dot{q}_d) f_1(q_d, \dot{q}_d) - J_I b^{-1}(q_d, \dot{q}_d) \zeta^{-2}(q_d) \dot{\zeta}(q_d, \dot{q}_d) \ddot{q}_d \\
& + J_I b^{-1}(q_d, \dot{q}_d) A_f(q_d, \dot{q}_d) \zeta^{-1}(q_d) \ddot{q}_d + b^{-1}(q_d, \dot{q}_d) \zeta^{-1}(q_d) A_f(q_d, \dot{q}_d) \\
& (M_e(q_d) + M_g(q_d) + M_v(\dot{q}_d)) + b^{-1}(q_d, \dot{q}_d) \zeta^{-1}(q_d) \\
& \left(\dot{M}_e(q_d, \dot{q}_d) + \dot{M}_g(q_d, \dot{q}_d) + \dot{M}_v(\dot{q}_d, \ddot{q}_d)\right) - b^{-1}(q_d, \dot{q}_d) \zeta^{-2}(q_d) \dot{\zeta}(q_d, \dot{q}_d) \\
& (M_e(q_d) + M_g(q_d) + M_v(\dot{q}_d)) .
\end{aligned} \tag{5–5}
$$

Based on the universal function approximation property [69], the unknown function in (5–5) can be approximated by a multi-layer NN which is defined as

$$f_{2d} = W^T \sigma\left(V^T X_d\right) + \varepsilon, \tag{5–6}$$

where $X_d(q_d, \dot{q}_d, \ddot{q}_d) \in \mathbb{R}^4$ is defined as

$$X_d \triangleq \begin{pmatrix} 1 & q_d & \dot{q}_d & \ddot{q}_d \end{pmatrix}^T, \tag{5–7}$$

and $W \in \mathbb{R}^{n \times 1}$, $V \in \mathbb{R}^{4 \times n}$ denote the ideal weights for the hidden layer neurons and the input layer neurons, respectively, where the number of hidden layer neurons is selected

as n. $\varepsilon(X_d) \in \mathbb{R}$ denotes the reconstruction error. Since $X_d(q_d, \dot{q}_d, \ddot{q}_d)$ depends on the known bounded desired trajectory, the NN input is guaranteed to lie on a compact set.

Assumption 6: The activation function $\sigma(\cdot)$ and its first order derivative with respect to its arguments $\sigma'(\cdot)$ are bounded by known constants [47].

Assumption 7: The reconstruction error $\varepsilon(X_d)$ and its first order derivative with respect to its arguments $\varepsilon'(X_d)$ are bounded by known constants [47].

By using (4–9) $-$(5–2) and (5–6) , the open-loop error system for $e_2(t)$ can be obtained as

$$J\dot{e}_2 = -\frac{1}{2}\dot{J}e_2 + f_2 - f_{2d} + W^T\sigma\left(V^TX_d\right) + \frac{1}{2}\dot{J}e_2 + J\ddot{q}_d + \tau_2 + \varepsilon - u. \quad (5\text{–}8)$$

Let $\hat{W}(t) \in \mathbb{R}^{n\times 1}$, $\hat{V}(t) \in \mathbb{R}^{4\times n}$ be the estimated weights for W, V, and $\sigma(X_d)$, $\hat{\sigma}(X_d, t)$, $\hat{\sigma}'(X_d, t)$, $\tilde{\sigma}(X_d, t)$, $\tilde{W}(t) \in \mathbb{R}^{n\times 1}$, $\tilde{V}(t) \in \mathbb{R}^{4\times n}$ be defined as

$$\sigma \triangleq \sigma(V^TX_d), \quad (5\text{–}9)$$

$$\hat{\sigma} \triangleq \sigma(\hat{V}^TX_d), \quad (5\text{–}10)$$

$$\hat{\sigma}' \triangleq \frac{\partial\left(\sigma(\hat{V}^TX)\right)}{\partial\left(\hat{V}^TX\right)}\Big|_{\hat{V}^TX=\hat{V}^TX_d}, \quad (5\text{–}11)$$

$$\tilde{\sigma} \triangleq \sigma - \hat{\sigma}, \quad (5\text{–}12)$$

$$\tilde{W} \triangleq W - \hat{W}, \quad (5\text{–}13)$$

$$\tilde{V} \triangleq V - \hat{V}. \quad (5\text{–}14)$$

By using a Taylor series approximation, $\tilde{\sigma}(X_d, t)$ can be expressed as

$$\tilde{\sigma} = \hat{\sigma}'\tilde{V}^TX_d + o(\tilde{V}^TX_d)^2,$$

where $o(\cdot)^2 \in \mathbb{R}$ denotes higher order terms. By using (5–9) $-$(7–7) , $W^T\sigma(V^TX_d)$ can be expressed as

$$W^T\sigma(V^TX_d) = \hat{W}^T\hat{\sigma}'\tilde{V}^TX_d + W^T\hat{\sigma} + \tilde{W}^T\hat{\sigma}'\tilde{V}^TX_d + W^To(\tilde{V}^TX_d)^2. \quad (5\text{–}15)$$

Based on (5–9) −(5–15) , the error system in (5–8) can be expressed as

$$J\dot{e}_2 = -\frac{1}{2}\dot{J}e_2 + f_3 - u + W^T\hat{\sigma} + \hat{W}^T\hat{\sigma}'\tilde{V}^T X_d, \qquad (5\text{–}16)$$

where $f_3(q, \dot{q}, \ddot{q}, q_d, \dot{q}_d, \ddot{q}_d, t) \in \mathbb{R}$ are defined as

$$\begin{aligned} f_3 \triangleq{}& f_2 - f_{2d} + \tilde{W}^T\hat{\sigma}'\tilde{V}^T X_d + W^T o(\tilde{V}^T X_d)^2 - J\alpha_1^2\dot{e} \\ &+ J\left(\alpha_1 + \alpha_2\right)\dot{e}_1 + \frac{1}{2}\dot{J}e_2 + J\dddot{q}_d + \tau_2 + \varepsilon. \end{aligned}$$

If the update laws $\dot{\hat{W}}(t) \in \mathbb{R}^{n\times 1}$, $\dot{\hat{V}}(t) \in \mathbb{R}^{4\times n}$ are selected as

$$\dot{\hat{W}} \triangleq proj(\Gamma_w\hat{\sigma}\hat{e}_2), \ \dot{\hat{V}} \triangleq proj(\Gamma_v X_d\hat{e}_2\hat{W}^T\hat{\sigma}'), \qquad (5\text{–}17)$$

where $proj(\cdot)$ is a smooth projection operator [62].

$$\hat{e}_2\tilde{W}^T\hat{\sigma} + \hat{e}_2\hat{W}^T\hat{\sigma}'\tilde{V}^T X_d + \dot{G}_1 = 0, \qquad (5\text{–}18)$$

where $G_1(t) \in \mathbb{R}$ is defined as

$$G_1 \triangleq \frac{1}{2}tr\left(\tilde{W}^T\Gamma_w^{-1}\tilde{W}\right) + \frac{1}{2}tr\left(\tilde{V}^T\Gamma_v^{-1}\tilde{V}\right),$$

where $\Gamma_w \in \mathbb{R}^{n\times n}$, $\Gamma_v \in \mathbb{R}^{4\times 4}$ are positive definite matrices and $tr(\cdot)$ denotes the trace of a matrix. It is straightforward to show that $G_1(t) \geq 0$. Since $proj(\cdot)$ guarantees $\hat{W}(t)$, $\hat{V}(t)$ to be bounded, $\tilde{W}(t)$, $\tilde{V}(t)$ are bounded by using (5–13) and the fact that W and V are bounded. Since $X_d(q_d, \dot{q}_d, \ddot{q}_d)$ is bounded, the following bound can be obtained as

$$\left|\tilde{W}^T\hat{\sigma} + \hat{W}^T\hat{\sigma}'\tilde{V}^T X_d\right| \leq a_1, \qquad (5\text{–}19)$$

where $a_1 \in \mathbb{R}$ is a known positive constant. Since $W, V, \sigma(\cdot), \hat{W}(t), \tilde{W}(t), \tilde{V}(t), \hat{\sigma}(X_d)$, $\sigma'(\hat{V}^T X_d), o(\tilde{V}^T X_d)$, and $\varepsilon(X_d)$ are bounded, using the Mean Value Theorem, (5–19) and the assumption that $\dddot{q}_d(t)$ is bounded, $f_3(q, \dot{q}, \ddot{q}, q_d, \dot{q}_d, \ddot{q}_d, t) \in \mathbb{R}$ can be bounded as

$$|f_3| \leq a_2 + \rho_1\left(\|z_f\|\right)\|z_f\|, \qquad (5\text{–}20)$$

where $a_2 \in \mathbb{R}$ is a positive constant, $z_f(e(t), e_1(t), e_2(t)) \in \mathbb{R}^3$ is defined as

$$z_f \triangleq \left(\begin{array}{ccc} e & e_1 & e_2 \end{array} \right)^T,$$

and $\rho_1 \left(\|z_f\| \right) \in \mathbb{R}$ is a positive, globally invertible function. Based on (5–16), (5–17), and the subsequent stability analysis, the control input is designed as

$$u = k_f \hat{e}_2 + \hat{W}^T \hat{\sigma}, \tag{5–21}$$

where $k_f \in \mathbb{R}$ is a positive control gain. After substituting (5–21) into (5–16), the closed-loop error system can be obtained as

$$J \dot{e}_2 = -\frac{1}{2} \dot{J} e_2 + f_3 + \tilde{W}^T \hat{\sigma} + \hat{W}^T \hat{\sigma}' \tilde{V}^T X_d - k_f \hat{e}_2. \tag{5–22}$$

5.3   Observer Design

The objective of this section is to design an observer/identifier to generate the estimation of $\ddot{\hat{q}}(t)$, which is used in $\hat{e}_2(t)$ in (5–4), so that the controller in (5–21) can be implemented with only measurements of $q(t)$ and $\dot{q}(t)$.

To facilitate the following observer design, define $x(t)$, $\hat{x}(t)$, $\tilde{x}(t)$, $r(t) \in \mathbb{R}^2$, $z(t) \in \mathbb{R}^4$ as

$$x \triangleq \left(\begin{array}{cc} q & \dot{q} \end{array} \right)^T, \tag{5–23}$$

$$\hat{x} \triangleq \left(\begin{array}{cc} \hat{q} & \dot{\hat{q}} \end{array} \right)^T, \tag{5–24}$$

$$\tilde{x} \triangleq x - \hat{x}, \tag{5–25}$$

$$r \triangleq \dot{\tilde{x}} + \alpha \tilde{x} = \left(\begin{array}{cc} r_1 & r_2 \end{array} \right)^T, \tag{5–26}$$

$$z \triangleq \left(\begin{array}{cc} \tilde{x}^T & r^T \end{array} \right)^T, \tag{5–27}$$

where $\alpha \triangleq \alpha_1 + \alpha_2 \in \mathbb{R}$ is a constant control gain. By using (5–2) and (5–4), the difference between $e_2(t)$ and $\hat{e}_2(t)$ yields the acceleration estimation error as

$$\hat{e}_2 - e_2 = r_2, \tag{5–28}$$

which can be bounded as

$$|r_2| \leq \|r\|. \tag{5–29}$$

After substituting (2–2), and (4–1), the dynamics in (2–1) can be expressed as

$$J_I \ddot{q} + M_e + M_g + M_v + \tau_d = \zeta x_f, \tag{5–30}$$

which can be rewritten as

$$\dot{x} = -\alpha x + g_1 + d, \tag{5–31}$$

where $x(t)$ is defined in (5–23) and $g_1\left(q, \dot{q}\right), d\left(t\right) \in \mathbb{R}^2$ are defined as

$$g_1 \triangleq \alpha x + \begin{pmatrix} \dot{q} \\ -J_I^{-1}\left(M_e + M_g + M_v\right) + J_I^{-1}\zeta x_f \end{pmatrix},$$

$$d \triangleq \begin{pmatrix} 0 \\ -J_I^{-1}\tau_d \end{pmatrix}.$$

Let $g_{1d}\left(q_d, \dot{q}_d\right) \in \mathbb{R}^2$ be defined as

$$g_{1d} \triangleq \alpha x_d + \begin{pmatrix} \dot{q}_d \\ f_d \end{pmatrix},$$

where $f_d\left(q_d, \dot{q}_d\right) \in \mathbb{R}$ is defined as

$$f_d \triangleq J_I^{-1}\zeta\left(q_d\right) x_f\left(q_d, \dot{q}_d\right) - J_I^{-1}\left(M_e\left(q_d\right) + M_g\left(q_d\right) + M_v\left(\dot{q}_d\right)\right),$$

and $x_d\left(\begin{array}{cc} q_d & \dot{q}_d \end{array} \right) \in \mathbb{R}^2$ is defined as

$$x_d \triangleq \left(\begin{array}{cc} q_d & \dot{q}_d \end{array} \right)^T.$$

The unknown function $g_{1d}(q_d, \dot{q}_d) \in \mathbb{R}^2$ can be approximated by a multi-layer NN with a reconstruction error as

$$g_{1d} = W_1^T \sigma_1 (V_1^T x_d) + \varepsilon_1,$$

where $W_1 \in \mathbb{R}^{n_1 \times 2}$, $V_1 \in \mathbb{R}^{2 \times n_1}$ denote the ideal weights for the hidden layer neurons and the input layer neurons, respectively, where the number of hidden layer neurons is selected as n_1; $\varepsilon_1(x_d) \in \mathbb{R}$ denotes the reconstruction error.

Assumption 8: The activation function $\sigma_1(\cdot)$ and its first order derivative with respect to its arguments $\sigma_1'(\cdot)$ are bounded by known constants [47].

Assumption 9: The reconstruction error $\varepsilon_1(x_d)$ and its first order derivative with respect to its arguments $\varepsilon_1'(x_d)$ are bounded by known constants [47].

The dynamics in (5–31) can be rewritten as

$$\dot{x} = -\alpha x + g_1 - g_{1d} + W_1^T \sigma_1 (V_1^T x_d) + \varepsilon_1 + d. \tag{5–32}$$

Based on (5–32), a multi-layer dynamic NN observer is designed as

$$\dot{\hat{x}} = -\alpha \hat{x} + \hat{W}_1^T \sigma_1 (\hat{V}_1^T \hat{x}) + \mu, \tag{5–33}$$

where $\hat{W}_1(t) \in \mathbb{R}^{n_1 \times 2}$, $\hat{V}_1(t) \in \mathbb{R}^{2 \times n_1}$ denote the estimated weights for W_1, V_1, and $\mu(\tilde{x}) \in \mathbb{R}^2$ is defined as

$$\mu \triangleq k\tilde{x} - k\tilde{x}(0) + \int_0^t k\alpha\tilde{x}d\tau, \tag{5–34}$$

where $k \in \mathbb{R}$ is positive control gain.

Based on (5–32) and (5–33) , the observer error dynamics can be written as

$$\dot{\tilde{x}} = -\alpha \tilde{x} + \varepsilon_1 + \varepsilon_2 + g_1 - g_{1d} + d - \mu, \tag{5–35}$$

where $\varepsilon_2(x) \in \mathbb{R}^2$ is defined as

$$\varepsilon_2 \triangleq W_1^T \sigma_1 (V_1^T x_d) - \hat{W}_1^T \sigma_1 (\hat{V}_1^T \hat{x}). \tag{5–36}$$

After some algebraic manipulation, the time derivative of (5–36) can be written as

$$\dot{\varepsilon}_2 = W_1^T \sigma_1' V_1^T \dot{x}_d - \dot{\hat{W}}_1^T \hat{\sigma}_1(\hat{V}_1^T \hat{x}) - \hat{W}_1^T \hat{\sigma}_1' \dot{\hat{V}}_1^T \hat{x} - W_1^T \hat{\sigma}_1' V_1^T \dot{\hat{x}} \qquad (5\text{–}37)$$

$$+\tilde{W}_1^T \hat{\sigma}_1' \tilde{V}_1^T \dot{\hat{x}} + \hat{W}_1^T \hat{\sigma}_1' \tilde{V}_1^T \dot{\hat{x}} + \tilde{W}_1^T \hat{\sigma}_1' \hat{V}_1^T \dot{\hat{x}},$$

where $\tilde{W}_1(t) \triangleq W_1 - \hat{W}_1(t) \in \mathbb{R}^{n_1 \times 2}$, $\tilde{V}_1(t) \triangleq V_1 - \hat{V}_1(t) \in \mathbb{R}^{2 \times n_1}$ denote the estimated mismatches for the ideal weight estimates. Based on the subsequent stability analysis, the update laws $\dot{\hat{W}}_1(t) \in \mathbb{R}^{n_1 \times 2}$, $\dot{\hat{V}}_1(t) \in \mathbb{R}^{2 \times n_1}$ are designed as

$$\dot{\hat{W}}_1 \triangleq proj(\Gamma_{w1} \hat{\sigma}_1' \hat{V}_1^T \dot{\hat{x}} \tilde{x}^T), \ \dot{\hat{V}}_1 \triangleq proj(\Gamma_{v1} \dot{\hat{x}} \tilde{x}^T \hat{W}_1^T \hat{\sigma}_1'), \qquad (5\text{–}38)$$

where $\Gamma_{w1} \in \mathbb{R}^{n_1 \times n_1}$, $\Gamma_{v1} \in \mathbb{R}^{2 \times 2}$ are positive definite gain matrices. Based on (5–38),

$$\tilde{x}^T \left(\hat{W}_1^T \hat{\sigma}_1' \tilde{V}_1^T \dot{\hat{x}} + \tilde{W}_1^T \hat{\sigma}_1' \hat{V}_1^T \dot{\hat{x}} \right) + \dot{G}_2 = 0, \qquad (5\text{–}39)$$

where $G_2(t) \in \mathbb{R}$ is defined as

$$G_2 \triangleq \frac{1}{2} tr \left(\tilde{W}_1^T \Gamma_{w1}^{-1} \tilde{W}_1 \right) + \frac{1}{2} tr \left(\tilde{V}_1^T \Gamma_{v1}^{-1} \tilde{V}_1 \right).$$

By using the Mean Value Theorem, Assumptions $8 - 9$ and (5–38), the following inequalities can be obtained

$$N_1 \leq \rho_2(\|y\|) \|y\| + a_3, \qquad (5\text{–}40)$$

$$N_2 \leq a_4 \|z\| + a_5 \|z_f\| + a_6, \qquad (5\text{–}41)$$

where $N_1(y), N_2(y) \in \mathbb{R}$ are defined as

$$N_1 \triangleq W_1^T \sigma_1' V_1^T \dot{x}_d - \dot{\hat{W}}_1^T \hat{\sigma}_1(\hat{V}_1^T \hat{x}) - \hat{W}_1^T \hat{\sigma}_1' \dot{\hat{V}}_1^T \hat{x} - W_1^T \hat{\sigma}_1' V_1^T \dot{\hat{x}} + \tilde{W}_1^T \hat{\sigma}_1' \tilde{V}_1^T \dot{\hat{x}} \quad (5\text{–}42)$$

$$+\dot{\varepsilon}_1 + \dot{d} + \dot{g}_1(q, \dot{q}, \ddot{q}) - \dot{g}_1(q_d, \dot{q}_d, \ddot{q}_d),$$

$$N_2 \triangleq \hat{W}_1^T \hat{\sigma}_1' \tilde{V}_1^T \dot{\hat{x}} + \tilde{W}_1^T \hat{\sigma}_1' \hat{V}_1^T \dot{\hat{x}}, \qquad (5\text{–}43)$$

73

and $a_i \in \mathbb{R}$, $i = 4 - 7$ are positive constants, $\rho_2(\|y\|) \in \mathbb{R}$ is positive, globally invertible function and $y(t) \in \mathbb{R}^7$ is defined as $y(t) \triangleq \left(\begin{array}{cc} z^T(t) & z_f^T(t) \end{array} \right)^T$. By using (5–23), (5–26), (5–37), (5–42), and (5–43), the observer error system in (5–35) can be rewritten as

$$\dot{r} = -kr + N_1 + N_2. \tag{5–44}$$

5.4 Stability Analysis

Theorem 5.1. *The closed-loop system in (5–22) and the observer system in (5–33) together with the control law in (5–21) and (5–34) and the update laws in (5–17) and (5–38) ensure that all closed-loop signals are bounded, and the tracking error is semi-global uniformly ultimately bounded (SUUB) provided the control gains k, k_f, α, α_1, α_2 are selected according to the following conditions:*

$$\alpha_1 > \frac{1}{2}, \quad \alpha_2, k > 1, \quad k_f > 2, \tag{5–45}$$

$$\min(\alpha_1 - \frac{1}{2}, \alpha_2 - 1, \frac{1}{4}k_f - \frac{1}{2}) \quad > \quad a_5, \tag{5–46}$$

$$\min(\alpha - \frac{1}{2}, \frac{1}{2}k - \frac{1}{2}k_f \quad) > \quad 2a_4 + a_5, \tag{5–47}$$

where a_4, $a_5 \in \mathbb{R}$ are positive constants introduced in (5–41) .

Proof. Let $\mathcal{D} \subset \mathbb{R}^9$ be a domain containing $\varphi(t) = 0$, where $\varphi(t) \in \mathbb{R}^9$ is defined as

$$\varphi \triangleq \left(\begin{array}{ccc} y^T & \sqrt{G_1} & \sqrt{G_2} \end{array} \right)^T,$$

and consider the Lyapunov candidate function $V_L(\varphi) : \mathcal{D} \to \mathbb{R}$, which is continuously differentiable positive definite function defined as

$$V_L \triangleq \frac{1}{2}e^2 + \frac{1}{2}e_1^2 + \frac{1}{2}Je_2^2 + \frac{1}{2}\tilde{x}^T\tilde{x} + \frac{1}{2}r^Tr + G_1 + G_2, \tag{5–48}$$

which satisfies the following inequalities

$$U_1(\varphi) \leq V_L(\varphi, t) \leq U_2(\varphi). \tag{5–49}$$

In (5–49), $U_1(\varphi)$, $U_2(\varphi) \in \mathbb{R}$ are continuous positive definite functions defined as

$$U_1(\varphi) \triangleq \frac{1}{2} min(1, \xi_0) \left\| \varphi \right\|^2, \ U_2(\varphi) \triangleq max(1, \frac{1}{2}\xi_1) \left\| \varphi \right\|^2.$$

Taking time derivative of (5–48), substituting the dynamics in (5–22) and (5–44) , and using (5–28) yields

$$
\begin{aligned}
\dot{V}_L \ = \ & ee_1 - \alpha_1 e^2 + e_1 e_2 - \alpha_2 e_1^2 + (\hat{e}_2 - r_2) \left(\tilde{W}^T \hat{\sigma} + \hat{W}^T \hat{\sigma}' \tilde{V}^T X_d \right) \\
& + e_2 f_3 - k_f e_2 (e_2 + r_2) + r^T N_1 + r^T N_2 - k r^T r \\
& + \tilde{x}^T r - \tilde{x}^T \alpha \tilde{x} + \dot{G}_1 + \dot{G}_2.
\end{aligned}
$$

Using the Young's Inequality together with (5–18)−(5–20), (5–29) and (5–39)−(5–41) yields

$$
\begin{aligned}
\dot{V}_L \ \leq \ & -\left(\alpha_1 - \frac{1}{2} \right) e^2 - (\alpha_2 - 1) e_1^2 - \frac{1}{2} (k_f - 1) e_2^2 + a_1 \left\| r \right\| + a_2 \left\| z_f \right\| \\
& + \rho_1 (\left\| z_f \right\|) \left\| z_f \right\| \left| e_2 \right| + \frac{1}{2} k_f \left\| r \right\|^2 + \rho_2 (\left\| y \right\|) \left\| y \right\| \left\| r \right\| + a_3 \left\| r \right\| \\
& + 2 \left\| z \right\| (a_4 \left\| z \right\| + a_5 \left\| z_f \right\| + a_6) - \left(k - \frac{1}{2} \right) r^T r - \left(\alpha - \frac{1}{2} \right) \tilde{x}^T \tilde{x},
\end{aligned}
$$

which can be rewritten as

$$
\begin{aligned}
\dot{V}_L \ \leq \ & -2\lambda_1 \left\| z_f \right\|^2 - 2\lambda_2 \left\| z \right\|^2 + a_2 \left\| z_f \right\| + (a_1 + 2a_6) \left\| z \right\| - \frac{1}{4} k r^T r + a_3 \left\| r \right\| \\
& - \frac{1}{4} k r^T r + \rho_2 (\left\| y \right\|) \left\| y \right\| \left\| r \right\| - \frac{1}{4} k_f e_2^2 + \rho_1 (\left\| z_f \right\|) \left\| z_f \right\| \left| e_2 \right|,
\end{aligned}
$$

where λ_1, $\lambda_2 \in \mathbb{R}$ are positive constants that can be made arbitrarily large by increasing the control gains k, k_f, α, α_1, α_2, which are defined as

$$
\begin{aligned}
\lambda_1 \ &\triangleq \ \frac{1}{2} \left(min(\alpha_1 - \frac{1}{2}, \alpha_2 - 1, \frac{1}{4} k_f - \frac{1}{2}) - a_5 \right), \\
\lambda_2 \ &\triangleq \ \frac{1}{2} \left(min(\alpha - \frac{1}{2}, \frac{1}{2} k - \frac{1}{2} - \frac{1}{2} k_f) - (2a_4 + a_5) \right).
\end{aligned}
$$

By completing the squares, the following inequality can be upper bounded as

$$\dot{V}_L \leq -\left(\lambda_1 - \frac{\rho_1^2}{k_f}\right)\|z_f\|^2 - \lambda_2\|z\|^2 + \frac{\rho_2^2}{k}\|y\|^2 + \lambda_3$$

$$\leq -\lambda_4\|y\|^2 + \lambda_3,$$

where $\lambda_3,\ \lambda_4 \in \mathbb{R}$ are defined as

$$\lambda_3 \triangleq \frac{a_2^2}{4\lambda_1} + \frac{(a_1 + 2a_6)^2}{4\lambda_2} + \frac{a_3^2}{k},$$

$$\lambda_4 \triangleq min\left(\lambda_1 - \frac{\rho_1^2}{k_f} - \frac{\rho_2^2}{k}, \lambda_2 - \frac{\rho_2^2}{k}\right).$$

If $\|y(0)\|^2 > \frac{\lambda_3}{\lambda_4}$ and the sufficient conditions in (5–45)–(5–47) are satisfied, $V(t)$ is asymptotically decreasing until $\|y(t)\|^2$ enters the ultimate bound $\frac{\lambda_3}{\lambda_4}$. The region of attraction $\mathcal{D}$ is defined as

$$\mathcal{D} \triangleq \left\{\varphi(t) \subset \mathbb{R}^9 \mid \|\varphi\| \leq \min(\rho^{-1}(\lambda k k_f), \rho_2^{-1}(\sqrt{\lambda_2 k}))\right\}, \tag{5–50}$$

where $\rho^{-1}(\cdot) \in \mathbb{R}$ is the inverse of the function $\rho(\cdot) \triangleq k\rho_1^2 + k_f\rho_2^2 \in \mathbb{R}$, . The region of attraction $\mathcal{D}$ in (5–50) can be made arbitrarily large to include any initial condition by increasing the control gain k and k_f (i.e., a semi-global type of stability result). The ultimate bound $\frac{\lambda_3}{\lambda_4}$ can be made arbitrarily small by increasing the control gain k and k_f. Hence, the tracking error is semi-global uniformly ultimately bounded (SUUB).

The inequality in (5–49) and the fact that $\dot{V}(t) \leq 0$ when $\|y(t)\|^2 > \frac{\lambda_3}{\lambda_4}$ can be used to show that $e(t), e_1(t), e_2(t), \tilde{x}(t), r(t), G_1(t), G_2(t) \in \mathcal{L}_\infty$ in $\mathcal{D}$. Given $e(t), e_1(t), e_2(t), \tilde{x}(t), r(t) \in \mathcal{L}_\infty$ in $\mathcal{D}$ and using (5–1), (5–2), and (5–26), standard linear analysis methods can be used to prove that $\dot{e}_1(t), \dot{e}_2(t), \dot{\tilde{x}}(t) \in \mathcal{L}_\infty$ in $\mathcal{D}$. Using (4–9), (5–1), (5–2), and the assumption that $q_d(t)$ and its derivatives are bounded up to third order, $q(t), \dot{q}(t), \ddot{q}(t) \in \mathcal{L}_\infty$ in $\mathcal{D}$ can be proven. Given $q(t), \dot{q}(t), \ddot{q}(t), \dot{\tilde{x}}(t) \in \mathcal{L}_\infty$ and using (5–25), it can be shown that $\hat{q}(t), \dot{\hat{q}}(t), \ddot{\hat{q}}(t) \in \mathcal{L}_\infty$ in $\mathcal{D}$. Using (5–4), it can be shown $\hat{e}_2(t) \in \mathcal{L}_\infty$ in $\mathcal{D}$. Given W, V, W_1, V_1 are bounded by assumptions and $\hat{W}(t), \hat{V}(t), \hat{W}_1(t), \hat{V}_1(t)$ are bounded by using $proj(\cdot), u(t) \in \mathcal{L}_\infty$ in (5–21) in $\mathcal{D}$ can be shown.

Given $\dot{e}_1(t)$, $\dot{e}_2(t)$, $\dot{\tilde{x}}(t) \in \mathcal{L}_\infty$ and using (5–35), it can be shown that $\mu(t) \in \mathcal{L}_\infty$ in $\mathcal{D}$. The definition for $\varphi(t)$ can be used to prove that $\varphi(t)$ is continuous in $\mathcal{D}$. $\qquad\square$

5.5 Simulation

Simulations are performed using a modified muscle model given in [70]. The controller computes a voltage as the input to the simulated muscle dynamics. The simulation results are shown in Figures 5-1−5-4. for the control gains

$$
\begin{aligned}
k_f &= 0.05,\ \alpha_1 = 20,\ \alpha_2 = 20, \\
\Gamma_w &= diag([1,1,1,1,1,0.1]) * 0.01, \\
\Gamma_v &= diag([1,1,0.1,0.01]) * 0.01, \\
k &= diag([96,112]),\ \alpha = 20, \\
\Gamma_{w_1} &= [0.02, 0.02, 0.02, 0.02, 0.02]^T, \\
\Gamma_{v_1} &= [0.02, 0.02, 0.02, 0.02, 0.02].
\end{aligned}
$$

Figure 5-1 and Figure 5-2 depict the tracking performance. The control input depicted in Figure 5-3 is within a typical range for quadriceps stimulation. Figure 5-4 depicts the acceleration estimation.
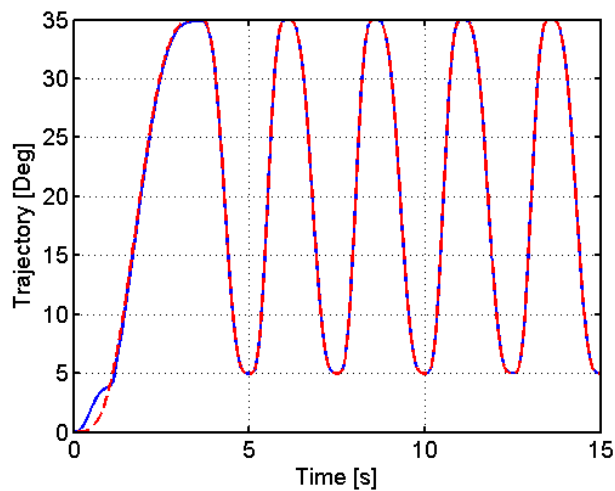

Figure 5-1. Actual (solid) and desired (dashed) trajectories
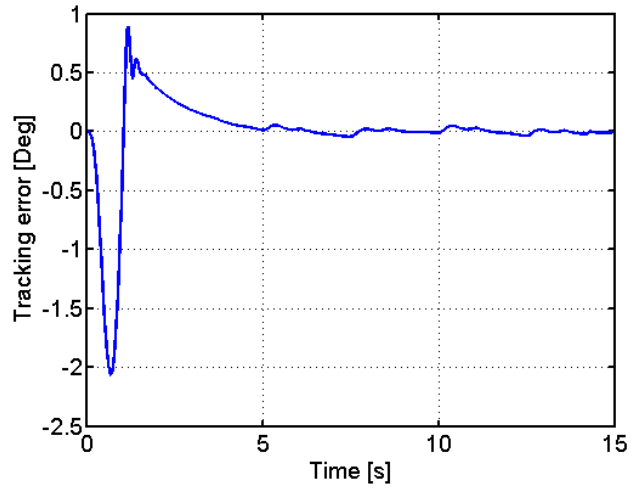
Figure 5-2. Limb position tracking error
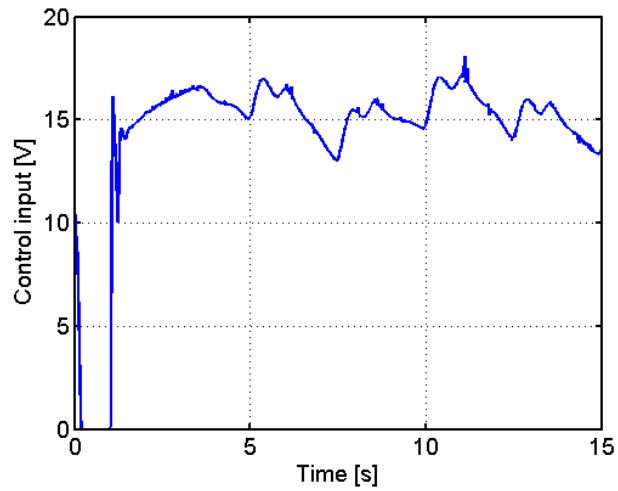
Figure 5-3. Unmodulated input control voltage
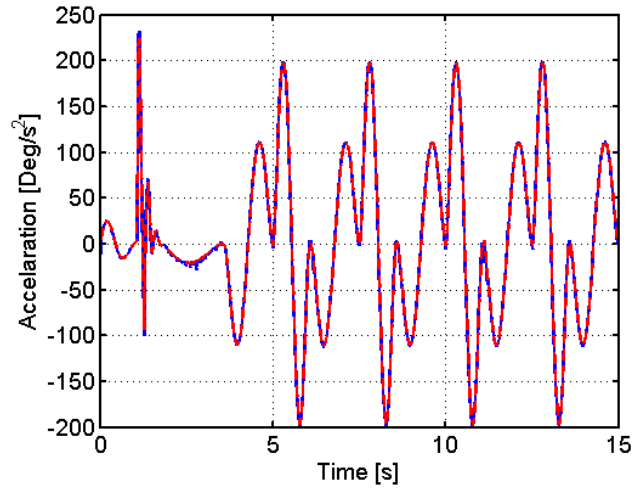
Figure 5-4. Estimated (solid) and actual (dashed) accelerations

CHAPTER 6
IDENTIFICATION-BASED CLOSED-LOOP NEUROMUSCULAR ELECTRICAL STIMULATION LIMB TRACKING WITH A PULSED MODULATED CONTROL INPUT

In Chapter 4, a NMES controller is designed and analyzed considering the pulse modulated control input which brings together an analysis of the controller and modulation scheme. A limitation of the design is that acceleration has to be used to implementation of the controller because the acceleration obtained from position derivation is noisy. In Chapter 5, an identification-based controller is developed for the muscle-limb model which includes an uncertain first order dynamic system that models muscle contraction dynamics. The controller developed can be implemented by only using position and velocity signals. In this chapter, based on the two approaches in Chapters 4 and 5, a muscle activation model with a pulse modulated control input is developed to capture the discontinuous nature of muscle activation, and an identification-based closed-loop NMES controller is designed and analyzed for the uncertain pulse muscle activation model. A feedforward NN term is included in the controller to achieve better tracking performance. Semi-global uniformly ultimately bounded (SUUB) tracking is guaranteed. The closed-loop system is analyzed through Lyapunov-based methods and a pulse frequency related gain condition is obtained. Experiment results are provided to illustrate the performance of the developed controller.

6.1 Muscle Activation and Limb Model

The dynamics used in this chapter are the same as those in the Chapter 4.

6.2 Controller Development

The control objective is to ensure the knee angle $q(t)$ tracks a desired trajectory, denoted by $q_d(t) \in \mathbb{R}$, which is an essential task in many rehabilitative exercises and function restoration tasks. To quantify the tracking objective, a lower limb angular tracking error, denoted by $e_1(t) \in \mathbb{R}$, is defined in (3–1). To facilitate the subsequent control design and stability analysis, filtered tracking errors denoted by $e_2(t)$, $e_3(t) \in \mathbb{R}$,

are also defined in (3–2) and (3–3). An error estimation is designed based on (5–3) as in (5–4).

To facilitate the subsequent analysis, let $f_{2d}(q_d, \dot{q}_d, \ddot{q}_d) \in \mathbb{R}$ be defined as

$$
\begin{aligned}
f_{2d} \triangleq \ & b^{-1}(q_d, \dot{q}_d) f_1(q_d, \dot{q}_d) - J_I b^{-1}(q_d, \dot{q}_d) \zeta^{-2}(q_d) \dot{\zeta}(q_d, \dot{q}_d) \ddot{q}_d \\
& + J_I b^{-1}(q_d, \dot{q}_d) A_f(q_d, \dot{q}_d) \zeta^{-1}(q_d) \ddot{q}_d + b^{-1}(q_d, \dot{q}_d) \zeta^{-1}(q_d) A_f(q_d, \dot{q}_d) \\
& (M_e(q_d) + M_g(q_d) + M_v(\dot{q}_d)) + b^{-1}(q_d, \dot{q}_d) \zeta^{-1}(q_d) \\
& \left(\dot{M}_e(q_d, \dot{q}_d) + \dot{M}_g(q_d, \dot{q}_d) + \dot{M}_v(\dot{q}_d, \ddot{q}_d) \right) - b^{-1}(q_d, \dot{q}_d) \zeta^{-2}(q_d) \dot{\zeta}(q_d, \dot{q}_d) \\
& (M_e(q_d) + M_g(q_d) + M_v(\dot{q}_d)).
\end{aligned}
\tag{6–1}
$$

Based on the universal function approximation property [69], the unknown function in (6–1) can be approximated by a multi-layer NN which is defined as

$$
f_{2d} = W^T \sigma\left(V^T X_d\right) + \varepsilon,
\tag{6–2}
$$

where $X_d(q_d, \dot{q}_d, \ddot{q}_d) \in \mathbb{R}^4$ is defined as in (5–7), and $W \in \mathbb{R}^{n_0 \times 1}$, $V \in \mathbb{R}^{4 \times n_0}$ denote the bounded ideal weights for the hidden layer neurons and the input layer neurons, respectively, where the number of hidden layer neurons is selected as n_0, and $\varepsilon(X_d) \in \mathbb{R}$ denotes the reconstruction error. Since $X_d(q_d, \dot{q}_d, \ddot{q}_d)$ depends on the known bounded desired trajectory, the NN input is guaranteed to lie on a compact set.

Assumption 10: The activation function $\sigma(\cdot)$ and its first order derivative with respect to its arguments $\sigma'(\cdot)$ are bounded by known constants [47].

Assumption 11: The reconstruction error $\varepsilon(X_d)$ and its first order derivative $\varepsilon'(X_d)$ are bounded by known constants [47].

By using (4–9) $-$(5–2) and (6–2), the open-loop error system for $e_2(t)$ is

$$
\begin{aligned}
J\dot{e}_2 = \ & -\frac{1}{2}\dot{J}e_2 + f_2 - f_{2d} + W^T \sigma\left(V^T X_d\right) + \frac{1}{2}\dot{J}e_2 - J\alpha_1^2 \dot{e} \\
& + J(\alpha_1 + \alpha_2)\dot{e}_1 + J\dddot{q}_d + \tau_2 + \varepsilon - u.
\end{aligned}
\tag{6–3}
$$

Let $\hat{W}(t) \in \mathbb{R}^{n_0 \times 1}$, $\hat{V}(t) \in \mathbb{R}^{4 \times n_0}$ be the estimated weights for W, V, and $\sigma(X_d, t)$, $\hat{\sigma}(X_d, t)$, $\hat{\sigma}'(X_d, t)$, $\tilde{\sigma}(X_d, t)$, $\tilde{W}(t) \in \mathbb{R}^{n_0 \times 1}$, $\tilde{V}(t) \in \mathbb{R}^{4 \times n_0}$ be defined as (5–9)−(7–7). By using a Taylor series approximation, $\tilde{\sigma}(X_d, t)$ can be expressed as $\tilde{\sigma} = \hat{\sigma}' \tilde{V}^T X_d + o(\tilde{V}^T X_d)^2$, where $o(\cdot)^2 \in \mathbb{R}^{n_0 \times 1}$ denotes higher order terms. By using (5–9)−(7–7), $W^T \sigma(V^T X_d)$ can be expressed as

$$W^T \sigma(V^T X_d) \;\; = \;\; \hat{W}^T \hat{\sigma}' \tilde{V}^T X_d + W^T \hat{\sigma} + \tilde{W}^T \hat{\sigma}' \tilde{V}^T X_d + W^T o(\tilde{V}^T X_d)^2. \tag{6–4}$$

The update laws $\dot{\hat{W}}(t) \in \mathbb{R}^{n \times 1}$, $\dot{\hat{V}}(t) \in \mathbb{R}^{4 \times n}$ can be arbitrarily selected as

$$\dot{\hat{W}} \triangleq proj(\cdot), \dot{\hat{V}} \triangleq proj(\cdot), \tag{6–5}$$

where $proj(\cdot)$ is a smooth projection operator [62]. Gradient-based update laws were used in the following experiments. Since $proj(\cdot)$ guarantees $\hat{W}(t), \hat{V}(t)$ are bounded,

$$\left| \hat{W}^T \hat{\sigma} \right| \leq a_1, \tag{6–6}$$

where $a_1 \in \mathbb{R}$ is a known positive constant.

The error system in (6–3) can be expressed as

$$J \dot{e}_2 \;\; = \;\; -\frac{1}{2} \dot{J} e_2 + f_3 + \hat{W}^T \hat{\sigma} - u, \tag{6–7}$$

where $f_3(q, \dot{q}, \ddot{q}, q_d, \dot{q}_d, \ddot{q}_d, t) \in \mathbb{R}$ is defined as

$$\begin{aligned} f_3 \;\; &\triangleq \;\; f_2 - f_{2d} + \tilde{W}^T \hat{\sigma} + \hat{W}^T \hat{\sigma}' \tilde{V}^T X_d + \tilde{W}^T \hat{\sigma}' \tilde{V}^T X_d + W^T o(\tilde{V}^T X_d)^2 \\ &\quad - J \alpha_1^2 \dot{e} + J(\alpha_1 + \alpha_2) \dot{e}_1 + \frac{1}{2} \dot{J} e_2 + J \dddot{q}_d + \varepsilon + \tau_2. \end{aligned}$$

Since $W, V, \sigma(\cdot)$, and $\varepsilon(X_d)$ are bounded, using the Mean Value Theorem, (6–5), and the assumption that $\dddot{q}_d(t)$ is bounded, $f_3(q, \dot{q}, \ddot{q}, q_d, \dot{q}_d, \ddot{q}_d, \dddot{q}_d, t) \in \mathbb{R}$ can be bounded as

$$|f_3| \leq a_2 + \rho_1(\|z_f\|) \|z_f\|, \tag{6–8}$$

where $a_2 \in \mathbb{R}$ is a positive constant, $z_f(e(t), e_1(t), e_2(t)) \in \mathbb{R}^3$ is defined as $z_f \triangleq \begin{pmatrix} e & e_1 & e_2 \end{pmatrix}^T$, and $\rho_1(\|z_f\|) \in \mathbb{R}$ is a positive, globally invertible function. Based on (6–7), (6–5), and the subsequent stability analysis, the control input is designed as

$$v = k_f \hat{e}_2 + \hat{W}^T \hat{\sigma}, \tag{6–9}$$

where $k_f \in \mathbb{R}$ is a positive control gain. After substituting (4–7), (6–9) into (6–7), the closed-loop error system can be obtained as

$$J\dot{e}_2 = \begin{cases} -\frac{1}{2}\dot{J}e_2 + f_3 - k_f\hat{e}_2, & nT \le t < nT + d \\ -\frac{1}{2}\dot{J}e_2 + f_3 + \hat{W}^T\hat{\sigma}, & otherwise \end{cases}, \tag{6–10}$$

$$n = 0, 1, 2, 3...$$

6.3   Observer Design

The development of the observer is the same as that in Chapter 5.

6.4   Stability Analysis

Theorem 6.1. *The controller in (4–7) and (5–34) along with the update laws in (6–5) and (5–38), and the observer in (5–33) ensure that all closed-loop signals are bounded, and the tracking error is semi-global uniformly ultimately bounded (SUUB) in the sense that $\|\varphi(t)\|$ uniformly converges to a ball with a constant radius provided the control gains are selected sufficiently large based on the initial conditions of the states (see the subsequent stability analysis) and the following sufficient conditions are satisfied:*

$$\alpha_1 > \frac{1}{2}, \quad \alpha_2, k > 1, \quad k_f > 2, \tag{6–11}$$

$$\min(\alpha_1 - \frac{1}{2}, \alpha_2 - 1, \frac{1}{4}k_f - \frac{1}{2}) \quad > \quad \frac{1}{2}a_5, \tag{6–12}$$

$$\min(\alpha - \frac{1}{2}, \frac{1}{2}k - \frac{1}{2}k_f - \frac{1}{2} - \frac{1}{2}a_5) \quad > \quad a_4, \tag{6–13}$$

$$\gamma_1\left(\frac{d}{T-d}\right) \quad > \quad \gamma_3, \tag{6–14}$$

83

where a_4, $a_5 \in \mathbb{R}$ *are positive constants introduced in (5–41)*, T, $d \in \mathbb{R}$ *are introduced in (4–7)*, $\gamma_3 \in \mathbb{R}$ *is a known positive bounding constant, and* $\gamma_1 \in \mathbb{R}$ *is a gain constant that can be made arbitrarily large by selecting* $\alpha_1, \alpha_2, k_f, k \in \mathbb{R}$ *in (5–1),(5–2), (6–9), and (5–34) arbitrarily large.*

Proof. Consider the Lyapunov candidate function $V(\varphi) : \mathbb{R}^7 \to \mathbb{R}$, which is continuously differentiable positive definite function defined as

$$V \triangleq \frac{1}{2}e^2 + \frac{1}{2}e_1^2 + \frac{1}{2}Je_2^2 + \frac{1}{2}\tilde{x}^T\tilde{x} + \frac{1}{2}r^Tr, \tag{6–15}$$

which satisfies the following inequalities

$$\beta_1 \|\varphi\|^2 \leq V \leq \beta_2 \|\varphi\|^2, \tag{6–16}$$

where β_1, $\beta_2 \in \mathbb{R}$ are positive constants defined as $\beta_1 \triangleq \frac{1}{2}\min(1, \xi_0)$, $\beta_2 \triangleq \frac{1}{2}\max(1, \xi_1)$. Taking time derivative of (6–15, substituting the dynamics in (6–7) and (5–44) and using (5–2) and (5–28) yields

$$\begin{aligned}
\dot{V} &= ee_1 - \alpha_1 e^2 + e_1 e_2 - \alpha_2 e_1^2 + e_2 f_3 + e_2 \hat{W}^T\hat{\sigma} - e_2 u + r^T N_1 + r^T N_2 \\
&\quad -kr^Tr + \tilde{x}^Tr - \tilde{x}^T\alpha\tilde{x}.
\end{aligned}$$

The function $V(\varphi(t))$ can be expressed in segments $V_n(\varphi, \tau)$, where $V_n(\varphi, \tau) \in \mathbb{R}$ is defined as

$$V_n(\varphi, \tau) \triangleq V(\varphi(nT + \tau)), \tag{6–17}$$

where $\tau \triangleq t - nT$, $n \triangleq \lfloor t/T \rfloor$. Using the Young's Inequality together with (6–8), (5–29), (5–40), and (5–41) on the interval $0 \leq \tau < d$, yields

$$\begin{aligned}
\dot{V}_n(\varphi, \tau) \leq &-2\lambda_1 \|z_f\|^2 - \lambda_2 \|z\|^2 + a_2 \|z_f\| - \frac{1}{4}kr^Tr + (a_3 + a_6)\|r\| \\
&-\frac{1}{4}kr^Tr + \rho_2(\|\varphi\|)\|\varphi\|\|r\| - \frac{1}{4}k_f e_2^2 + \rho_1(\|z_f\|)\|z_f\||e_2|,
\end{aligned}$$

where $\lambda_1,\ \lambda_2 \in \mathbb{R}$ are defined as

$$
\begin{aligned}
\lambda_1 &\triangleq \frac{1}{2}\left(\min(\alpha_1 - \frac{1}{2}, \alpha_2 - 1, \frac{1}{4}k_f - \frac{1}{2}) - \frac{1}{2}a_5\right), \\
\lambda_2 &\triangleq \min(\alpha - \frac{1}{2}, \frac{1}{2}k - \frac{1}{2}k_f - \frac{1}{2} - \frac{1}{2}a_5) - a_4,
\end{aligned}
$$

provided the sufficient conditions in (6–11)−(6–13) are satisfied. Completing the squares yields

$$
\dot{V}_n \ (\varphi, \tau) \le \ -\left(\lambda_1 - \frac{\rho_1^2}{k_f}\right)\|z_f\|^2 - \lambda_2\|z\|^2 + \frac{\rho_2^2}{k}\|\varphi\|^2 + \frac{a_2^2}{4\lambda_1} + \frac{(a_3 + a_6)^2}{k}. \quad (6\text{–}18)
$$

Let a set $\mathcal{D}$ be defined as

$$
\mathcal{D} \triangleq \left\{ \varphi\,(t) \subset \mathbb{R}^7 \mid \|\varphi\| \le \min(\rho^{-1}\,(\lambda_1 k k_f)\,, \rho_2^{-1}\left(\sqrt{\lambda_2 k}\right)) \right\}, \quad (6\text{–}19)
$$

where $\rho^{-1}\,(\cdot) \in \mathbb{R}$ is the inverse of the function $\rho\,(\cdot) \triangleq k\rho_1^2 + k_f\rho_2^2 \in \mathbb{R}$. Using (6–16), (6–18) can be rewritten as

$$
\dot{V}_n\,(\varphi, \tau) \le -\gamma_1 V_n + \gamma_2,\ \forall\,\|\varphi\| \in \mathcal{D}, \quad (6\text{–}20)
$$

where $\gamma_1,\ \gamma_2 \in \mathbb{R}$ are defined as

$$
\begin{aligned}
\gamma_1 &\triangleq \frac{1}{\beta_2}\min\left(\lambda_1 - \frac{\rho_1^2}{k_f} - \frac{\rho_2^2}{k}, \lambda_2 - \frac{\rho_2^2}{k}\right), \\
\gamma_2 &\triangleq \frac{a_2^2}{4\lambda_1} + \frac{(a_3 + a_6)^2}{k}.
\end{aligned}
$$

The region of attraction $\mathcal{D}$ in (6–19) can be made arbitrarily large to include any initial condition by increasing the control gain k and k_f (i.e., a semi-global result).

Likewise, on the interval $d \le \tau < T$,

$$
\dot{V}_n(\varphi, \tau) \ \le \ \frac{1}{2}\gamma_3 V_n(\varphi, \tau) + \gamma_4 \quad (6\text{–}21)
$$

where $\gamma_3,\ \gamma_4 \in \mathbb{R}$ are known positive bounding constants that depend on constants defined in (6–8), (5–29), (5–40), and (5–41), which are independent of the gain selection.

Using (6–15) and (6–17), $\dot{V}_n(\varphi, \tau)$ is

$$\dot{V}_n(\varphi, \tau) \leq \begin{cases} -\gamma_1 V_n(\varphi, \tau) + \gamma_2, & 0 \leq \tau < d \\ \gamma_3 V_n(\varphi, \tau) + \gamma_4, & d \leq \tau < T \end{cases},$$

which can be solved to obtain $V_n(\varphi, d)$ and $V_n(\varphi, T)$ as

$$V_n(\varphi, d) \leq \left(V_n(\varphi, 0) - \frac{\gamma_2}{\gamma_1} \right) e^{-\gamma_1 d} + \frac{\gamma_2}{\gamma_1}, \tag{6–22}$$

$$V_n(\varphi, T) \leq \left(V_n(\varphi, d) + \frac{\gamma_4}{\gamma_3} \right) e^{\gamma_3(T-d)} - \frac{\gamma_4}{\gamma_3}. \tag{6–23}$$

By using (6–22) and (6–23), and the fact that $V_{n+1}(z, 0) = V_n(z, T)$,

$$\begin{aligned} \tilde{V}_n &\triangleq V_{n+1}(\varphi, 0) - V_n(\varphi, 0), \tag{6–24} \\ &\leq V_n(\varphi, d)e^{\gamma_3(T-d)} - V_n(\varphi, 0) + \frac{\gamma_4}{\gamma_3}(e^{\gamma_3(T-d)} - 1), \\ &\leq V_n(\varphi, 0)(e^{-\gamma_1 d}e^{\gamma_3(T-d)} - 1) + \frac{\gamma_2}{\gamma_1}(1 - e^{-\gamma_1 d})e^{\gamma_3(T-d)} \\ &\quad + \frac{\gamma_4}{\gamma_3}(e^{\gamma_3(T-d)} - 1). \end{aligned}$$

If the condition in (6–14) is satisfied and $V(\varphi(nT)) > \beta_1 \bar{d}^2$, then $V(\varphi(nT)) < V(\varphi((n+1)T))$ i.e.,

$$V(\varphi(0)) > V(\varphi(T)) > V(\varphi(2T)) > \cdots \tag{6–25}$$

where $\bar{d} \in \mathbb{R}$ is defined as

$$\bar{d} \triangleq \sqrt{\frac{\frac{\gamma_4}{\gamma_3}(1 - e^{-\gamma_3(T-d)}) + \frac{\gamma_2}{\gamma_1}(1 - e^{-\gamma_1 d})}{\beta_1(e^{-\gamma_3(T-d)} - e^{-\gamma_1 d})}}, \tag{6–26}$$

and the size of $\bar{d}$ is determined based on the period, pulse width, and control gains.

Given (6–15), (6–16), (6–19), and (6–25), $\|e(t)\|$ is semi-global uniformly ultimately bounded [68, Theorem 4.18]in the sense that

$$\|e(t)\| \leq \|\varphi(t)\| < \bar{d}, \ \forall t \geq \overline{T}(\bar{d}, \|\varphi(0)\|), \forall \|\varphi(0)\| \in \mathcal{D},$$

Table 6-1. The tracking errors for a sinusoidal trajectory with a period of 2.5s and ROM between 5° and 60° (Data are coming from Table 4-1). The stimulation frequency is 30Hz.

Subject	RMS	Steady state RMS (10-20s)	Steady state peak (10-20s)
A-left	4.01	3.26	5.18
A-right	4.07	3.43	3.75
B-left	4.41	3.44	6.35
B-right	3.91	3.19	5.27
C-left	3.83	3.83	8.44
C-right	4.03	3.89	4.61
Mean	4.04	3.51	5.60
STD	0.18	0.27	1.49

where $\overline{T}\left(\bar{d}, \|\varphi(0)\|\right) \in \mathbb{R}$ is a positive constant that denotes the ultimate time to reach the ball. □

6.5   Experiments

The proposed controller was implemented on able-bodied volunteers (3 males, ages 26-42 yrs.) to evaluate the performance. The same test bed and procedure were used as in Chapter 2. The stimulation frequency was 30Hz and no weight was attached to the weight bar. No low-pass filter was used to smooth the feedback signals. Any sufficiently smooth desired trajectory could have been selected. One trajectory was a sinusoidal trajectory with a period of 2.5s and range of motion (ROM) between 5° and 60° which was used in Chapter 4 (see Figure 6-1).

To illustrate that the proposed controller can achieve better results, the tracking errors using the controller proposed in Chapter 4 is re-listed in Table 6-1. Note that Table 6-1 is the same date as in Table 4-1, printed here for comparison. The steady state RMS and peak error were calculated from the interval 10-20s.

The experiments results from the proposed controller in this chapter are summarized in Table 6-2. Same subjects were used as in Chapter 4. The peak tracking error was calculated as $max(|e(t)|)$. The steady state RMS and peak errors using the proposed controller are both statistically lower (student T-test, one tail, paired, p<0.05) than the results obtained using the controller in Chapter 4. No statistical difference was

determined in the total RMS error because the controller with a feedforward NN term

had bigger transient errors. A representative trial (i.e., A-left in Table 6-2) is shown in

Figures 6-2 and 6-3.

Table 6-2. The tracking errors for a sinusoidal trajectory with a period of 2.5s and ROM
between 5° and 60°. The stimulation frequency is 30Hz. The * indicates a
statistically significant difference (p<0.05) when compared to the results from
Chapter4 (Table 6-1).

| Subject	RMS	Steady state RMS	Steady state peak
A-left	4.69	1.82	5.18
A-right	4.47	1.42	3.75
B-left	2.91	2.22	6.35
B-right	3.24	2.43	5.27
C-left	6.05	3.18	8.44
C-right	4.95	2.13	4.61
Mean	4.37	2.20*	5.60*
STD	1.05	0.54	1.49
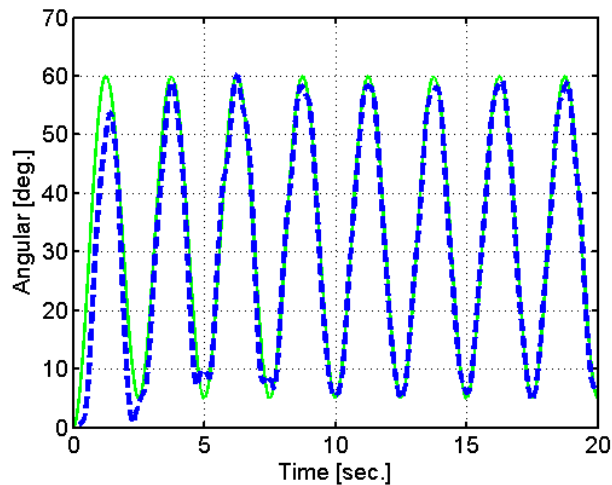
Figure 6-1. Performance of a representative sinusoidal trajectory tracking experiment.
The desired trajectory is plotted as a solid line and the measured trajectory
is plotted as a dashed line.

To illustrate the ability of tracking more complex trajectories, an irregular continuous

trajectory with varied period and ROM was selected (see Figure 6-4). The tracking

errors are summarized in Table 6-3. A comparable tracking performance was achieved.

A representative trial (i.e. D-left in Table 6-3) is given in Figure 6-4.
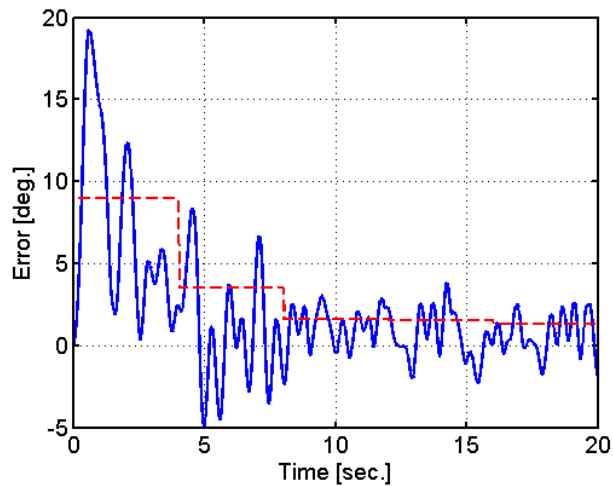
Figure 6-2. Tracking error of a representative sinusoidal trajectory tracking experiment. The tracking error is plotted as a solid line and the RMS error over every 4 seconds is plotted as a dashed line.

Table 6-3. The tracking errors for an irregular trajectory

| Subject	RMS	Peak
A-left	3.89	10.1
A-right	3.45	13.6
B-left	3.89	13
B-right	3.45	13.15
D-left	2.73	8.49
Mean	3.48	11.67
STD	0.42	2.01
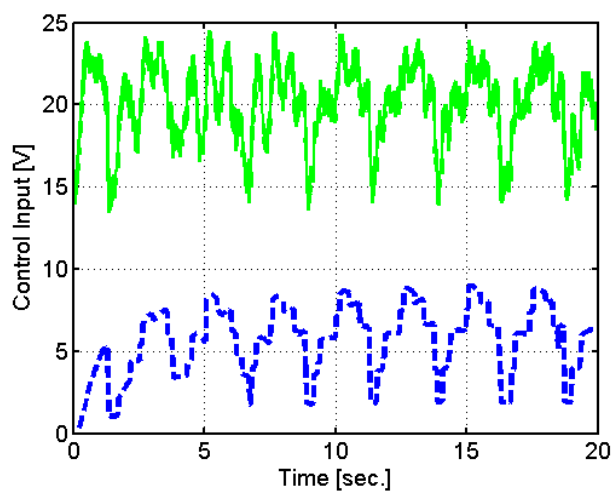
Figure 6-3. Control input (Voltage) for a representative sinusoidal trajectory tracking experiment. The total control input is plotted as a solid line and the contribution of NN is plotted as a dashed line.
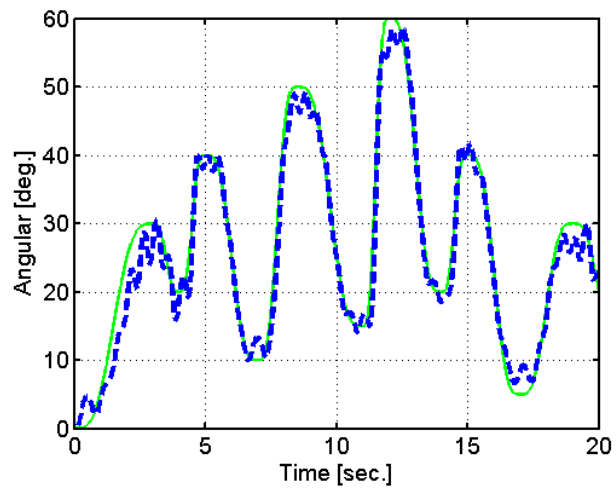
Figure 6-4. Trajectory tracking performance of an irregular trajectory. The desired trajectory is plotted as a solid line and the measured trajectory is plotted as a dashed line.

CHAPTER 7
HYBRID NEUROMUSCULAR ELECTRICAL STIMULATION TRACKING CONTROL OF ANKLE

NMES is an effective rehabilitation tool for gait retraining for individuals suffering from various neurological disorders. Traditionally, NMES is only delivered to activate ankle dorsiflexor muscles during the swing phase of the gait to correct "foot drop". Recent research indicates that improved functional ambulation can be achieved by delivering NMES to both the plantarflexor and dorsiflexor muscles during gait. Closed-loop electrical stimulation has the potential to yield positive rehabilitative outcomes by enabling accurate and precise limb motions during gait retraining. Naturally, the motion of ankle during gait is an event-driven system combining continuous evolution of the angle between the foot and shank, alternate moving segments of the foot and shank, and alternate activation of the plantarflexor and dorsiflexor muscles. In this chapter, a switched sliding mode based controller is developed to ensure that the ankle tracks a designed or recorded normal trajectory during gait which can be used for gait retraining. Semi-global asymptotic tracking of the hybrid controller is analyzed using multiple Lyapunov functions and the performance is illustrated though simulations.

7.1 Muscle Activation and Limb Model

While the arcs of ankle motion during walking are not large, they are critical for progression and shock absorption during stance [42]. During normal gait, the arcs of ankle motion continuously plantarflex and then dorsiflex. During the stance phase, the ankle plantarflexes, dorsiflexes and then plantarflexes again. During the swing phase the ankle only dorsiflexes. The activated muscles switch between dorsiflexor and plantarflexor muscles during each gait cycle.

Each gait cycle starts from heel strike, the beginning of the stance phase. The ankle position starts at neutral. The dorsiflexor muscle (tibialis anterior) becomes active immediately after heel strike to toe strike to decelerate the rate of plantar flexion, which contributes to shock absorption, body weight acceptance, and limb progression.

Throughout heel strike to toe strike phase, the moving segment is the foot and the leg remains relatively stationary. After toe strike, the forefoot contacts the floor and the foot becomes stationary. The moving segment is the leg (shank). The plantarflexor (calf muscles) gradually increases eccentric contraction to control ankle dorsiflexion and provide critical stabilization that allows both the foot and tibia to move forward and provide forward propulsion (push-off). By the end of terminal stance, with the weight shifting to the other leg, the stabilizing force in the foot goes away, and the foot is free to plantarflex corresponding to the activation of plantarflexor muscle (gastrosoleus) while the onset of dorsiflexor muscle (tibialis anterior) activity decelerates the foot fall (this coactivation of dorsiflexor and plantarflexor muscles is modeled as the activation of plantarflexor muscles only for simplicity). At toe-off, the swing phase begins and the second arc of dorsiflexion starts. Dorsiflexor muscles activate again to lift the foot clear of the ground. At the end of the swing phase the ankle position returns to neutral preparing for heel contact [42]. A summary of the gait cycle is provided in Table 7-1.

Table 7-1. Summary of ankle motions, activated muscle groups, and limb movements during gait cycle

	Gait Cycle			
	Stance Phase			Swing Phase
Ankle Motion	Planta-	Dorsi-	Planta-	Dorsi-
Activated Muscle Group	Dorsi-	Planta-	Planta-	Dorsi-
Moving Part	Foot	Shank	Shank	Foot
Switching Signal	1	2	3	4

The dynamics of a muscle-limb system is modeled as the same as that in Chapter 2. To capture the switching property of gait cycle, the ankle dynamics can be modeled as

$$J_{\zeta_\sigma} \ddot{q} = -M_{\zeta_\sigma} - \tau_{d\zeta_\sigma} + u_\sigma, \qquad (7–1)$$

where $\sigma : [0, \infty) \to \mathcal{P}$, denotes a piecewise constant switching signal which can be expressed as

$$\sigma = p, \ p \in \mathcal{P} \triangleq \left\{ \ 1, \ \ 2, \ \ 3, \ \ 4 \ \right\}. \tag{7–2}$$

For example, $\sigma(t)$ could be the signal from foot switches indicating the transition of gait phases.

7.2 Control Design

The control objective is to ensure that the ankle follows designed or recorded ankle trajectories during normal gait, which is essential in rehabilitative exercises and function restoration.

To quantify the tracking objective and facilitate the subsequent control design and stability analysis, an angular position tracking error, denoted by $e(t) \in \mathbb{R}$ and a filtered tracking error, denoted by $r(t) \in \mathbb{R}$, are defined as in (2–9). The control objective is to ensure that the ankle follows designed or recorded ankle trajectories during normal gait, which is essential in rehabilitative exercises and function restoration.

Controllers are designed for each subsystem individually, which is indicated by a subscript $p \in \mathcal{P} \triangleq \left\{ \ 1, \ \ 2, \ \ 3, \ \ 4 \ \right\}$. Taking the derivative of $r(t)$ in (2–9), multiplying both sides by $J_{\zeta p,}$ and using (7–1) and (2–9), yields

$$J_{\zeta p}\dot{r} = J_{\zeta p}(\ddot{q}_d + \alpha \dot{e}) + M_{\zeta_p} + \tau_{d\zeta p} - u_p. \tag{7–3}$$

Based on (7–30 and the subsequent stability analysis, the control law is defined as

$$u_p = k_{s_p}r + e + \beta_p sgn(r), \tag{7–4}$$

where $k_{s_p}, \beta_p \in \mathbb{R}$ are adjustable gains, and $y(t) \in \mathbb{R}^2$ is defined as

$$y = \begin{bmatrix} e & r \end{bmatrix}. \tag{7–5}$$

93

After substituting (7–4) into (7–3) and performing some algebraic manipulation, the closed-loop error dynamics can be expressed as

$$J_{\zeta_p}\dot{r} = -\frac{1}{2}\dot{J}_{\zeta_p}r + \tilde{N}_p + N_{D_p} - k_{s_p}r - e - \beta_p sgn\left(r\right),\qquad(7\text{–}6)$$

where the auxiliary functions $N_p\left(\dot{e}, r, q, \dot{q}, \ddot{q}_d\right)$, $N_{D_p}\left(q_d, \dot{q}_d, \ddot{q}_d, t\right)$, $\tilde{N}_p\left(\dot{e}, r, q, \dot{q}, q_d, \dot{q}_d, \ddot{q}_d, t\right) \in \mathbb{R}$ are defined as

$$N_p \triangleq \frac{1}{2}\dot{J}_{\zeta_p}r + J_{\zeta_p}\left(\ddot{q}_d + \alpha\dot{e}\right) + M_{\zeta_p},\qquad(7\text{–}7)$$

$$\tilde{N}_p \triangleq N_p - J_{\zeta_p}\left(q_d\right)\ddot{q}_d - M_{\zeta_p}\left(q_d, \dot{q}_d\right),$$

$$N_{D_p} \triangleq J_{\zeta_p}\left(q_d\right)\ddot{q}_d + M_{\zeta_p}\left(q_d, \dot{q}_d\right) + \tau_{d\zeta_p}.$$

The following inequality can be developed based on Assumption 1 and 2,

$$\left|N_{D_p}\right| \leq \xi_{4_p},\qquad(7\text{–}8)$$

where $\xi_{4_p} \in \mathbb{R}$ is a known positive constant. The control gain k_c can be adjusted to reduce ξ_{4_p}. The Mean Value Theorem can be used to develop the following upper bound

$$\left|\tilde{N}_p\right| \leq \rho_p(\|y\|)\|y\|,\qquad(7\text{–}9)$$

where $\rho_p(\|y\|) \in \mathbb{R}$ is a positive, globally invertible function.

7.3 Stability Analysis

For each gait cycle, let $t_0 = 0$ and $t_4 = T$, where $T \in \mathbb{R}$ denotes the period of a gait cycle. The time interval between two switches, denoted by $T_i \in \mathbb{R}$, $i = 1, 2, 3, 4$, is defined as

$$T_i = t_i - t_{i-1},\qquad(7\text{–}10)$$

where t_i denote the switching times. Define γ_{1_p}, $\gamma_{2_p} \in \mathbb{R}$, $p \in \mathcal{P}$ as

$$\gamma_{1_p} \triangleq \frac{1}{2} \min(1, \xi_{0_p}), \tag{7–11}$$

$$\gamma_{2_p} \triangleq \frac{1}{2} \max(1, \xi_{1_p}), \tag{7–12}$$

where ξ_{0_p}, ξ_{1_p} are introduced in (2–8).

Theorem 7.1. *The control law $u(t) = u_{\sigma(t)}(t)$ ensures all closed-loop signals are bounded and semi-global asymptotic tracking in the sense that $|e(t)| \to 0$ as $t \to \infty$, provided the control gains are selected sufficiently large based on the initial conditions of the states (see the subsequent stability analysis) and the following sufficient conditions are satisfied:*

$$\beta_p > \xi_{4_p}, \quad p \in \mathcal{P}, \tag{7–13}$$

$$\sum_{p=1}^{4} \frac{\gamma_{3_p}}{\gamma_{2_p}} T_p > \sum_{p=1}^{4} \log\left(\frac{\gamma_{2_p}}{\gamma_{1_p}}\right), \tag{7–14}$$

are satisfied, where $\beta_p \in \mathbb{R}$ is introduced in (7–4), ξ_{4_p} is introduced in (7–8) γ_{1_p}, $\gamma_{2_p} \in \mathbb{R}$, are introduced in (7–11), and (7–12), and $\gamma_{3_p} \in \mathbb{R}$ are positive constants determined by the initial condition of the system and the control gains α and k_{s_p}.

Proof. For each phase indicated by $\sigma(t)$, consider a continuously differentiable, radially unbounded, positive definite function $V_p(e, r, t) \in \mathbb{R}$, $p \in \mathcal{P}$ defined as

$$V_p = \frac{1}{2}e^2 + \frac{1}{2}r^2 J_{\zeta_p}. \tag{7–15}$$

Using (2–8), $V_p(e, r, t)$ can be upper and lower bounded as

$$\gamma_{1_p} \|y\|^2 \le V_p \le \gamma_{2_p} \|y\|^2, \tag{7–16}$$

where γ_{1_p}, $\gamma_{2_p} \in \mathbb{R}$ are defined in (7–11) and (7–12). After taking the time derivative of (7–15), and using (2–9) and (7–6), $\dot{V}_p(e, r, t)$ can be expressed as

$$\dot{V}_p = -\alpha e^2 - k_{s_p} r^2 - \beta_p |r| + \tilde{N}_p r + N_{D_p} r.$$

Using (7–9) and (7–8), $\dot{V}_p(t)$ can be upperbounded as

$$\dot{V}_p \leq -\alpha e^2 - k_{s_p} r^2 + \rho_p(\|y\|)\,|r|\,\|y\| - \beta_p\,|r| + \xi_{4_p}\,|r|,$$

which can be further upperbounded as

$$\dot{V}_p \leq -\left(min(\alpha, \frac{3}{4}k_{s_p}) - \frac{\rho_p^2(\|y\|)}{k_{s_p}}\right)\|y\|^2 \leq -\gamma_{3_p}\|y\|^2, \tag{7–17}$$

provided the sufficient conditions in (7–13) is satisfied, and where $\gamma_{3p} \in \mathbb{R}$ is a positive constant provided α and k_{s_p} are selected sufficiently large based on the initial condition of the activated subsystem. The region of attraction $\mathcal{D}_p$ is defined as

$$\mathcal{D}_p \triangleq \left\{ y(t) \subset \mathbb{R}^2 \mid \|y\| \leq \rho_p^{-1}\left(\sqrt{min(\alpha, \frac{3}{4}k_{s_p})k_{s_p}})\right) \right\}, \tag{7–18}$$

That is, the region of attraction can be made arbitrarily large to include any initial conditions by increasing the control gain α and k_{s_p} (i.e., a semi-global type of stability result). Using (7–16) and (7–17), and solving the resulting differential equation yields

$$V_p(t) \leq V_p(0)\,e^{-\lambda_p t}, \tag{7–19}$$

where $\lambda_p \in \mathbb{R}$ is a constant defined as

$$\lambda_p \triangleq \frac{\gamma_{3_p}}{\gamma_{2_p}}. \tag{7–20}$$

Provided the condition in (7–13) is satisfied, the control input and all the closed-loop signals are bounded during $\sigma(t) = p$ in $\mathcal{D}_p$.

Even though each controller is exponentially stable, additional development is required to examine the stability of the composite system. To this end, (7–16) can be used to conclude

$$V_{\sigma(t_i)}(t_i) \leq \mu_i V_{\sigma(t_{i-1})}(t_i), \tag{7–21}$$

where $\sigma(t_i) = i + 1$, and the constant $\mu_i \in \mathbb{R}$, $i = 1, 2, 3, 4$ is defined as

$$\mu_i \triangleq \frac{\gamma_{2_{\sigma(t_i)}}}{\gamma_{1_{\sigma(t_{i-1})}}}. \tag{7–22}$$

From (7–19) and (7–21),

$$\begin{aligned} V_{\sigma(t_i)}(t_i) &\leq \mu_i V_{\sigma(t_{i-1})}(t_i) \\ &\leq \mu_i V_{\sigma(t_{i-1})}(t_{i-1}) e^{-\lambda_{\sigma(t_{i-1})} T_i}. \end{aligned} \tag{7–23}$$

Iterating (7–23) for $i = 1$ to 4 yields

$$\begin{aligned} V_{\sigma(t_4)}(t_4) &\leq \mu_4 V_{\sigma(t_3)}(t_4) \leq \\ \mu_4 V_{\sigma(t_3)}(t_3) e^{-\lambda_4 T_4} &\leq \mu V_{\sigma(t_0)}(t_0) e^{-\lambda}, \end{aligned} \tag{7–24}$$

where $\mu, \lambda \in \mathbb{R}$ are defined as

$$\mu \triangleq \mu_1 \mu_2 \mu_3 \mu_4, \tag{7–25}$$

$$\lambda \triangleq \lambda_1 T_1 + \lambda_2 T_2 + \lambda_3 T_3 + \lambda_4 T_4. \tag{7–26}$$

Based on (7–16) and (7–24), the following inequality can be developed:

$$\begin{aligned} V_1(t_4) - V_1(t_0) &\leq -\left(1 - \mu e^{-\lambda}\right) V_1(t_0) \\ &\leq -\left(1 - \mu e^{-\lambda}\right) \gamma_{1_1} \|y(t_0)\|^2. \end{aligned} \tag{7–27}$$

This result can be generalized as

$$V_{\sigma(t_i)}(t_i + T) - V_{\sigma(t_i)}(t_i) \leq -\left(1 - \mu e^{-\lambda}\right) \gamma_{1_{\sigma(t_i)}} \|y(t_i)\|^2. \tag{7–28}$$

Provided α, k_s and β_p are selected sufficient large, and

$$1 - \mu e^{-\lambda} > 0, \tag{7–29}$$

(7–15), (7–16), (7–17), and (7–28) can be used to conclude asymptotic tracking [43, 71]. The switched control law $u(t) = u_{\sigma(t)}(t)$ ensures all closed-loop signals are bounded,

and $|e(t)| \to 0$ as $t \to \infty$ in $\mathcal{D}$. The region of attraction $\mathcal{D}$ is defined as

$$\mathcal{D} \triangleq \mathcal{D}_1 \cap \mathcal{D}_2 \cap \mathcal{D}_3 \cap \mathcal{D}_4. \tag{7-30}$$

The region of attraction can be made arbitrarily large to include any initial conditions by increasing the control gain α and k_{s_p} (i.e., a semi-global type of stability result). $\qquad \square$

7.4 Simulation

Simulations are performed using a modified model based on the model given in [70]. The controller computes a voltage as an input to the simulated muscle model. The simulation results are shown in Figs. 7-1−7-3. A desired trajectory is designed to simulate an average trajectory (cf. the experimental data in [42]) which is given as

$$q_d = 90 + pf + (ps - pf)\left(10(\frac{tt}{d})^3 - 15(\frac{tt}{d})^44 + 6(\frac{tt}{d})^5)\right),$$

where $pf = A(i), ps = A(i+1), tt = t(\mathrm{mod}T) - T_t(i), d = T_t(i+1) - T_t(i)$, where $T \in \mathbb{R}$ is the gait period; $T_t \in \mathbb{R}^5$ is the time period for each phase; $A \in \mathbb{R}^4$ is the amplitude of each phase; and $i \in \mathbb{R}$ is the phase indicator defined as $T = 2.5s, T_t = [\ 0 \quad 0.12T \quad 0.48T \quad 0.62T \quad T \ ], A = [\ 0 \quad -7 \quad 10 \quad -20 \ ]$, and

$$i = \begin{cases} 1 & 0 \le t(\mathrm{mod}T) < 0.12T \\ 2 & 0.12T \le t(\mathrm{mod}T) < 0.48T \\ 3 & 0.48T \le t(\mathrm{mod}T) < 0.62T \\ 4 & 0.62T \le t(\mathrm{mod}T) < T. \end{cases}$$

The gains of the controller are selected as

$$\alpha = 2, k_s = [\ 5 \quad 5 \quad 5 \quad 5 \ ], k_c = [\ 22 \quad 22 \quad 22 \quad 22 \ ], \beta = [\ 0.2 \quad 1.2 \quad 0.4 \quad 0.3 \ ].$$

The tracking performance is shown in Figure 7-1. Asymptotic decrease of tracking error is depicted in Figure 7-2. The control inputs in Figures 7-3 and 7-4 are in the range

98

of $15 - 30V$. The control inputs are within a typical range and the tracking error indicate the controller can yield functional gaits.
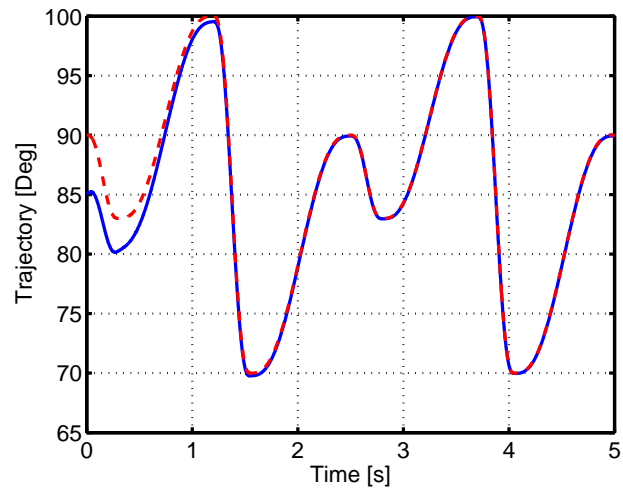

Figure 7-1. Actual (solid line) and desired (dashed line) trajectories
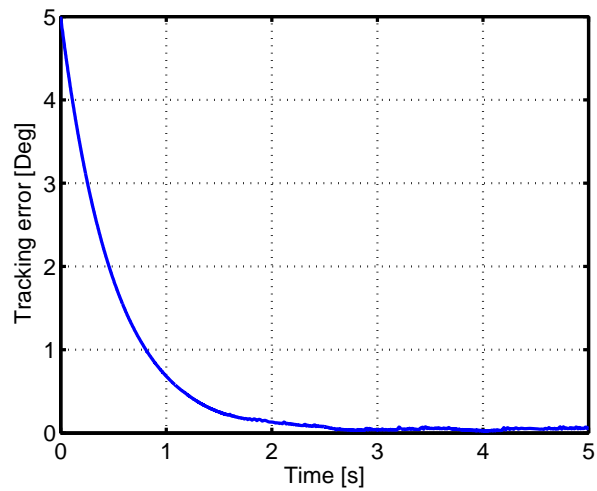

Figure 7-2. Tracking error
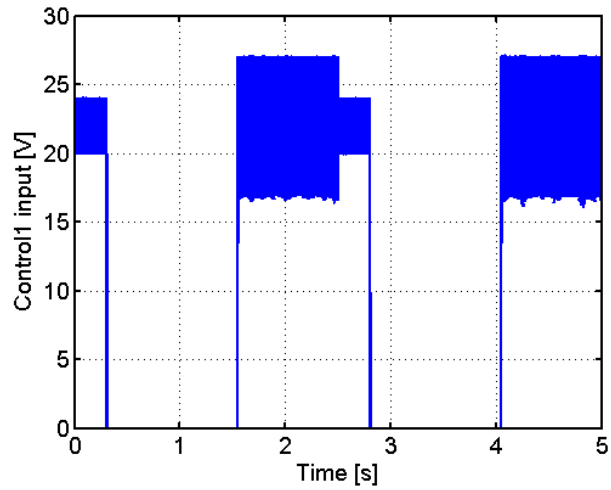
Figure 7-3. Computed voltage as control input for the dosiflexation muscle group
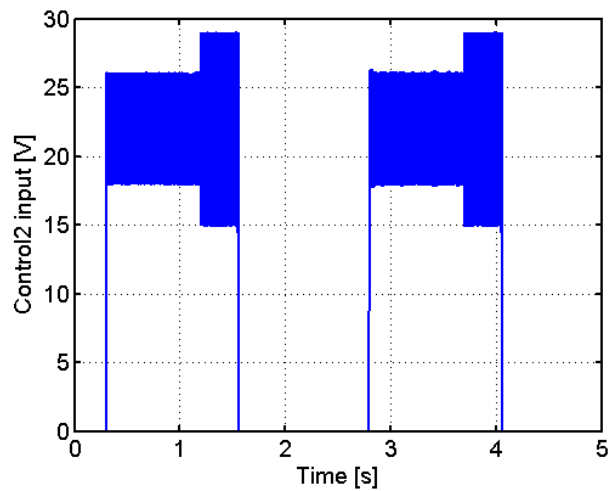
Figure 7-4. Computed voltage as control input for the plantaflexation muscle group

CHAPTER 8
CONCLUSION AND FUTURE WORK

8.1 Conclusion

Millions of people suffering from disability and paralysis could benefit from advancements in closed-loop NMES. Potentially, more efficient rehabilitation and more precise motor function can be achieved through closed-loop control of NMES. In this dissertation, Lyapunov-based methods are used to design and analyze NMES controllers. Varied problems are addressed to build the framework for future research and to improve the efficacy and the performance of the closed-loop NMES controller.

In Chapter 2, an adaptive inverse optimal NMES controller is developed for lower limb trajectory tracking in the presence of parametric uncertainty and external disturbances in the muscle activation and limb dynamics model. A Lyapunov-based stability analysis is used to prove that the developed NN-based controller yields uniformly ultimately bounded (UUB) tracking while simultaneously minimizing a cost functional. Experiments on able bodied volunteers validate the performance of the proposed controller for a limb tracking task for walking speed trajectories and a functional stand from a sitting position task. Experiments also illustrate the ability to alter the control performance through weighting the cost function.

In Chapter 3, a NMES controller that achieves asymptotic tracking and minimizes a quadratic cost functional is achieved. The overall control structure asymptotically converges to an optimal controller for a specific dynamic system. The resulting controller achieves asymptotic error tracking while converging to an optimal controller. A NN feedforward component is incorporated with a RISE feedback controller to improve the transient and steady state response and reduce the control effort. A Lyapunov-based analysis is used to prove the lower limb asymptotically tracks a desired time varying angular trajectory. The controller is also proven to asymptotically minimize a given cost functional. Experiments on healthy normal volunteers validate the performance of the

proposed controller for a limb tracking task for walking speed trajectories. Experiments also illustrate the ability to alter the control performance through weighting the cost function.

In Chapter 4, a muscle activation model with a pulse modulated control input is analyzed. A closed-loop NMES controller is designed based on an uncertain muscle activation model. The controller ensures that the knee angle tracks a desired trajectory which can be used for rehabilitation and functional restoration purposes. A Lyapunov-based method is used to conclude UUB tracking based on sufficient conditions on the gains and modulation parameters. For the first time, an analysis of the controller with modulation scheme is illustrated.

In Chapter 5, a system identifier is developed to identify the limb dynamics and estimate acceleration. The controller can be implemented only using position and velocity signals. Acceleration is not required to implement the controller as it was required in [5] and [37]. For the first time, an identification-based controller is developed for the muscle-limb model which includes an uncertain first order dynamic system that models muscle contraction dynamics. The parameters of the limb dynamics and the muscle contraction model are unknown. The designed identifier-controller system is analyzed through Lyapunov methods. Semi-global uniformly ultimately bounded (SUUB) tracking and asymptotic identification are guaranteed. Simulation results are provided to illustrate the controller performance.

In Chapter 6, ankle motion control is modeled as a hybrid system and a switched controller comprised of multiple sliding mode based controllers is designed for the first time to enable the ankle to track desired trajectories during gait. Semi-global asymptotic tracking result of the switched controller during gait is analyzed based on multiple Lyapunov functions and the performance is illustrated though simulations.

8.2   Future Work

The work in this dissertation addresses some important challenges in closed-loop control of NMES. Frameworks are developed to facilitate future research. However, several remaining questions need for further investigation:

1. Optimal frameworks are developed to facilitate a practitioner's ability to balance control efforts and performance. How can different rehabilitation goals be achieved by selecting procedures that emphasize on tracking performance over that emphasize on repetition numbers? More work has to be done to develop optimal controller that includes overall control input instead of just partial feedback of the total control effort like the current approaches.

2. Reducing muscle fatigue is still an open question. Approaches by selecting different modulation strategies related to stimulation intensity, frequency, and interval have been published. How to incorporate these open-loop results into the closed-loop controller design to improve the fatigue resistance performance could be a path worth to pursue. In Chapter 4, a hybrid analysis is demonstrated and future results can build on frequency optimization.

3. One cause of the early onset of muscle fatigue is due to synchronous recruitment of motor units. Asynchronous excitement of motor units can be achieved by using multiple surface or implanted electrodes. Controllers that can handle the rapid switching between pairs of electrodes should be developed to investigate the possibility to reduce fatigue.

4. Most muscles work collaboratively. A controller that can organize the agonist and the antagonist and utilize co-contractions would be highly valued in the application of functional restoration.

5. Current approaches are based on one joint models, these results can be extended to multi-joint situations to solve more realistic clinic problems.

6. Modern biomedical techniques such as MRI (magnetic resonance imaging), NIRS (near infrared spectroscopy) can provide inside muscle metabolic information. Incorporating these useful information into closed-loop control design is interesting and promising to reducing muscle fatigue.

REFERENCES

[1] G. Lyons, T. Sinkjaer, J. Burridge, and D. Wilcox, "A review of portable fes-based neural orthoses for the correction of drop foot," *IEEE Trans. Neur. Sys. and Rehab. Eng.,*, vol. 10, no. 4, pp. 260 –279, Dec. 2002.

[2] J. J. Abbas and H. J. Chizeck, "Feedback control of coronal plane hip angle in paraplegic subjects using functional neuromuscular stimulation," *IEEE Trans. Biomed. Eng.*, vol. 38, no. 7, pp. 687–698, 1991.

[3] N. Lan, P. E. Crago, and H. J. Chizeck, "Control of end-point forces of a multijoint limb by functional neuromuscular stimulation," *IEEE Trans. Biomed. Eng.*, vol. 38, no. 10, pp. 953–965, 1991.

[4] ——, "Feedback control methods for task regulation by electrical stimulation of muscles," *IEEE Trans. Biomed. Eng.*, vol. 38, no. 12, pp. 1213–1223, 1991.

[5] T. Schauer, N. O. Negard, F. Previdi, K. J. Hunt, M. H. Fraser, E. Ferchland, and J. Raisch, "Online identification and nonlinear control of the electrically stimulated quadriceps muscle," *Control Eng. Pract.*, vol. 13, pp. 1207–1219, 2005.

[6] K. Stegath, N. Sharma, C. Gregory, and W. E. Dixon, "An extremum seeking method for non-isometric neuromuscular electrical stimulation," in *Proc. IEEE Int. Conf. Syst. Man Cybern.*, Montreal, Canada, October 2007, pp. 2528–2532.

[7] N. Lan, H. Feng, and E. Crago, "Neural network generation of muscle stimulation patterns for control of arm movements," *IEEE Trans. Rehabil. Eng.*, vol. 2, no. 4, pp. 213–224, 1994.

[8] J. J. Abbas and H. J. Chizeck, "Neural network control of functional neuromuscular stimulation systems: computer simulation studies," *IEEE Trans. Biomed. Eng.*, vol. 42, no. 11, pp. 1117–1127, Nov. 1995.

[9] D. Graupe and H. Kordylewski, "Artificial neural network control of FES in para-plegics for patient responsive ambulation," *IEEE Trans. Biomed. Eng.*, vol. 42, no. 7, pp. 699–707, July 1995.

[10] G.-C. Chang, J.-J. Lub, G.-D. Liao, J.-S. Lai, C.-K. Cheng, B.-L. Kuo, and T.-S. Kuo, "A neuro-control system for the knee joint position control with quadriceps stimulation," *IEEE Trans. Rehabil. Eng.*, vol. 5, no. 1, pp. 2–11, Mar. 1997.

[11] J. A. Riess and J. J. Abbas, "Adaptive neural network control of cyclic movements using functional neuromuscular stimulation," *IEEE Trans. Neural Syst. Rehabil. Eng.*, vol. 8, pp. 42–52, 2000.

[12] H. Kordylewski and D. Graupe, "Control of neuromuscular stimulation for ambulation by complete paraplegics via artificial neural networks," *Neurol. Res.*, vol. 23, no. 5, pp. 472–481, 2001.

[13] N. Sharma, C. M. Gregory, M. Johnson, and W. E. Dixon, "Modified neural network-based electrical stimulation for human limb tracking," in *Proc. IEEE Int. Symp. Intell. Control*, San Antonio, Texas, September 2008, pp. 1320–1325.

[14] D. G. Zhang and K. Y. Zhu, "Simulation study of FES-assisted standing up with neural network control," in *Proc. Annu. Int. Conf. IEEE Eng. Med. Biol. Soc.*, vol. 6, 2004, pp. 4118–4121.

[15] J. P. Giuffrida and P. E. Crago, "Functional restoration of elbow extension after spinal-cord injury using a neural network-based synergistic FES controller," *IEEE Trans. Neural Syst. Rehabil. Eng.*, vol. 13, no. 2, pp. 147–152, 2005.

[16] Y. Chen and Z. Wang, "Formation control: a review and a new consideration," in *Proc. IEEE/RSJ Int. Conf. Intell. Robot. Syst.*   IEEE, 2005, pp. 3181–3186.

[17] K. Kurosawa, R. Futami, T. Watanabe, and N. Hoshimiya, "Joint angle control by FES using a feedback error learning controller," *IEEE Trans. Neural Syst. Rehabil. Eng.*, vol. 13, pp. 359–371, 2005.

[18] A. Pedrocchi, S. Ferrante, E. De Momi, and G. Ferrigno, "Error mapping controller: a closed loop neuroprosthesis controlled by artificial neural networks," *J. Neuroeng. Rehabil.*, vol. 3, no. 1, p. 25, 2006.

[19] S.-J. Kim, M. Fairchild, A. Iarkov, J. Abbas, and R. Jung, "Adaptive control of movement for neuromuscular stimulation-assisted therapy in a rodent model," *IEEE Trans. Biomed. Eng.*, vol. 56, no. 2, pp. 452 –461, feb. 2009.

[20] A. Ajoudani and A. Erfanian, "A neuro-sliding-mode control with adaptive modeling of uncertainty for control of movement in paralyzed limbs using functional electrical stimulation," *IEEE Trans. Biomed. Eng.*, vol. 56, no. 7, pp. 1771–1780, Jul. 2009.

[21] J. Lujan and P. Crago, "Automated optimal coordination of multiple-DOF neuromuscular actions in feedforward neuroprostheses," *IEEE Trans. Biomed. Eng.*, vol. 56, no. 1, pp. 179–187, Jan. 2009.

[22] N. Sharma, K. Stegath, C. M. Gregory, and W. E. Dixon, "Nonlinear neuromuscular electrical stimulation tracking control of a human limb," *IEEE Trans. Neural Syst. Rehabil. Eng.*, vol. 17, no. 6, pp. 576–584, 2009.

[23] S. A. Binder-Macleod and L. Snyder-Mackler, "Muscle fatigue: clinical implications for fatigue assessment and neuromuscular electrical stimulation," *Phys. Ther.*, vol. 73, no. 12, pp. 902–910, Dec 1993.

[24] C. Lynch and M. Popovic, "Functional electrical stimulation," *IEEE Contr. Syst. Mag.*, vol. 28, no. 2, pp. 40 –50, April 2008.

[25] R. Maladen, R. Perumal, A. Wexler, and S. Binder-Macleod, "Effects of activation pattern on nonisometric human skeletal muscle performance," *J. Appl. Physiol.*, vol. 102, no. 5, pp. 1985–91, 2007.

[26] S. Binder-Macleod, J. Dean, and J. Ding, "Electrical stimulation factors in poten-tiation of human quadriceps femoris," *Muscle Nerve*, vol. 25, no. 2, pp. 271–9, 2002.

[27] J. Mizrahi, "Fatigue in muscles activated by functional electrical stimulation," *Crit. Rev. Phys. Rehabil. Med.*, vol. 9, no. 2, pp. 93–129, 1997.

[28] C. M. Gregory, W. E. Dixon, and C. S. Bickel, "Impact of varying pulse frequency and duration on muscle function during nmes," *Muscle and Nerve*, vol. 35, pp. 504–509, 2007.

[29] R. A. Freeman and P. V. Kokotovic, *Robust Nonlinear Control Design: State-Space and Lyapunov Techniques*.   Boston, MA: Birkšauser„ 1996.

[30] M. Krstic and H. Deng, *Stabilization of Nonlinear Uncertain Systems*.   Springer, 1998.

[31] Y. Kim and F. Lewis, "Optimal design of CMAC neural-network controller for robot manipulators," *IEEE Trans. Syst. Man Cybern. Part C Appl. Rev.*, vol. 30, no. 1, pp. 22 –31, feb 2000.

[32] K. Dupree, P. Patre, Z. Wilcox, and W. E. Dixon, "Asymptotic optimal control of uncertain nonlinear systems," *Automatica*, vol. 47, no. 1, pp. 99–107, 2011.

[33] P. H. Peckham and J. S. Knutson, "Functional electrical stimulation for neuromuscu-lar applications," *Annu. Rev. Biomed. Eng.*, vol. 7, pp. 327–360, 2005.

[34] T. Kesar, L.-W. Chou, and S. A. Binder-Macleod, "Effects of stimulation frequency versus pulse duration modulation on muscle fatigue." *J. Electromyogr. Kinesiol.*, vol. 18, no. 4, pp. 662–671, Aug 2008.

[35] D. V. Knudson, *Fundamentals of biomechanics*.   Springer-Verlag New York Inc., 2003.

[36] N. Sharma, S. Bhasin, Q. Wang, and W. E. Dixon, "Predictor-based control for an uncertain Euler-Lagrange system with input delay," *Automatica*, vol. 47, no. 11, pp. 2332–2342, 2011.

[37] N. Sharma, P. Patre, C. Gregory, and W. E. Dixon, "Nonlinear control of nmes: Incorporating fatigue and calcium dynamics," in *Proc. ASME Dyn. Syst. Control Conf.*, Hollywood, CA, October 2009, pp. 705–712.

[38] S. Bhasin, R. Kamalapurkar, H. T. Dinh, and W. Dixon, "Robust identification-based state derivative estimation for nonlinear systems," *IEEE Trans. Automat. Control*, T.A.

[39] P. W. Duncan, K. J. Sullivan, A. L. Behrman, S. P. Azen, S. S. Wu, S. E. Nadeau, B. H. Dobkin, D. K. Rose, J. K. Tilson, and L. E. A. P. S. I. Team, "Protocol for the

locomotor experience applied post-stroke (LEAPS) trial: a randomized controlled trial." *BMC Neurol*, vol. 7, p. 39, 2007.

[40] D. G. Embrey, S. L. Holtz, G. Alon, B. A. Brandsma, and S. W. McCoy, "Functional electrical stimulation to dorsiflexors and plantar flexors during gait to improve walking in adults with chronic hemiplegia." *Arch. Phys. Med. Rehabil.*, vol. 91, no. 5, pp. 687–696, May 2010.

[41] T. M. Kesar, R. Perumal, D. S. Reisman, A. Jancosko, K. S. Rudolph, J. S. Higginson, and S. A. Binder-Macleod, "Functional electrical stimulation of ankle plantarflexor and dorsiflexor muscles: effects on poststroke gait." *Stroke*, vol. 40, no. 12, pp. 3821–3827, Dec 2009.

[42] J. Perry, *Gait analysis : normal and pathological function*. Harry C. Benson, 1992.

[43] D. Liberzon and A. Morse, "Basic problems in stability and design of switched systems," *IEEE Contr. Syst. Mag.*, vol. 19, no. 5, pp. 59–70, 1999.

[44] M. Ferrarin and A. Pedotti, "The relationship between electrical stimulus and joint torque: A dynamic model," *IEEE Trans. Rehabil. Eng.*, vol. 8, no. 3, pp. 342–352, 2000.

[45] W. L. Buford, Jr., F. M. Ivey, Jr., J. D. Malone, R. M. Patterson, G. L. Peare, D. K. Nguyen, and A. A. Stewart, "Muscle balance at the knee - moment arms for the normal knee and the ACL - minus knee," *IEEE Trans. Rehabil. Eng.*, vol. 5, no. 4, pp. 367–379, 1997.

[46] F. L. Lewis, "Neural network control of robot manipulators," *IEEE Expert*, vol. 11, no. 3, pp. 64–75, 1996.

[47] F. L. Lewis, R. Selmic, and J. Campos, *Neuro-Fuzzy Control of Industrial Systems with Actuator Nonlinearities*. Philadelphia, PA, USA: Society for Industrial and Applied Mathematics, 2002.

[48] R. A. Freeman and P. V. Kokotovic, "Optimality of robust nonlinear feedback control," Univ. California, Santa Barbara, CCEC-11-09-93, Tech. Rep., Nov 1993.

[49] M. Krstic and P. Tsiotras, "Inverse optimal stabilization of a rigid spacecraft," *IEEE Trans. Autom. Control*, vol. 44, no. 5, pp. 1042–1049, May 1999.

[50] W. J. Crochetiere, L. Vodovnik, and J. B. Reswick, "Electrical stimulation of skeletal muscle–a study of muscle as an actuator." *Med Biol Eng*, vol. 5, no. 2, pp. 111–125, Mar 1967.

[51] J. Hausdorff and W. Durfee, "Open-loop position control of the knee joint using electrical stimulation of the quadriceps and hamstrings," *Med. Biol. Eng. Comput.*, vol. 29, pp. 269–280, 1991.

[52] R. Riener and J. Quintern, *Biomechanics and Neural Control of Posture and movement*, J. Winters and P. E. Crago, Eds.   Springer-Verlag New York, Inc, 2000.

[53] R. Riener, J. Quintern, and G. Schmidt, "Biomechanical model of the human knee evaluated by neuromuscular stimulation," *J. Biomech.*, vol. 29, pp. 1157–1167, 1996.

[54] M. K. Z. Li, "Optimal design of adaptive tracking controllers for non-linear systems," *Automatica*, vol. 33, pp. 1459–1473, 1997.

[55] Y. Kim, F. Lewis, and D. Dawson, "Intelligent optimal control of robotic manipulator using neural networks," *Automatica*, vol. 36, no. 9, pp. 1355–1364, 2000.

[56] A. Filippov, "Differential equations with discontinuous right-hand side," *Am. Math. Soc. Transl.*, vol. 42 no. 2, pp. 199–231, 1964.

[57] A. F. Filippov, *Differential Equations with Discontinuous Right-hand Sides*.   Kluwer Academic Publishers, 1988.

[58] G. V. Smirnov, *Introduction to the theory of differential inclusions*.   American Mathematical Society, 2002.

[59] J. P. Aubin and H. Frankowska, *Set-valued analysis*.   Birkhäuser, 2008.

[60] D. Shevitz and B. Paden, "Lyapunov stability theory of nonsmooth systems," *IEEE Trans. Autom. Control*, vol. 39 no. 9, pp. 1910–1914, 1994.

[61] B. Paden and S. Sastry, "A calculus for computing Filippov's differential inclusion with application to the variable structure control of robot manipulators," *IEEE Trans. Circuits Syst.*, vol. 34 no. 1, pp. 73–82, 1987.

[62] M. Krstic, P. V. Kokotovic, and I. Kanellakopoulos, *Nonlinear and Adaptive Control Design*.   John Wiley & Sons, 1995.

[63] B. Xian, D. M. Dawson, M. S. de Queiroz, and J. Chen, "A continuous asymptotic tracking control strategy for uncertain nonlinear systems," *IEEE Trans. Autom. Control*, vol. 49, pp. 1206–1211, 2004.

[64] P. M. Patre, W. MacKunis, K. Kaiser, and W. E. Dixon, "Asymptotic tracking for uncertain dynamic systems via a multilayer neural network feedforward and RISE feedback control structure," *IEEE Trans. Automat. Control*, vol. 53, no. 9, pp. 2180–2185, 2008.

[65] F. H. Clarke, *Optimization and nonsmooth analysis*.   SIAM, 1990.

[66] J. M. Y. Giat and M. Levy, "A musculotendon model of the fatigue pro̅les of paralyzed quadriceps muscle under fes," *IEEE Trans. Biomed. Eng.*, vol. 40, pp. 664–674, 1993.

[67] F. Zajac, "Muscle and tendon: properties, models, scaling, and application to biomechanics and motor control," *Crit. Rev. Biomed. Eng.*, vol. 17, no. 4, pp. 359–411, 1989.

[68] H. K. Khalil, *Nonlinear Systems*, 3rd ed.   Prentice Hall, 2002.

[69] G. Cybenko, "Approximation by superpositions of a sigmoidal function," *Math. Control Signals Syst.*, vol. 2, pp. 303–314, 1989.

[70] M. Ferrarin, F. Palazzo, R. Riener, and J. Quintern, "Model-based control of FES-induced single joint movements," *IEEE Trans. Neural Syst. Rehabil. Eng.*, vol. 9, no. 3, pp. 245–257, Sep. 2001.

[71] R. Goebel, R. Sanfelice, and A. Teel, "Hybrid dynamical systems," *IEEE Contr. Syst. Mag.,*, vol. 29, no. 2, pp. 28 –93, 2009.

BIOGRAPHICAL SKETCH

Qiang Wang was born in Hubei, China. He received his bachelor's degree in biomedical engineering from Huazhong University of Science and Technology. He received his master's and PhD degrees in biomedical engineering from Peking Union Medical College. He joined the Nonlinear Controls and Robotics (NCR) research group to pursue his second doctoral degree in electrical engineering, under the advisement of Dr. Warren E. Dixon. He received his PhD in electrical and computer engineering from the University of Florida in the Fall of 2012.